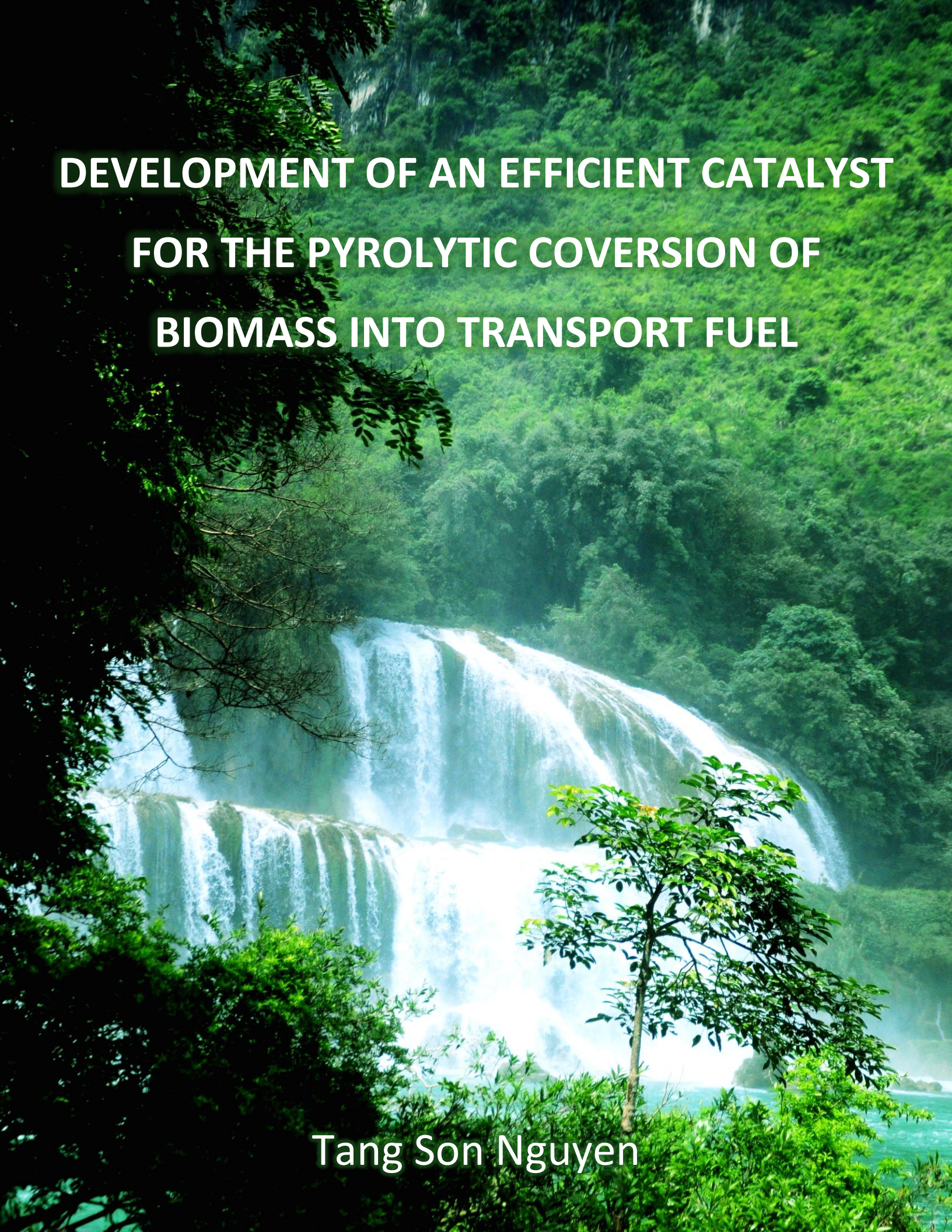

# DEVELOPMENT OF AN EFFICIENT CATALYST FOR THE PYROLYTIC COVERSION OF BIOMASS INTO TRANSPORT FUEL

Tang Son Nguyen

# DEVELOPMENT OF AN EFFICIENT CATALYST FOR THE PYROLYTIC CONVERSION OF BIOMASS INTO TRANSPORT FUEL

**Tang Son Nguyen**

## Promotion committee

| | | |
|---|---|---|
| Prof. Dr. Ir. J.W.M. Hilgenkamp | Chairman | University of Twente, The Netherlands |
| Prof. Dr. K. Seshan | Promoter | University of Twente, The Netherlands |
| Prof. Dr. Ir. L. Lefferts | Promoter | University of Twente, The Netherlands |
| Prof. Dr. Ir. W.P.M.G van Swaaij | | University of Twente, The Netherlands |
| Prof. Dr. Ir. W. Prins | | University of Ghent, Belgium |
| Prof. Dr. J. H. Bitter | | University of Wageningen, The Netherlands |
| Prof. Dr. Ir. G. Brem | | University of Twente, The Netherlands |
| Dr. P. O'Connor | | BIOeCON, The Netherlands |

The research described in this thesis was conducted in the Catalytic Processes and Materials (CPM) group at University of Twente, The Netherlands. This work was financially supported by STW-GSPT under project number 07972.

ISBN: 978-90-365-3796-4

Publisher: Gildeprint, Enschede, The Netherlands



Cover design: The cover picture is designed by Bùi Hương Liên based on a picture taken by Lê Việt Anh at Ban Gioc Fall, Cao Bang, Vietnam. The theme of the cover illustrates the wonder of nature and thus represents the key goal of my PhD project: shaping a sustainable future for us and for our children *via* development of greener processes.

# DEVELOPMENT OF AN EFFICIENT CATALYST FOR THE PYROLYTIC CONVERSION OF BIOMASS INTO TRANSPORT FUEL

DISSERTATION

to obtain

the degree of doctor at the University of Twente,

on the authority of the rector magnificus,

Prof. Dr. H. Brinksma

on account of the decision of the graduation committee,

to be publicly defended on

Thursday December 4th 2014 at 12:45 hrs

by


## Tang Son Nguyen

Born on 25 October 1983

in Hanoi, Vietnam

This dissertation has been approved by the promoters

Prof. Dr. K. Seshan

Prof. Dr. Ir. L. Lefferts

Dành tặng bố mẹ và vợ yêu

Dedicated to my parents and my wife

“The training is nothing! The will is everything!
The will to act.”

- Ra’s al Ghul

**Contents**

# Summary

Fast pyrolysis is a promising technique to convert biomass into a liquid fuel/fuel precursor, known as bio-oil. However, compared to conventional crude oil, bio-oil has much higher oxygen content which results in various detrimental properties and limits its application. Thus the first part of this thesis aims to develop an efficient catalyst to upgrade bio-oil into high quality fuel *via* de-oxygenation and hydro-deoxygenation. The second part is dedicated to study the nature of the active specie in the newly-developed catalyst and to gain more insight into the catalytic conversion of lignin *via* a model compound study.

The first part of the thesis starts with **Chapter 3**. In this chapter, Faujasite materials with different $H^+$ and $Na^+$ concentrations including H-FAU, $Na_{0.2}H_{0.8}$-FAU and Na-FAU were applied as catalysts in the pyrolysis of white pine, with the goal to lower the oxygen content of bio-oil. Two methods to establish the catalyst-feed contact, *i.e. in situ* and post-treatment, were compared and it was shown that the post-treatment was superior to *in-situ* when it comes to bio-oil oxygen removal efficiency. It was shown that the amount of $H^+$ and $Na^+$ of the catalyst plays an important role in the product yields and product distribution. The higher the concentration of $H^+$ of the catalyst is, the lower the liquid yield, and the higher the solid and gas yields are obtained. The two of major problems with bio-oil, namely the corrosiveness and instability, were shown to be mainly caused by carbonyl and carboxylic acid compounds, respectively. The best catalyst candidate is $Na_{0.2}H_{0.8}$-FAU, which reduced the most acid and carbonyl compounds while boosted the amount of the desirable phenolic and hydrocarbon compounds compared to non-catalytic experiment and to the other two catalysts. $Na_{0.2}H_{0.8}$-FAU also removed the most oxygen as $CO_2$, resulting in an oil with lowest oxygen content (38 wt.%) and highest energy content (24 MJ $kg^{-1}$) compared to other materials. It was shown possible to regenerate the spent catalyst without changing its crystalline structure and catalytic performance.

The catalytic system shown in **Chapter 3** was improved further in **Chapter 4** by employing $\gamma$-$Al_2O_3$ as the support for $Na^+$. $\gamma$-$Al_2O_3$ was selected because of its mesoporous nature, which allows access to bulkier biomass oxygenates and likely reduces the problem of coking/pore blockage compared to microporous FAU zeolites. Compared to non-catalytic pyrolysis, catalytic upgrading in the presence of $Na_2CO_3$/$\gamma$-$Al_2O_3$ results in higher level of selective de-oxygenation with the oxygen ending up in heterogeneous char or removed as

COx. Characterization of the catalyst using SEM and XRD has shown that sodium carbonate is well-dispersed on the support γ-$Al_2O_3$. TGA and $^{23}Na$ MAS NMR study suggested the formation of new hydrated sodium phase, which is likely responsible for the high activity of the catalyst. This hydrated phase is proposed to be formed by the coordination between sodium ion and the hydroxyl group of alumina. It has been shown that catalytic oil has much lower oxygen content (12.3 wt.%) compared to non-catalytic oil (42.1 wt.%). This comes together with a tremendous increase in the energy density (37 compared to 19 MJ $kg^{-1}$) approaching that of fuel oil (40 MJ $kg^{-1}$). Decarboxylation of carboxylic acids was favoured on the catalyst, resulting to an oil almost neutral (TAN= 3.8 mg KOH/g oil and pH=6.5). However, the mentioned decarboxylation also resulted in the formation of carbonyls, which correlates to low stability of the oil.

**Chapter 5** continues with the study on the active specie in $Na_2CO_3$/γ-$Al_2O_3$ catalyst which was briefly mentioned in **Chapter 4** but with a higher level of details**.** It was shown possible to achieve very high de-oxygenation degree of bio-oil with $Na_2CO_3$/γ-$Al_2O_3$ catalyst compared to $Na_2CO_3$, γ-$Al_2O_3$ and non-catalytic experiment. XRD analyses have shown that a good dispersion of $Na_2CO_3$ on γ-$Al_2O_3$ was achieved using wet impregnation followed by calcination of the obtained materials. It was revealed in TGA analyses that, in the supported catalysts, the sodium active specie likely existed in a state different from that in pure $Na_2CO_3$. This was shown by the difference in decomposition temperature between the two. $^{1}H$ and $^{23}Na$ MAS NMR spectra of the supported catalysts with different concentration of $Na_2CO_3$ (10, 20, 33, 50 and 100 wt.%) showed that in the samples with low concentration (10, 20 wt.%) sodium presented in a different state compared to that in high concentration samples and to pure $Na_2CO_3$. This state is proposed to be hydrated sodium specie, formed by the coordination between sodium ions and hydroxyl groups on the surface of γ-$Al_2O_3$. The fact that the 20 wt.% $Na_2CO_3$/γ-$Al_2O_3$ sample the most active catalyst in the de-oxygenation of bio-oil suggests that this hydrated specie is the one responsible for this superior activity of the catalyst. $^{27}Al$ MAS NMR spectra of γ-$Al_2O_3$ and the supported catalysts with different $Na_2CO_3$ loadings have revealed two peaks corresponding to the tetrahedral and octahedral Al. It can be observed that there is a downshift in the resonance signal of the tetrahedral Al in the supported catalysts compared to that of γ-$Al_2O_3$. This can be a result of the interaction between absorbed $Na^+$ ions and oxygen atoms of γ-alumina which causes a deshielding effect on Al atoms. The chemical shifts of the octahedral Al also varied depending on the loading of

sodium carbonate, but with a lesser extent. Regeneration of the catalyst was carried out in air at 600$^{o}$C and the regenerated material shows to have lower activity towards de-oxygenation compared to fresh catalyst. The alumina support was hardly affected during regeneration while there is change in the hydrated specie and this change is likely responsible for the deactivation of the catalyst.

In **Chapter 6**, the conversion of lignin-derived compounds in bio-oil over catalysts was studied using vanillyl alcohol as the model compound. It has been shown that this model compound has undergo consecutive reactions to form methoxy phenols, phenols, and eventually hydrocarbons with increasing degree of deoxygenation. The degree of deoxygenation of vanillyl alcohol was shown to increase with the increase in number of acid sites in catalysts. γ-$Al_2O_3$ material with the highest number of acid sites has resulted in the highest yield of aromatic hydrocarbons, accompanied by the highest yields of coke and gas compared to other materials used in this study. Two pathways have been shown leading to the formation of hydrocarbons from vanillyl alcohol, which are: (i) decomposition of vanillyl alcohol into small hydrocarbon fragments and the subsequent aromatization into final products and (ii) direct deoxygenation of this model compound over catalysts. Cyclic ketones, phenol derivatives and aromatic hydrocarbons were detected among the pyrolysis products of vanillyl alcohol and biomass. The concentrations of those components change in presence of different catalysts and the trends of changes are similar in both biomass and vanillyl alcohol pyrolysis. However, the rates of changes are different, which illustrates the difference in catalytic efficiency towards different biomass components.

The hydro-deoxygenation of bio-oil was investigated in **Chapter 7**. It was shown in **Chapter 4** that catalytic upgrading in the presence of $Na_2CO_3$/γ-$Al_2O_3$ results in higher level of selective de-oxygenation but leads to the formation of more harmful carbonyls. The study in **Chapter 7** was carried out to solve that problem using the combination of catalytic de-oxygenation and hydrogenation. It was shown that hydro-deoxygenation using Pt-$Na_2CO_3$/γ-$Al_2O_3$ co-catalysts reduced the amount of carbonyl compounds in bio-oil. However, the bulk quality of bio-oil (*i.e.* oxygen content, heating value) remained unchanged or became worse compared to the single catalyst, *i.e.* Pt/γ-$Al_2O_3$ and $Na_2CO_3$/γ-$Al_2O_3$. This low catalytic activity can be attributed to the interaction between the 2 precursors, namely choloroplatinic acid and sodium carbonate, which in turn resulted in the agglomeration of Pt particles and lower surface area of the support. The dual-bed system in which the sodium and platinum

components were separated has proven to be a very promising approach. Dual-bed operation has shown to achieve the highest de-oxygenation level of bio-oil among all the catalytic systems. This was achieved *via* the removal of harmful carbonyls and enhancement of the desirable hydrocarbons, leading to a heating value higher than that of traditional fuel oil (42 MJ $kg^{-1}$). n-butane possesses similar performance compared to $H_2$ as a hydrogen source for biomass hydro-pyrolysis, opening new possibility for economical hydrogen sources for bio-oil treating (for *e.g.* natural gas).

# Samenvatting

Snelle pyrolyse is een veelbelovende techniek om biomassa om te zetten naar vloeibare brandstof/brandstofprecursor, beter bekend als bio-olie. Echter, in vergelijking met conventionele ruwe olie heeft bio-olie een hoger zuurstofgehalte waardoor het nadelige eigenschappen en beperkte toepassingen heeft. Daarom richt het eerste deel van deze thesis zich op het ontwikkelen van een efficiënte katalysator om bio-olie op te waarderen naar brandstof van hoge kwaliteit *via* de-oxygenatie en hydro-deoxygenatie. Het tweede deel is gericht op het bestuderen van de aard van de actieve deeltjes in de nieuw-ontwikkelde katalysator en op het verwerven van meer inzicht in de katalytische conversie van lignine *via* een modelcomponentenstudie.

Het eerste deel van de thesis begint met **Hoofdstuk 3**. In dit hoofdstuk werden Faujasietmaterialen met verschillende $H^+$- en $Na^+$-concentraties, waaronder H-FAU, $Na_{0.2}H_{0.8}$-FAU en Na-FAU, gebruikt als katalysator voor de pyrolyse van witte den, met als doel het zuurstofgehalte van de bio-olie te verlagen. Twee methoden om het contact tussen de katalysator en de voeding te creëren, i.e. *in situ* en nabehandeling, werden vergeleken en er werd aangetoond dat nabehandeling beter was dan *in-situ* als het op de efficiëntie van de verwijdering van zuurstof uit bio-olie aankomt. Er werd aangetoond dat de hoeveelheid $H^+$ en $Na^+$ van de katalysator een belangrijke rol speelt in de productopbrengsten en productdistributie. Hoe hoger de concentratie van $H^+$ van de katalysator is, hoe lager de vloeistofopbrengst is en hoe hoger de verkregen opbrengt van vaste stof en gas. Er werd aangetoond dat de twee belangrijkste problemen van bio-olie, namelijk de corrosiviteit en instabiliteit, voornamelijk worden veroorzaakt door respectievelijk carbonyl- en carboxylzuurgroepen. De beste katalysatorkandidaat is $Na_{0.2}H_{0.8}$-FAU, welke de meeste zuur- en carbonylgroepen reduceerde en de hoeveelheid gewenste fenol- en koolwaterstofgroepen verhoogde in vergelijking tot het ongekatalyseerde experiment en de andere twee katalysatoren. $Na_{0.2}H_{0.8}$-FAU verwijderde ook de meeste zuurstof als $CO_2$, wat resulteerde in een olie met het laagste zuurstofgehalte (38 gewichts%) en de hoogste energie-inhoud (24 MJ $kg^{-1}$) in vergelijking met andere materialen. Er werd aangetoond dat het mogelijk is om de gebruikte katalysator te regenereren zonder de kristallijne structuur en katalytische prestaties te veranderen.

**Samenvatting**

Het katalytische systeem dat werd getoond in **Hoofdstuk 3** werd verder verbeterd in **Hoofdstuk 4** door γ-$Al_2O_3$ te gebruiken als de drager voor $Na^+$. γ-$Al_2O_3$ werd geselecteerd vanwege haar mesoporeuze structuur, wat de toegang van grote zuurstofhoudende biomassamoleculen mogelijk maakt en het probleem van koolafzetting/blokkering van de poriën vermindert in vergelijking tot microporeuze FAU zeolieten. In vergelijking tot ongekatalyseerde pyrolyse resulteert katalytische opwaardering in de aanwezigheid van $Na_2CO_3$/γ-$Al_2O_3$ in een hogere mate van selectieve de-oxygenatie waarbij de zuurstof in de heterogene kool terechtkomt of wordt verwijderd als $CO_x$. Karakterisering van de katalysator met behulp van SEM en XRD heeft laten zien dat natriumcarbonaat goed gedispergeerd op de γ-$Al_2O_3$ drager is. TGA en $^{23}Na$ MAS NMR studie suggereren de vorming van een nieuwe gehydrateerde natriumfase, welke waarschijnlijk verantwoordelijk is voor de hoge activiteit van de katalysator. Er wordt voorgesteld dat deze gehydrateerde fase wordt gevormd door de coördinering tussen het natriumion en de hydroxylgroep van alumina. Het is aangetoond dat katalytische olie een veel lager zuurstofgehalte (12.3 gewichts%) heeft in vergelijking tot niet-katalytische olie (42.1 gewichts%). Dit komt samen in een ongelooflijke toename in energiedichtheid (37 vergeleken met 19 MJ $kg^{-1}$) wat die van stookolie (40 MJ $kg^{-1}$) benadert. Decarboxylering van carboxylzuur kreeg de voorkeur op de katalysator, wat resulteerde in een bijna pH-neutrale olie (TAN = 3.8 mg KOH/g olie en pH = 6.5). De genoemde decarboxylering resulteerde echter ook in de vorming van carbonylgroepen, wat samenhangt met een lage stabiliteit van de olie.

**Hoofdstuk 5** gaat verder met de studie van de actieve deeltjes in de $Na_2CO_3$/γ-$Al_2O_3$ katalysator, welke al kort werd genoemd in **Hoofdstuk 4**, maar dan meer in detail. Er werd aangetoond dat het mogelijk is om een hoge mate van de-oxygenatie van de bio-olie te bereiken met de $Na_2CO_3$/γ-$Al_2O_3$ katalysator in vergelijking met $Na_2CO_3$, γ-$Al_2O_3$ en het ongekatalyseerde experiment. XRD analyses hebben aangetoond dat een goede dispersie van $Na_2CO_3$ op γ-$Al_2O_3$ werd bereikt met behulp van ‘natte’ impregnatie gevolgd door calcinatie van de verkregen materialen. In de TGA analyses werd onthuld dat, in de gedragen katalysatoren, de actieve natriumdeeltjes vermoedelijk in een andere staat voorkomen dan in puur $Na_2CO_3$. Dit werd aangetoond door het verschil in decompositietemperatuur tussen de twee. $^{1}H$ en $^{23}Na$ MAS NMR spectra van de gedragen katalysatoren met verschillende concentraties van $Na_2CO_3$ (10, 20, 33, 50 en 100 gewichts%) lieten zien dat in de samples met een lage concentratie (10, 20 gewichts%) natrium in een andere staat aanwezig was dan in de

samples met een hoge concentratie en puur $Na_2CO_3$. Er wordt voorgesteld dat deze staat bestaat uit gehydrateerde natriumdeeltjes, gevormd door de coördinering tussen natriumionen en hydroxylgroepen op het oppervlak van γ-$Al_2O_3$. Het feit dat het 20 gewichts% $Na_2CO_3$/γ-$Al_2O_3$ sample de meest actieve katalysator voor de de-oxygenatie van bio-olie is, suggereert dat deze gehydrateerde deeltjes verantwoordelijk zijn voor de superieure activiteit van de katalysator. $^{27}$Al MAS NMR spectra van γ-$Al_2O_3$ en van de gedragen katalysatoren met verschillende $Na_2CO_3$ beladingen, hebben twee pieken onthuld die met tetraëdrisch en octaëdrisch Al corresponderen. Een verschuiving naar beneden werd waargenomen in het resonantiesignaal van het tetraëdrische Al in de gedragen katalysatoren ten opzichte van die van γ-$Al_2O_3$. Dit kan komen door de interactie tussen de geabsorbeerde $Na^+$-ionen en zuurstofatomen van γ-$Al_2O_3$, wat een 'deshielding' effect veroorzaakt op de Al atomen. De chemische verschuivingen van het octaëdrische Al varieerden ook afhankelijk van de belading van natriumcarbonaat, maar in mindere mate. Regeneratie van de katalysator werd uitgevoerd in lucht bij 600$^o$C en het geregenereerde materiaal vertoonde lagere activiteit naar deoxygenatie in vergelijking met de ongebruikte katalysator. De aluminadrager werd nauwelijks aangetast tijdens de regeneratie terwijl er een verandering is in het gehydrateerde deeltje en deze verandering is vermoedelijk verantwoordelijk voor de deactivering van de katalysator.

In **Hoofdstuk 6** werd de conversie van componenten in bio-olie afkomstig van lignine over katalysatoren bestudeerd door vanillylalcohol als modelcomponent te gebruiken. Er werd aangetoond dat dit modelcomponent opeenvolgende reacties ondergaat waarbij methoxyfenolen, fenolen en uiteindelijk koolwaterstoffen met een toenemende mate van deoxygenatie worden gevormd. Er werd aangetoond dat de mate van deoxygenatie van vanillylalcohol toeneemt met de toename van het aantal zuurgebieden in katalysatoren. γ-$Al_2O_3$ materiaal met het hoogste aantal zuurgebieden resulteerde in de hoogste opbrengst van aromatische koolwaterstoffen, alsmede de hoogste opbrengst van kool en gas in vergelijking tot andere materialen die in deze studie zijn gebruikt. Twee paden die leiden tot de vorming van koolwaterstoffen uit vanillylalcohol werden getoond, namelijk (i) decompositie van vanillylalcohol in kleine koolwaterstoffragmenten en de daaropvolgende aromatisering tot het uiteindelijke product en (ii) directe deoxygenatie van dit modelcomponent over katalysatoren. Cyclische ketonen, fenolderivaten en aromatische koolwaterstoffen werden gedetecteerd in de pyrolyseproducten van vanillylalcohol en biomassa. De concentraties van deze componenten

veranderen in de aanwezigheid van verschillende katalysatoren en de trends van deze veranderingen zijn gelijk voor de pyrolyse van biomassa en van vanillylalcohol. Echter, de mate van verandering is anders, wat het verschil in katalytische efficiëntie naar verschillende biomassacomponenten illustreert.

De hydro-deoxygenatie van bio-olie werd onderzocht in **Hoofdstuk 7**. In **Hoofdstuk 4** werd aangetoond dat katalytische opwaardering in de aanwezigheid van $Na_2CO_3/\gamma\text{-}Al_2O_3$ resulteert in een hogere mate van selectieve de-oxygenatie maar ook tot de vorming van meer schadelijke carbonylgroepen. De studie in **Hoofdstuk 7** werd uitgevoerd om dat probleem op te lossen door gebruikt te maken van de combinatie van katalytische deoxygenatie en hydrogenatie. Er werd aangetoond dat hydro-deoxygenatie met behulp van $Pt\text{-}Na_2CO_3/\gamma\text{-}Al_2O_3$ co-katalysatoren het aantal carbonylgroepen in bio-olie verminderde. Echter, de bulkkwaliteit van bio-olie (*i.e.* zuurstofgehalte, verbrandingswaarde) bleef onveranderd of werd slechter in vergelijking tot de individuele katalysator, *i.e.* $Pt/\gamma\text{-}Al_2O_3$ en $Na_2CO_3/\gamma\text{-}Al_2O_3$. Deze lage katalytische activiteit kan worden toegeschreven aan de interactie tussen de 2 precursors, namelijk hexachloorplatinazuur en natriumcarbonaat, wat vervolgens resulteerde in de agglomeratie van Pt-deeltjes en een lager contactoppervlak van de drager. Het duale-bedsysteem waarin natrium- en platinacomponenten werden gescheiden heeft bewezen een veelbelovende aanpak te zijn. Duale-bedoperatie heeft laten zien onder alle katalysatorsystemen de hoogste mate van de-oxygenatie van bio-olie te bereiken. Dit werd bereikt *via* de verwijdering van schadelijke carbonylgroepen en verbetering van de gewenste koolwaterstoffen, wat leidde tot een verbrandingswaarde die hoger is dan die van traditionele stookolie (42 MJ $kg^{-1}$). n-butaan bezit vergelijkbare prestaties als $H_2$ as waterstofbron voor de hydro-pyrolyse van biomassa, wat nieuwe mogelijkheden biedt voor zuinige waterstofbronnen voor de behandeling van bio-olie (voor *e.g.* aardgas).

# Chapter 1

## Catalytic cracking of biomass feedstock into fossil fuel additives

**Abstract.** Biofuels have gained considerable interest in recent years because of the high crude oil prices, energy security concerns and potential climate change consequences over the utilization of fossil fuel. Pyrolysis can directly produce a liquid fuel precursor from biomass, which can be readily stored or transported. This process can utilize various inedible sources of lignocellulosic biomass, for *e.g.* agricultural residues and waste, and hence does not compete with food production. The liquid fuel precursor, named bio-oil or bio-crude, has the potential to be processed in a refinery plant to generate liquid fuel. However, this bio-oil requires a significant upgrade to become an acceptable feedstock for refinery plants due to its high oxygen content. Coupling of pyrolysis of biomass with upgrade of the formed bio-oil by catalytic de-oxygenation is a promising way to produce sustainable fuels.

## 1.1. Bridging the energy gap- what are our options?

The world's population will rise by more than 30% from 2010 to 2050, exceeding 9 billion people, based on an UN 2010 projection [1]. This rapid growth is placing a tremendous stress on Earth's resources and the natural environment, creating a scarcity of food and water and leading to problems such as deforestation, increased global warming, *etc*. Among those, the fast-growing imbalance between the rate of production and consumption of energy puts us on the edge of the greatest challenge that mankind has ever faced. Current global energy consumption is $4.1 \times 10^{20}$ J annually, which is equivalent to an instantaneous yearly-averaged consumption rate of $15 \times 10^{12}$ W [15 trillion watts, or 15 terawatts (TW)][2]. Projected population and economic growth will more than double this global energy consumption rate by the mid-21$^{st}$ century and more than triple the rate by 2100, even with aggressive conservation efforts. Hence, to contribute significantly to global primary energy supply, a prospective resource has to be capable of providing at least 1-10 TW of power for an extended period of time.

The threat of climate change imposes a second requirement on prospective energy resources: they must produce energy without the emission of additional greenhouse gases. Stabilization of atmospheric $CO_2$ levels at even twice their pre-anthropogenic value will require daunting amounts of carbon-neutral energy by mid-century. The needed levels are in excess of 10 TW, increasing after 2050 to support economic growth for an expanding population.

The three prominent options to meet this demand for carbon-neutral energy are: (i) fossil fuel use in conjunction with carbon sequestration, (ii) nuclear power, and (iii) solar power. The challenge for carbon sequestration is finding secure storage for the 25 billion metric tons of $CO_2$ produced annually on Earth [2]. At atmospheric pressure, this yearly global emission of $CO_2$ would occupy 12,500 km$^3$, equal to the volume of Lake Superior, the 4$^{th}$ biggest lake in the world by water volume. Beyond finding storage volume, carbon sequestration also must prevent leakage. A 1% leak rate would nullify the sequestration effort in a century, far too short a time to have lasting impact on climate change. Although many scientists are optimistic, the success of carbon sequestration on the required scale for sufficiently long times has not yet been demonstrated. $CO_2$ capture is not the only challenge related to the consumption of fossil fuels. In a recent report it is projected that with the current

consumption rate, the proven reserves of oil, natural gas and coal will be depleted in 53, 56 and 109 years, respectively [3]. There are also more positive speculations about the day the last oil drop runs out, but they all agree that these "unproven" reserves mostly exist in such forms, for *e.g.* shale oil, that are extremely expensive to extract or refine [4].

Nuclear power is a second conceptually viable option. Producing 10 TW of nuclear power would require construction of a new one-gigawatt-electric (1-GWe) nuclear fission plant somewhere in the world every other day for the next 50 years [2]. Once that level of deployment was reached, the terrestrial uranium resource base would be exhausted in 10 years. The required fuel would then have to be mined from seawater (requiring processing seawater at a rate equivalent to more than 1,000 Niagara Falls), or else breeder reactor technology would have to be developed and disseminated to countries wishing to meet their additional energy demand in this way.

The third option is to exploit renewable energy sources, of which solar energy is by far the most prominent. United Nations (U.N.) estimates indicate that the remaining global, practically exploitable hydroelectric resource is less than 0.5 TW [5]. The cumulative energy in all the tides and ocean currents in the world amounts to less than 2 TW [6]. The total geothermal energy at the surface of the Earth, integrated over all the land area of the continents, is 12 TW, of which only a small fraction could be practically extracted [6]. The total amount of globally extractable wind power has been estimated by the IPCC and others to be 2-4 TWe [7]. For comparison, the solar constant at the top of the atmosphere is 170,000 TW, of which, on average, 120,000 TW strikes the Earth (the remainder being scattered by the atmosphere and clouds). It is clear that solar energy can be exploited on the needed scale to meet global energy demand in a carbon-neutral fashion without significantly affecting the solar resource.

## 1.2. Sustainable production of biofuels

Sunlight, as shown above, provides by far the largest of all carbon-neutral energy sources. Of the 86PW solar radiation exergy incident on the land and oceans, approximately 10–20PW falls on plants and algae[6]. Converting sunlight to chemical exergy through photosynthesis at about 0.5–1.0% average efficiency, plants and algae have a net productivity of about 90 TW, with 65 TW on land and 25 TW in the ocean. Currently, these are used to

produced 1.5 TW in the form of wood fuel (direct combustion) and 0.15 TW of commercial bio-fuels (biodiesel, ethanol) [6]. Compared those numbers to the net productivity of biomass (90 TW), it can be easily seen that there is still a lot of space to harvest solar energy from this material. We currently exploit this solar resource through two main paths: (i) solar electricity and (ii) solar-derived fuel from biomass, among which the latter shows to be very promising. This is because plant biomass is the only current sustainable source of organic carbon, and biofuels, fuels derived from plant biomass, are the only current sustainable source of liquid fuels [8]. Biofuels generate significantly less greenhouse gas emissions than do fossil fuels and can even be greenhouse gas neutral if efficient methods for biofuels production are developed [9].

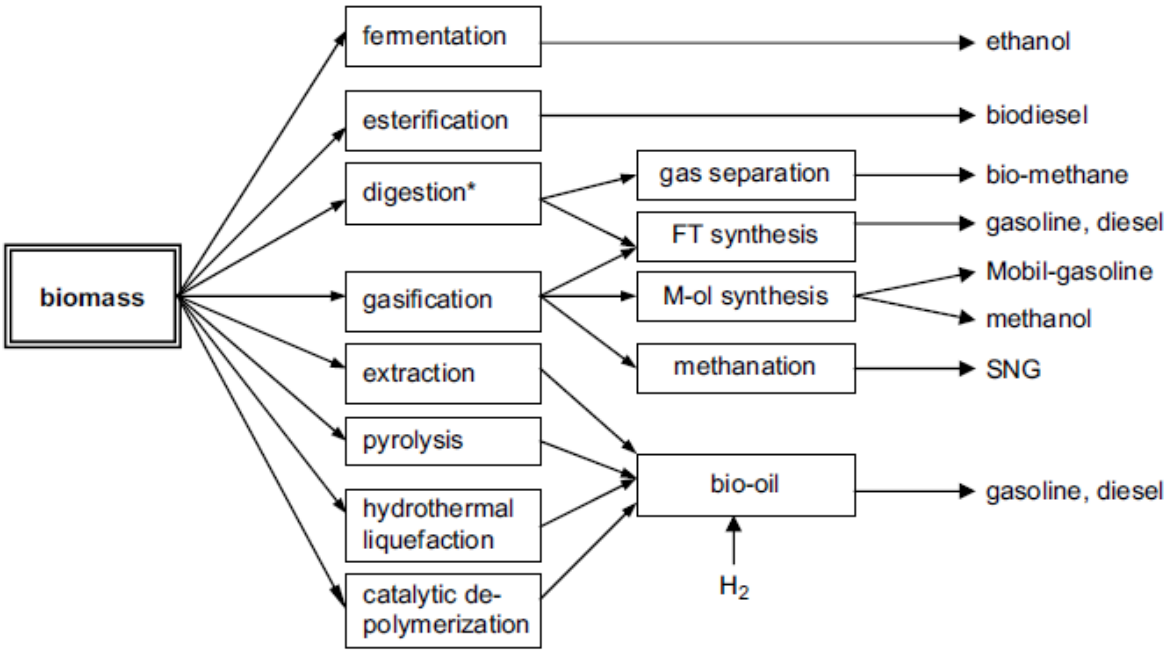


**Figure 1.1:** Main technological routes for the production of fuels from biomass as reported by Mudarov *et al* [10]. *Anaerobic digestion to biogas followed by its reforming to syngas; M-ol – methanol; SNG – substitute NG

Figure 1.1 depicts main technological routes to produce carbon-neutral alternative fuels (gas and liquid) from biomass. For the scope of our study, we are only interested in the generation of liquid fuels. Compared to gas fuels, liquid fuels contain more energy per volume. Moreover, they possess properties similar to conventional fuels and hence less investment and adjustment need to be made regarding the infrastructure and automotive engines. Conversion of biomass into liquid fuels can be classified into 3 main approaches: (i)

using bio/chemical techniques to convert biomass into bio-ethanol and bio-diesel; (ii) indirectly converting biomass feedstock into syngas and subsequent conversion of this product into liquid fuels; and (iii) using thermochemical methods to convert biomass into bio-oil and further upgrade to gasoline or diesel (Figure 1.1).

The first approach, also known as the production of first generation of bio-fuels, is commercially available. Examples are the production of ethanol by fermentation process of corn (US) or sugar cane (Brazil) and the generation of bio-diesel by transesterification of vegetable oils. In fact, bio-ethanol and bio-diesel are the most popular non-petroleum fuels nowadays, accounting for 90% of the biofuel market [11, 12]. However, it was estimated that if all corn and soybeans grown in US will be converted to ethanol and bio-diesel, they would replace only 18% of the gasoline and diesel fuel demand in the country [13]. The opponents of the corn ethanol option argue that it takes over 240 kilograms of corn – enough to feed one person for a whole year – is required to produce the 100 liters of ethanol needed to fill the gas tank of a modern sports utility vehicle [14]. Thus, biomass resource assessment conducted by many researchers implies that without seriously compromising food production, it would be practically impossible to produce enough crop-based fuels to replace the massive quantities of petroleum-based transportation fuels [10].

The second approach is mostly based on the well-established Fischer–Tropsch process. In this process, biomass feedstock is first gasified into syngas, which is in turn converted on a transitional metal-based catalyst to produce liquid hydrocarbons. Less popular is the methanol-to-gasoline (MTG) process developed by ExxonMobil in the 70s. In this process, syngas was converted to methanol and then to liquid hydrocarbons *via* the dimethyl ether intermediate. The advantages of this approach are that all of the biomass is converted into syngas, and these are established technologies. The disadvantage of all of these processes is that they have a low process thermal efficiency (PTE- defined as the energy in the product fuel divided by the energy of the biomass feedstock), typically around 16-50%; thus, a large amount of energy that was previously in the biomass is irreversibly lost in the biomass conversion steps [10]. Gasification of the biomass has a PTE of 75%, which represents the maximum PTE possible from syngas-derived fuels. Adding the energy required to produce and transport the biomass decreases the thermal efficiency even further [10].

The last approach is in fact very similar to the second one in the sense that both of them utilize thermochemical techniques to convert biomass into different intermediates/precursors,

followed by consequent conversion/upgrading of these intermediates/precursors into liquid fuels. However, the desired intermediate in this case is not syngas but a liquid oil, named bio-oil or bio-crude. Liquefaction and pyrolysis are the two major technologies to produce bio-oil [8]. Liquefaction occurs at 50-200 atm and 250-325°C, whereas pyrolysis typically occurs from 1 to 5 atm and 375-600°C [8]. Pyrolysis has a lower capital cost than liquefaction, and many pyrolysis technologies are currently being used commercially. The advantage of bio-oil production is that it requires only a single reactor, and a large fraction of the biomass energy (50-90%) can be converted into a liquid [8].

## 1.3. Bio-oil by fast pyrolysis

Pyrolysis is the thermal decomposition of materials in the absence of oxygen or when significantly less oxygen is present than required for complete combustion [15]. Pyrolysis of biomass, as mentioned previously, has the advantage of directly producing a liquid fuel precursor with lower capital cost than liquefaction and with higher energy efficiency than gasification. During pyrolysis the lignocellulosic structure of biomass disintegrates to smaller molecules due to the applied heat and the three products: solid (char), liquid (bio-oil) and gas are formed.

The general changes that occur during pyrolysis are enumerated as the following [15]: (1) Heat transfer from a heat source, to increase the temperature inside biomass material; (2) The initiation of primary pyrolysis reactions at this higher temperature releases volatiles and forms char; (3) The flow of hot volatiles toward cooler solids results in heat transfer between hot volatiles and cooler unpyrolyzed biomass; (4) Condensation of some of the volatiles in the cooler parts of biomass material, followed by secondary reactions, can produce tar; (5) Autocatalytic secondary pyrolysis reactions proceed while primary pyrolytic reactions (item 2, above) simultaneously occur in competition; and (6) Further thermal decomposition, reforming, water gas shift reactions, radicals recombination, and dehydrations can also occur, which are a function of the process's residence time/temperature/pressure profile. The residence time, heating rate, and temperature are the process parameters that determine the yield of gas, liquid and solid products in biomass pyrolysis (Table 1.1).

It can be seen that fast pyrolysis with short residence times (less than 2s), fast heating rates (up to $10^4$ $^oC$ $s^{-1}$), and moderate temperatures (≈ 550 $^oC$) favours liquid products (bio-oil). Generally fast pyrolysis processes produce 60-75 wt % of liquid bio-oil, 15-25 wt % of solid char, and 10-20 wt % of non-condensable gases, depending on the feedstock used [15].

**Table 1.1** Biomass pyrolysis technologies, reaction conditions, and products [15]

| Name | Residence time | Temperature ($^oC$) | Heating rate | Major products |
|---|---|---|---|---|
| conventional carbonization | hours-days | 300-500 | very low | char |
| pressurized carbonization | 15 min-2 h | 450 | medium | char |
| conventional pyrolysis | hours | 400-600 | low | char, liquids, gases |
| conventional pyrolysis | 5-30 min | 700-900 | medium | char, gases |
| fast pyrolysis | 0.1-2 s | 400-650 | high | liquids |
| fast pyrolysis | <1 s | 650-900 | high | liquids, gases |
| flash pyrolysis | <1 s | 1000-3000 | very high | gases |
| vacuum pyrolysis | 2-30 s | 350-450 | medium | liquids |
| pressurized hydro-pyrolysis | <10 s | <500 | high | liquids |

One option for the production of sustainable fuels is to use biomass-derived feedstocks/fuel precursors in existing petroleum refinery plants. Petroleum refineries are already built and use of this existing infrastructure for the production of biofuels therefore requires little capital investment [16].

The basic conceptual scheme of the biomass pyrolysis coupled with fuels production is shown in Figure 1.2. In the proposed scheme, solid heat carrier (sand) and catalyst transport char to a regenerator where it is combusted and catalyst regenerated. Heat from regenerator is integrated to the endothermic pyrolysis process similar to FCC scheme in a refinery.

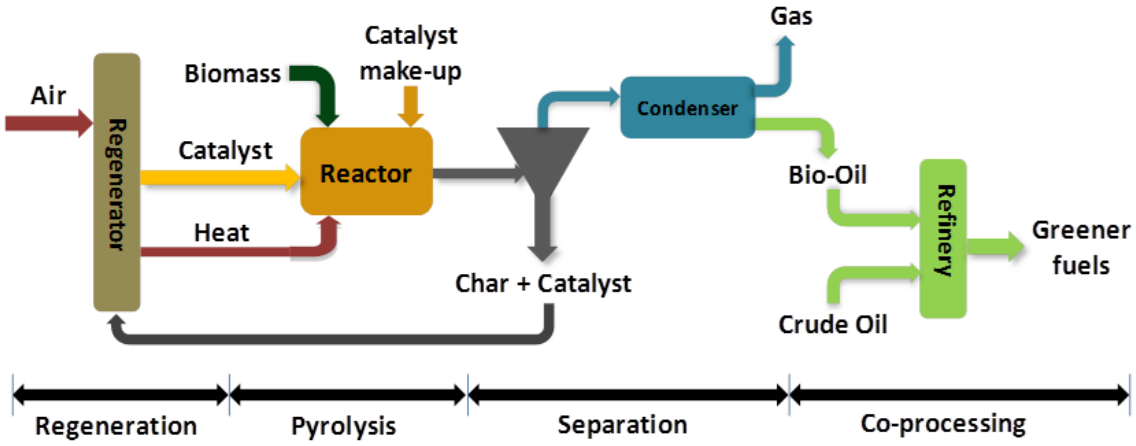


**Figure 1.2:** Conceptual scheme for green fuels from lignocellulosic biomass [16]

## 1.4. Properties of bio-oil- Problems identification

The liquid product formed during pyrolysis is commonly referred to as bio-oils. The multicomponent mixtures are derived primarily from depolymerization and fragmentation reactions of the three key building blocks of lignocellulose: cellulose, hemicellulose, and lignin. Thus, the chemical composition of bio-oil reflects the reactions which those three components have undergone during pyrolysis (Figure 1.3). Milne *et al.*[17] have summarized the chemical composition of bio-oils and the ranges these compositions may vary indifferent cases, which were shown in Figure 1.3. Milne's analysis is consistent with a more recent study by Branca *et al.* [18]. More than 400 organic compounds have been found in bio-oils. The concentrations of compounds in the bio-oil can vary by more than an order of magnitude. Among the listed compounds, phenols, guaiacols and syringols are formed from the lignin fraction, whereas the miscellaneous oxygenates, sugars, and furans form from the cellulose and hemicellulose biomass fraction. The esters, acids, alcohols, ketones, and aldehydes probably form from decomposition of the miscellaneous oxygenates, sugars, and furans [8]. However, complete chemical characterization of bio-oils is almost impossible mainly due to the presence of complex phenolic species from lignin decomposition, which can have molecular weights as high as 5000 g $mol^{-1}$. These species, also known as pyrolytic lignin, can make up up to 25 wt.% of bio-oil [15].

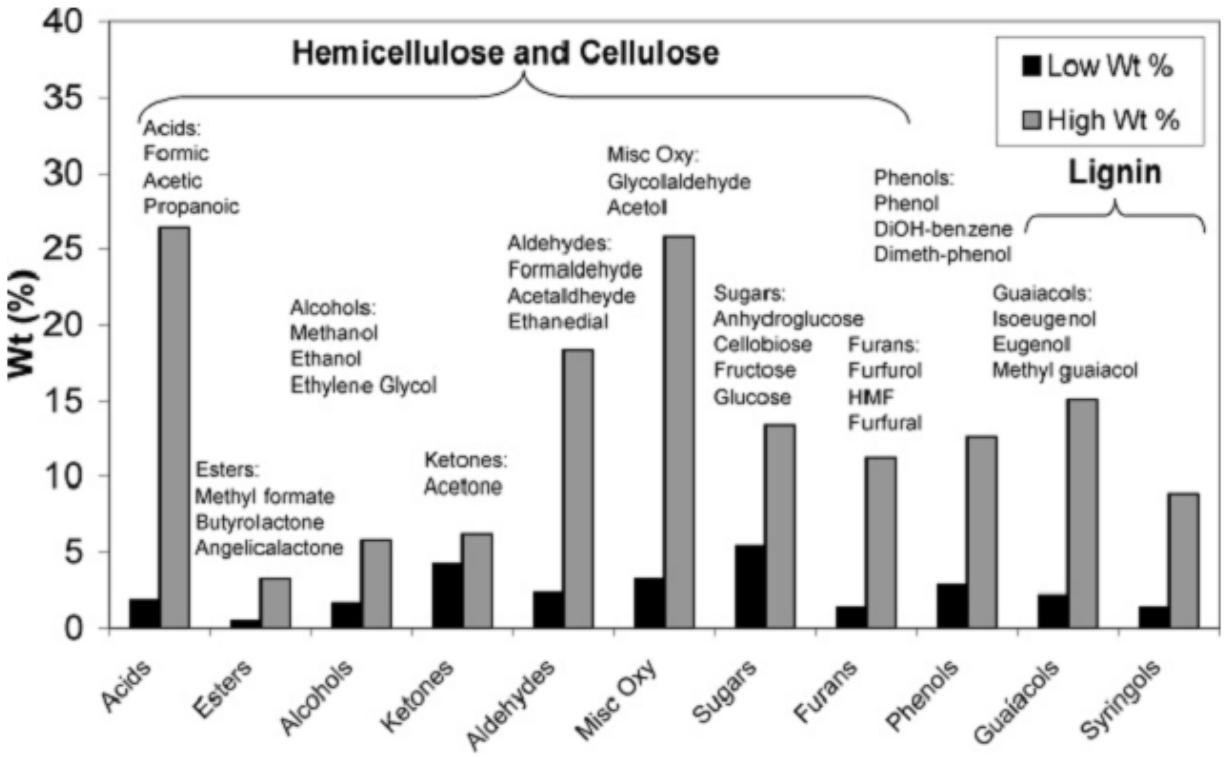


**Figure 1.3:** Chemical composition of bio-oils according to Milne *et al.* [17].The graph also shows the most abundant molecules of each of the components and the biomass fraction from which the components were derived. The concentration of a certain group of compounds in bio-oil can fluctuate between the low wt.% and high wt.%

As can be seen in Figure 1.3, most of the chemical compounds detectable in bio-oil contain oxygen. Proximate analysis of the bio-oil from wood pyrolysis gives a chemical formula of $CH_{1.4}O_{0.6}$, which corresponds to 40 wt % oxygen (similar to that in biomass). This high oxygen content in turn results in detrimental properties which prevent the application of bio-oil as a fuel. The important properties of bio-oil are compared to those of heavy fuel oil and summarized in Table 1.2. It can be seen that compared to fuel oil, bio-oil contains much more oxygen (42% compared to 1% in fuel oil). This directly results in a lower heating value of 19 $MJ.kg^{-1}$, about half of that of fuel oil. Carboxylic acids with possible concentration as high as 25 wt.% (Figure 1.3) makes bio-oil corrosive (pH = 2.6) and hence can be detrimental to various metal equipments during transporting and processing this liquid. Instability under storage is another negative property of bio-oil.

**Table 1.2** Typical properties of bio-oil and fuel oil

| Charateristic | Bio-oil | Fuel oil |
|---|---|---|
| water content (wt.%) | 34 | 0.1 |
| C (wt.%, dry) | 52 | 85.3 |
| H (wt.%, dry) | 5.7 | 11.5 |
| O (wt.%, dry) | 42 | 1 |
| HHV ($MJ.kg^{-1}$) | 19 | 40 |
| pH | 2.6 | 5.7 |

Diebold [19] has written a review on the chemical and physical mechanisms of the storage stability of fast pyrolysis bio-oils and concluded that the instable nature of bio-oil coming from various reactions, for *e.g.* condensation, which involve aldehydes, acids and alcohols. Other significant problems are incompatibility with conventional fuels, high viscosity and poor volatility [8]. All of those mention problems results from the presence of oxygenates in bio-oil. The removal of oxygen is thus necessary to convert bio-oil into a fuel which is universally accepted and economically attractive. De-oxygenation options for bio-oil will be discussed in the next section.

## 1.5. De-oxygenation of bio-oil

Methods for rejecting oxygen from biomass mainly include catalytic de-oxygenation [ref] and hydrogenation/hydro-dexygenation [16].

### *1.5.1. Hydrogenation/Hydro-deoxygenation*

Hydro-deoxygenation of bio-oils involves treating bio-oils at moderate temperatures (100-400 °C) with high-pressure $H_2$ in the presence of heterogeneous catalysts. Reviews on hydro-deoxygenation have been written by Furmisky [20] and Elliott *et al* [21]. Most hydro-deoxygenation work has focused on sulfided CoMo and NiMo-based catalysts, which are industrial hydrotreating catalysts for removal of sulfur, nitrogen, and oxygen from petrochemical feedstocks. $Pt/SiO_2$-$Al_2O_3$ [22], vanadium nitride [23], and Ru have also been used for hydro-deoxygenation. During hydro-deoxygenation, the oxygen in the bio-oil reacts with $H_2$ to form water and saturated C-C bonds. It is desirable to avoid hydrogenation of aromatics in the bio-oils, since this would decrease the octane number and increase $H_2$ consumption. Elliott and co-workers [21, 24, 25] developed a two-step hydrotreating process

for upgrading of bio-oils derived from pyrolysis, of which the results are summarized in Table 1.3.

**Table 1.3** Properties of bio-oil produced from pyrolysis, liquefaction and upgraded bio-oils

| Characteristic | High pressure liquefaction | Fast pyrolysis | Hydro-deoxygenated bio-oils |
|---|---|---|---|
| elemental analysis | | | |
| C (wt.%) | 72.6 | 43.5 | 85.3-89.2 |
| H (wt.%) | 8.0 | 7.3 | 10.5-14.1 |
| O (wt.%) | 16.3 | 49.2 | 0.0-0.7 |
| S (wt.%) | <45 | 29.0 | 0.005 |
| H/C molar | 1.21 | 1.23 | 1.40-1.97 |
| density (g/ml) | 1.15 | 24.8 | 0.796-0.926 |
| water content (wt.%) | 5.1 | 24.8 | 0.001-0.008 |
| HHV (MJ $kg^{-1}$) | 35.7 | 22.6 | 42.3-45.3 |
| viscosity (cP) | 15000 (61 $^{o}$C) | 59 (40 $^{o}$C) | 1.0-4.6 (23 $^{o}$C) |
| aromatic/aliphatic carbon | | | 38/62-22/78 |
| RON | | | 77 |
| distilation range (wt.%) | | | |
| IBP- 225 $^{o}$C | 8 | 44 | 97-36 |
| 225-350 $^{o}$C | 32 | coked | 0-41 |

It can be seen that the hydro-treated bio-oil has become much better in terms of fuel-compatibility compared to the other two oils. Its oxygen content decreased to almost zero while its energy content was boosted up to the level of diesel (45 MJ $kg^{-1}$). Other properties were also improved to the level of an acceptable fuel. In order to achive this, the bio-oil has undergone through 2 upgrading steps. The first step involves a low temperature (270 °C, 136 atm) catalytic treatment that hydrogenates the thermally unstable bio-oil compounds, which would otherwise thermally de-compose forming coke and plugging the reactor. The second step involves catalytic hydrogenation at higher temperature (400 °C, 136 atm). The same catalyst, a sulfided Co-Mo/$Al_2O_3$ or sulfided Ni-Mo/$Al_2O_3$, is used for both steps. This process can produce yield of 40 wt.% of refined oil, which contains less than 1 wt % oxygen. During this process, 20-30% of the carbon in the bio-oil is converted into gas-phase carbon, decreasing the overall yield. Catalyst stability and gum formation in the transporting lines were identified as major process uncertainties. As can be seen in Table 1.3, upgraded bio-oils have a research octane number (RON) of 77, and an aromatic/aliphatic carbon ratio of 38/62-

22/78. The octane number is lower than gasoline, and while aromatics do have a higher octane number they cause air pollution problems.

### *1.5.2. Catalytic de-oxygenation*

Many of the research in the field of catalytic de-oxygenation were carried out using zeolite catalysts. Zeolites contain active sites, usually acid sites, which can be generated in the zeolite framework. The strength and concentration of the active sites can be tailored for particular applications. Temperatures of 350-500 °C, atmospheric pressure and gas hourly space velocities of around 2 are used for zeolite upgrade [8]. During the upgrading process a number of reactions occur including dehydration, cracking, polymerization, de-oxygenation, and aromatization. The advantages of using zeolite catalysts or catalytic de-oxygenation in general are that no expensive $H_2$ is required, atmospheric processing reduces operating cost, and the temperatures are similar to those for bio-oil production. According to Bridgwater, this offers significant processing and economic advantages over hydrotreating [26]. Among the tested zeolites, H-MFI and H-FAU show to selectively enhance the formation of aromatic hydrocarbons from bio-oil. It was also reported that high yields of coke together with the formation of carcinogenic hydrocarbons are major problems [26].

The transformation of model bio-oil compounds, including alcohols, phenols, aldehydes, ketones, acids, and mixtures, have been studied over H-MFI catalysts by several authors [27-29]. It was reported that alcohols were converted first into olefins at temperatures around 200°C, then to higher olefins at 250°C, followed by paraffins and a small proportion of aromatics at 350°C. Phenol has a low reactivity on H-MFI and only produces small amounts of propylene and butanes. 2-Methoxyphenol also has a low reactivity to hydrocarbons and thermally decomposes generating coke. Acetaldehyde had a low reactivity on this catalyst, and it also underwent thermal decomposition leading to coking problems. Acetone, which is less reactive than alcohols, first is dehydrated to iso-butene at 250°C and then converts into $C_{5+}$ olefins at temperatures above 350°C. These olefins are then converted into $C_{5+}$ paraffins, aromatics, and light alkenes. Acetic acid is first converted to acetone, and consequently to other products as mentioned previously. Products from zeolite upgrading of acetic acid and acetone had considerably more coke than did products from alcohol feedstocks. Thus, different molecules in the bio-oils have a significant difference in reactivity

and coke formation rates. Gayubo *et al.* [29] recommended that the oil fractions that lead to thermal coking (such as aldehydes, oxyphenols, and furfurals) be removed from the bio-oil prior to zeolite upgrading.

### *1.5.3. Requirements of catalytic de-oxygenation*

Catalytic de-oxygenation is a promising route to upgrade bio-oil since it does not require use of other chemicals, for *e.g.*, alternative HDO process requires hydrogen, which is expensive and not easily available. The oxygen from bio-oil can be removed *via* $CO_2$, CO or $H_2O$. Among those $CO_2$ is the most favourable route because: (i) it is possible to remove two oxygen atoms per molecule of $CO_2$ and (ii) this route retains H and thus energy in bio-oil.

It has been shown that bio-oil contains hundreds of different compounds, which can be classified into different groups based on their functionalities. These groups consist of carboxylic acids, aldehydes/ketones, phenol derivatives, furan derivatives, hydrocarbons, among which:

(1) Furan derivatives and aliphatic hydrocarbons are of low (or zero) oxygen content and high energy content and thus the desirable products.

(2) Carboxylic acids cause bio-oils to be corrosive, aldehydes/ketones are the unstability precursors [19]. They also contains high amount of oxygen and thus the unwanted products.

(3) Phenol derivatives are milder in terms of acidity/basicity compared to carboxylic acids. Aromatic hydrocarbons are potentially carcinogenic agents. However, they both are of high energy content and high value and thus are allowed to present in small amount in bio-oils or can be sold separately as specialty chemicals.

For these reasons, to be efficient de-oxygenation of bio-oil should aim at: (i) oxygen removal as $CO_2$ and (ii) remove harmful oxygenates while retaining other oxygenates which have higher energy content. Catalyst design should attempt to optimise such selective de-oxygenation.

## 1.6. Scope and outline of the thesis

The main goal of this thesis is to develop an efficient catalyst for the de-oxygenation of biomass-derived fast pyrolysis oil (bio-oil) into fuel precursors, which can be co-processed with crude in green refineries. Part of this study also dedicates to gain insights about the active specie in the catalyst and investigate the possibilities to further improve quality of the precursor *via in situ* hydro-pyrolysis. Conversion of a model compound of lignin over different catalysts was also studied for a better understanding of the behaviour of this biomass component during catalytic pyrolysis.

Several zeolite materials, for *e.g.* H-MFI and H-FAU were known to enhance the hydrocarbon content of bio-oil and hence make it more promising as a fuel precursor. **Chapter 3** investigated the influences of H-FAU catalyst and its Na-exchanged materials in the upgrade of bio-oil. H-FAU was chosen because it has lower acidity and slightly bigger pores compared to H-MFI, which prevent severe cracking and allow the access of bigger biomass polymers to the catalytic sites. The effect of introducing $Na^+$ ions to the faujasite matrix was also studied. **Chapter 4** further investigates the activity of sodium-based materials by studying the conversion of bio-oil over $Na_2CO_3$ supported on γ-$Al_2O_3$ catalyst. This catalyst shows to be extremely efficient in de-oxygenation of bio-oil and was chosen for further study. **Chapter 5** dedicates to study the synergy between the two components of the $Na_2CO_3$/γ-$Al_2O_3$ catalyst and the consequence of the synergy to its catalytic performance. The nature of the catalytically active specie in this material was studied using TGA-MS and NMR techniques. A study about the regenerability of this catalyst was also carried out. Conversion of vanillyl alcohol as a model compound for lignin over different catalysts was studied in **Chapter 6,** aiming to elucidate the chemistry of C-C and C-O bonds cleavage over the materials. **Chapter 7** investigated the *in situ* hydro-pyrolysis of bio-oil over Pt and $Na_2CO_3$/γ-$Al_2O_3$ materials, either as a co-catalyst (single bed mode) or as two separated catalysts (dual bed mode). In this chapter the possibility to replace $H_2$ by n-butane, as a hydrogen source was also investigated. The conclusions and future outlook of this study were discussed in **Chapter 8**.

## References

[1] World population prospects: the 2012 revision, United Nations, 2012.
[2] Basic research needs for solar energy utilization, U.S. Department of energy, 2005.
[3] Statistical review of world energy, British Petroleum, 2013.

[4] J. Kjärstad, F. Johnsson, Energy Policy 37 (2009) 441-464.
[5] The 2010 energy statistics yearbook, United Nations, 2010.
[6] W.A. Hermann, Energy 31 (2006) 1685-1702.
[7] Climate change 2007: Working Group III: Mitigation of climate change, Intergorvemental panel on climate change, 2007.
[8] G.W. Huber, S. Iborra, A. Corma, Chemical Reviews 106 (2006) 4044-4098.
[9] C. Whittaker, M.C. McManus, G.P. Hammond, Energy Policy 39 (2011) 5950-5960.
[10] N.Z. Muradov, T.N. Veziroğlu, International Journal of Hydrogen Energy 33 (2008) 6804-6839.
[11] International energy outlook 2011, U.S. Energy Information Administration, 2011.
[12] A.K. Agarwal, Progress in Energy and Combustion Science 33 (2007) 233-271.
[13] J. Hill, E. Nelson, D. Tilman, S. Polasky, D. Tiffany, Proceedings of the National Academy of Sciences 103 (2006) 11206-11210.
[14] World development report 2008: Agriculture for development, World Bank, 2008.
[15] D. Mohan, C.U. Pittman, P.H. Steele, Energy & Fuels 20 (2006) 848-889.
[16] T.S. Nguyen, M. Zabeti, L. Lefferts, G. Brem, K. Seshan, Biomass and Bioenergy 48 (2013) 100-110.
[17] T. Milne, F. Agblevor, M. Davis, S. Deutch, D. Johnson, in: A.V. Bridgwater, D.G.B. Boocock (Eds.), Developments in Thermochemical Biomass Conversion, Springer Netherlands, 1997, pp. 409-424.
[18] C. Branca, P. Giudicianni, C. Di Blasi, Industrial & Engineering Chemistry Research 42 (2003) 3190-3202.
[19] J.P. Diebold, A review of the chemical and physical mechanisms of the storage stability of fast pyrolysis bio-oils, National Renewable Energy Laboratory, 2000.
[20] E. Furimsky, Applied Catalysis A: General 199 (2000) 147-190.
[21] D.C. Elliott, D. Beckman, A.V. Bridgwater, J.P. Diebold, S.B. Gevert, Y. Solantausta, Energy & Fuels 5 (1991) 399-410.
[22] Y.-H.E. Sheu, R.G. Anthony, E.J. Soltes, Fuel Processing Technology 19 (1988) 31-50.
[23] S. Ramanathan, S.T. Oyama, The Journal of Physical Chemistry 99 (1995) 16365-16372.
[24] D.C. Elliott, E.G. Baker, J. Piskorz, D.S. Scott, Y. Solantausta, Energy & Fuels 2 (1988) 234-235.
[25] D.C. Elliott, A. Oasmaa, Energy & Fuels 5 (1991) 102-109.
[26] A.V. Bridgwater, Applied Catalysis A: General 116 (1994) 5-47.
[27] A.G. Gayubo, A.T. Aguayo, A. Atutxa, R. Aguado, J. Bilbao, Industrial & Engineering Chemistry Research 43 (2004) 2610-2618.
[28] A.G. Gayubo, A.T. Aguayo, A. Atutxa, R. Aguado, M. Olazar, J. Bilbao, Industrial & Engineering Chemistry Research 43 (2004) 2619-2626.
[29] A.G. Gayubo, A.T. Aguayo, A. Atutxa, B. Valle, J. Bilbao, Journal of Chemical Technology & Biotechnology 80 (2005) 1244-1251.

# Chapter 2

## Experimental

**Abstract.** For this study an IR fast pyrolysis system was assembled and is described in this chapter. The methods used for catalyst and biomass sample preparation are mentioned. Details of catalyst characterization and analyses of products are discussed.

## 2.1. Fast pyrolysis set-up and experiment

The experimental set-up used in this study is shown schematically in Figure 2.1. The tubular quartz reactor consists of two compartments: the biomass bed and the catalyst bed, of which the inner diameter/length are 10/350 mm and 7/250 mm, respectively. In all experiments, 2 g of biomass sample was packed inside the biomass compartment. Before each experiment, the whole system was purged by a flow of 100 mL $min^{-1}$ of Ar for 30 min to guarantee an inert atmosphere during the pyrolysis. After the flushing period, the flow of Ar was reduced to 70 mL $min^{-1}$ and kept constant during experiments. For hydro-pyrolysis experiments discussed in Chapter 7, Ar flow was replaced with the flow of either (i) 35 vol.% $H_2$ in Ar or (ii) 100 vol.% n-butane.

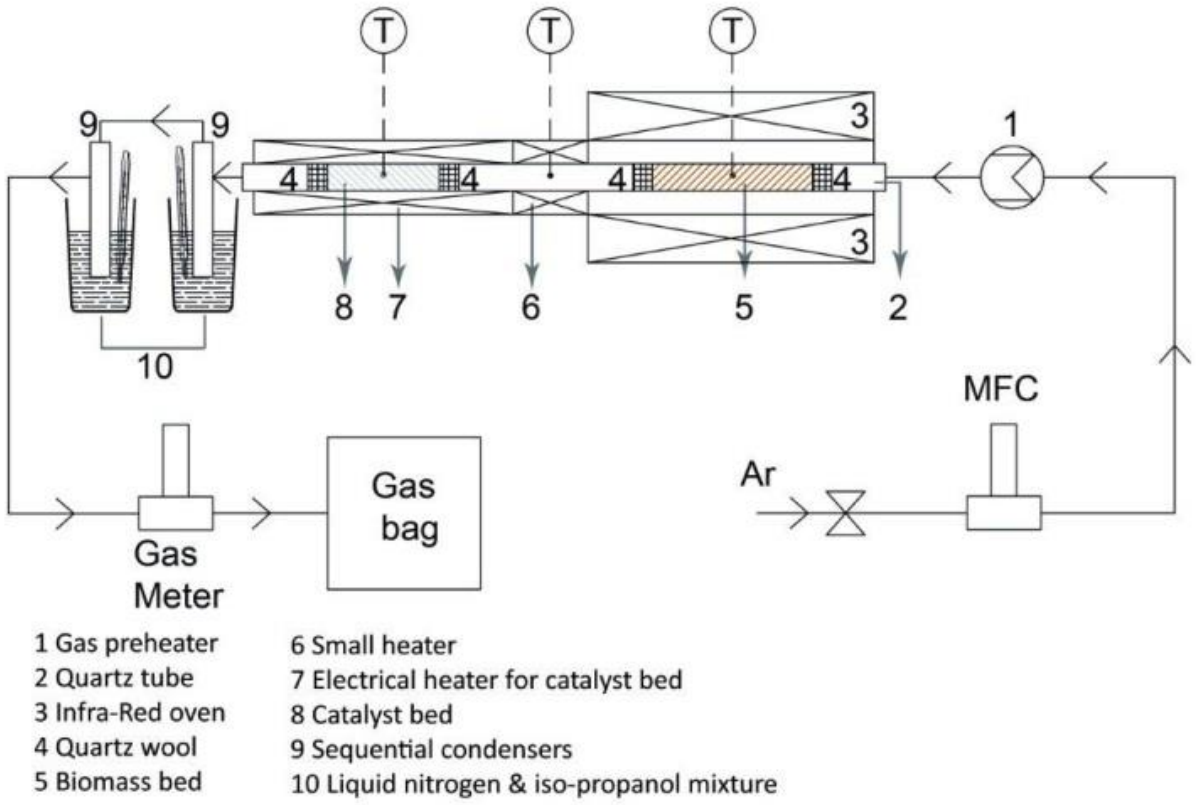


**Figure 2.1.** Schematic drawing of the fast pyrolysis experimental set-up

In Chapter 3, a low catalyst/biomass mass ratio of 0.1 was used, *i.e.* 2 g biomass and 0.2 g catalyst. This is to prevent coking and dehydration on the acid sites of catalyst, which result

in low yield of bio-oil. In this chapter, experiments were conducted in one of the two modes: mixing mode or post-treatment mode:

(1) In mixing mode, the biomass and catalyst were mixed and packed in the same compartment #5 (biomass bed). In this mode, the electrical furnace #7 was not used. Biomass-catalyst mixture was heated to the desired temperature using the IR furnace #3. Using the IR furnace, it is possible to raise the temperature to 500 $^{o}$C in less than 10 s.

(2) In the post-treatment mode, the biomass and catalyst were kept in compartment #5 and #8 (biomass and catalyst bed), respectively. In this experiment, catalyst in position #8, was brought to the required temperature by a separate electric furnace and maintained there. Pyrolysis experiment begins by activating the IR furnace and the vapours formed in compartment #5 travel through the catalyst bed.

For the rest of the study (Chapter 4-7), only the post-treatment mode was employed since it provides a better catalyst- pyrolysis vapour contact. In hydrogenation experiments shown in Chapter 6, an extra hydrogenation catalyst was employed. In this type of operation, named dual-bed system, the 2 catalysts were packed into 2 consecutive beds separated by quartz wool. The vapour evolved from biomass pyrolysis is pushed by the Ar flow into the first catalyst bed, where it is deoxygenated and later to the second bed where hydrogenation occurs. For the studies in Chapter 4-6, a catalyst/biomass mass ratio of 0.5 was used. For the dual-bed operation in Chapter 6, the total catalyst/biomass mass ratio is 1 (0.5 of each catalyst). For the model compound study in Chapter 7, the catalyst/model compound mass ratio was set at 1. Temperature was measured at points marked T in the figure using thermocouples. All biomass pyrolysis and catalytic upgrade of pyrolysis vapour were conducted at atmospheric pressure at 500$^{o}$C. The average temperature ramp applied to the biomass material during pyrolysis was 40 $^{o}$C.sec$^{-1}$. The mean vapour residence time inside the quartz reactor was 4 s, which was calculated based on the Ar flow rate.

Products of pyrolysis reactions were pushed by the Ar flow into two consecutive condensers immersed in isopropanol/liquid nitrogen mixture, at - 40 $^{o}$C to make sure that only non-condensable gases escaped for collection in a gas bag. Duration of experiments was set at 10 min to ensure collection of all products. This should not be mistaken with the pyrolysis reaction time (in the order of a few seconds). In Chapter 3-6 the mass balance was calculated as follows: The weight of the liquid products was considered equal to the gain in the weight

of the two condensers after experiments. The change in the weight of the quartz reactor before and after pyrolysis is equal to the amount of volatiles which has left the reactor during this process (weight of liquid + weight of gas). By applying the mass conservation law (weight of biomass = weight of solid + weight of liquid + weight of gas), it is possible to calculate the amount of solid products. Non-condensable gases collected in the gas bag were injected to a micro GC (using PPQ and MS 5A columns) to analyse the composition (based on volume fraction). The total volume of gas which flows to the bag was measured using a gas flow meter (Figure 2.1). This, together with composition analysed by the micro GC, provide the exact volume of each gas in the mixture. The ideal gas law was employed to calculate the molar amount of each gas and close the mass balance. In the model compound work shown in Chapter 7, there is no char formed and thus the solid yield is equal to the coke yield, which is determined by TGA experiment in air. The liquid yield is by the change in the weight of the 2 condensers. The gas yield is determined by difference, assuming that the yields of solid, liquid and gas make up to 100%.

## 2.2. Material preparation

### *2.2.1. Biomass*

Woodchips from the Canadian white pine (ThoroughBed ™, Long Beach Shavings Co.) were used as the feedstock in this study. Details of this material are given in Table 2.1.

**Table 2.1.** Main characteristics of the Canadian pine wood

| **Proximate analysis (mass fraction %)** | | | | | **Ultimate analysis (mass fraction %)** | | | |
|---|---|---|---|---|---|---|---|---|
| **Fixed carbon** | **Volatile** | **Ash** | **Moisture** | **HHV* (MJ kg$^{-1}$)** | **C** | **H** | **O**** | **N** |
| 14.5 | 78.4 | 2.6 | 4.5 | 16.1 | 48.3 | 5.8 | 45.4 | 0.5 |

*higher heating value **by difference

Prior to all experiments, the chips were ground by milling and sieved to particle sizes of 0.3-0.6 mm.

### *2.2.2. Catalyst*

Faujasite catalysts were obtained from Zeolyst (Na-FAU, $Na_{0.2}H_{0.8}$-FAU) and Albemarle (H-FAU). $Na_2CO_3$/ γ-$Al_2O_3$, Pt/ γ-$Al_2O_3$ and Pt-$Na_2CO_3$/ γ-$Al_2O_3$ catalysts were prepared by wet impregnation. The support γ-$Al_2O_3$ (Akzo Nobel) were prepared by crushing the extrudes and sieved to particle sizes of 0.3-0.6mm. The precursors are: $Na_2CO_3$ (ACS reagent grade >99.5%) from Sigma-Aldrich and $H_2PtCl_6.6H_2O$ (analytical grade >99.9%) from Alfa Aesar. The preparation steps are the following: The desired amount of a precursor was completely dissolved in $H_2O$ and later added to the support ($H_2O$/support = 5 w/w). The obtained slurry was mixed for 2 hours and then dried in a rotavap at 100°C under vacuum. The materials were finally calcined at 550°C for 10 hours under 200mL.min$^{-1}$ air flow. The catalyst Pt-$Na_2CO_3$/ γ-$Al_2O_3$ was prepared using co- and sequential-impregnation. In co-impregnation method, $Na_2CO_3$ and $H_2PtCl_6.6H_2O$ were dissolved in $H_2O$ at the same time before being added to the support. In sequential impregnation, $H_2PtCl_6.6H_2O$ was dissolved in $H_2O$ and added to the $Na_2CO_3$/ γ-$Al_2O_3$ catalyst, which was prepared in advance.

After calcination the catalysts were pelletized and sieved to particle sizes of 0.3-0.6 mm. Before each catalytic experiment, the catalysts were dried at 500°C for 60 min under Ar flow. This allows removal of free water presented, and hence, a better estimation of the mass balance of the experiments. For hydrogenation experiments using Pt-based catalysts, this step was carried out under $H_2$ flow to: (i) reduce Pt species to Pt metal and (ii) remove any residual Cl from the precursor.

## 2.3. Catalyst characterization and products analysis

### *2.3.1. Catalyst characterization*

The following techniques were used to characterize the catalysts:

**BET analysis:** Surface areas of catalysts were measured using ASAP 2400 Micromeritics equipment and later calculated based on BET theory. The analysis also gives information about the pore size distribution of the catalysts.

**TEM imaging:** TEM images were taken on a JEOL 2010F, equipped with EDX for elemental mapping.

**SEM imaging:** SEM images were taken on a Zeiss 1550 HR-SEM, equipped with EDX for elemental mapping.

**XRF analysis:** The loading of metal (Pt and Na) on the catalysts was determined using a Philips XRF spectrometer PW 1480.

**XRD analysis:** X-Ray diffractometer was recorded over the range $2\theta = 20\text{-}90^{o}$ on a Bruker D2 Phaser XRD device using Cu Kα1 radiation source.

**CO chemisorption:** Pt dispersion was measure by CO chemisorption on a Micromeritics Chemisorpt 2750 device. The dispersion was calculated based on the assumption that the stoichiometric ratio of the chemisorption between CO and Pt equals to 1:1. Before pulsing, the catalyst was reduced in $H_2$ at 400$^{o}$C for 1 h and then let to cool down to RT.

**TGA-MS:** The thermal decomposition of Na species (RT-1000$^{o}$C) in the catalysts was monitored using a Mettler Toledo TGA/SDTA851e device in 50 mL.min$^{-1}$ Ar flow and with a temperature ramp of 10$^{o}$C.min$^{-1}$. The amount of coke formed on catalysts was measure using the same equipment by heating the spent catalyst from RT-800$^{o}$C in in 50 mL.min$^{-1}$ air flow and with a temperature ramp of 10$^{o}$C.min$^{-1}$. The gaseous species evolved in those experiments was detected by a MS.

**NMR analysis:** All the magic angle spinning (MAS) solid state NMR (SSNMR) measurements were measured at Bruker AV-I 750MHz spectrometer with 17.6 Tesla magnetic field. In this field $^{27}$Al, $^{23}$Na and $^{1}$H resonate at 195.46, 198.41 and 750.13 MHz respectively. Standard 4 mm triple resonance MAS probe was used. All the samples were packed in 4mm zirconium rotor's and were spun at magic angle (54.74) at various spinning speeds. For $^{27}$Al MAS spectra, chemical shifts were referenced with respect to liquid $Al(NO_3)_3$ sample. An excitation pulse of 2 μs, corresponding to a $\pi/6$ pulse for $Al(NO_3)_3$ in solution was used with recycling delay of 1 s and total number of scans acquired were 32. Line broadening function of 10Hz and additional baseline correction was used for processing the data. For $^{23}$Na MAS spectra, chemical shifts were referenced with respect to liquid NaCl solution. An excitation pulse of 0.43 μs, corresponding to a $\pi/24$ pulse for NaCl in solution was used with recycling delay of 1 s and 32 scans were acquired. Line broadening function of 30Hz and additional baseline correction was used for processing the data. For $^{1}$H MAS NMR spectra, chemical shits were referenced with TMS. An excitation pulse of 2 μs, corresponding

to a 30 degree pulse was used with a recycle delay of 2 s and 32 scans were acquired. Line broadening of 10Hz and additional baseline correction was applied. All the NMR data were processed in Topspin 3.2 and MestReNova softwares.

### *2.3.2. Product analysis*

**GC analysis:** Gas products were analysed by a Varian Micro GC employing MS 5A and Poraplot Q (PPQ) columns. The temperature of both columns was kept at 70$^{o}$C and Ar was employed as the carrier gas. The run time is 3 min to make sure all the gas products evolve from the columns. MS 5A column was used to separate $H_2$, CO, $CH_4$ and PPQ for $CO_2$ and $C_2$-$C_3$ hydrocarbons separation.

**GC-MS analysis:** Chemical composition of bio-oil was analysed with an Agilant GC-MS, and using NIST database. TIC area percentage of a particular compound/family of compounds in different cases were compared and serve as a semi-quantitative indication of the selectivity of catalysts to that compound/family.

**TAN analysis:** Total acid number (TAN) of bio-oil samples was estimated by titration with 0.1 M KOH following the standard ASTM 664 using the titrator 785 DMP Titrino (Metrohm). In the measurement, the potential of the bio-oil/solvent solution was plotted against the amount of KOH (1 mol.$L^{-1}$) used to titrate. The end point was determined as the point with the highest slope.

**pH measurement:** pH of a bio-oil sample was measured using the titrator 785 DMP Titrino (Metrohm).

**Higher heating value:** The higher heating value of bio-oil was determined by a bomb calorimeter unit (C2000 Kikawerke).

**Water content analysis:** The water content of bio-oil (mass fraction) was determined using Karl Fischer titration (using Metrohm 787KF titrator).

**Gel permeation chromatography:** The weight distribution of bio-oils was analysed in the Agilent 1200 series gel permeation chromatography (GPC) equipped with a refractive index detector.

**Elemental analysis:** A Flash 2000 (Interscience) instrument was employed to analyze the elemental composition (C, H, and O mass fraction) of bio-oil and char. In this analysis, the samples were completely oxidized in $O_2$ and the [C], [H] mass fraction were calculated directly based on the amount of $CO_2$ and $H_2O$ formed, and the [O] mass fraction was obtained by difference.

# Chapter 3

## Catalytic upgrading of biomass pyrolysis vapours over Faujasite zeolite catalysts

*T.S. Nguyen, M. Zabeti, L. Lefferts, G. Brem, K. Seshan, Biomass Bioenery 48 (2013) 100*

**Abstract.** This chapter investigates the influence of Faujasite catalysts to the properties of bio-oil derived from pyrolysis of pinewood. Catalytic upgrading of bio-oil using Na-Faujasite, $Na_{0.2}H_{0.8}$-Faujasite, and H-Faujasite (Na-FAU, $Na_{0.2}H_{0.8}$-FAU, and H-FAU) were carried out in a fixed-bed reactor at 500 $^{o}$C. In the same condition, catalytic upgrading of bio-oil is shown to be superior to *in-situ* catalytic pyrolysis of biomass when it comes to quality of bio-oil. The yields of coke, gas and water increase while that of organic phase decreases proportional with the concentration of protons in catalysts. Compared to the other two catalysts, $Na_{0.2}H_{0.8}$-FAU removes the most oxygen from bio-oil, reduces amount of acids and aldehydes/ketones which result in a higher energy-contained and more stable oil with less corrosive property. However, the biggest contribution to the oxygen removal is *via* the formation of reaction water, which is not an optimum path. This leaves space for future development.

**Chapter 3**

## 3.1. Introduction

As discussed in Chapter 1, pyrolysis is a promising technique to convert biomass feeds into a valuable fuel precursor (bio-oil). This precursor can be processed together with crude in a traditional refinery plan to generate transportation fuels. However the biggest technical challenge for such a green refinery is the high oxygen content of the precursor, which leads to several detrimental properties [1]. Catalytic de-oxygenation is an economically attractive process to reduce the oxygen level of bio-oil as it does not require use of other chemicals, for *e.g.*, alternative HDO process requires hydrogen, which is expensive and not easily available [2, 3].

In general, de-oxygenation of biomass results in elimination of oxygen as carbon oxides, water and, depending on the extent of oxygen removal, a mixture of oxygen containing organic, aliphatic/aromatic, acids aldehydes, alcohols, *etc*. Complete de-oxygenation (Eq. 1) results in an aromatic hydrocarbon mixture (H/C ~1-1.2) due to the low hydrogen content of the starting biomass (H/C ~1.3) [4].

$$C_6H_8O_4 \rightarrow 4.6CH_{1.2} + 1.4\ CO_2 + 1.2\ H_2O \qquad \text{(Eq. 1)}$$

In the case of complete de-oxygenation (Eq. 1), the organic yield is about 42 % (mass fraction), and this corresponds to 50% energy recovery from the biomass feedstock. Incomplete de-oxygenation, *i.e*, retaining some of the oxygen in the organic fraction, will help enhance the liquid yields, however, this is an option only if the resulting product has properties that are compatible with fossil fuel / fuel additives (see Figure 1.2, Co-processing section).

The influence of H-MFI (ZSM-5) zeolite catalyst on the pyrolysis of biomass based on rice husks in a fixed-bed system has been investigated [5]. It was found that, in the presence of ZSM-5, oxygen in the feedstock was removed mostly as $H_2O$ at lower temperatures (< 500°C) and as $CO/CO_2$ at higher temperatures (> 550°C). At the higher temperatures, the bio-oils obtained from catalytic experiments contain significantly higher amounts of single ring and polycyclic aromatic hydrocarbons (PAH) because of deeper de-oxygenation. The evaluation of different commercial catalyst, including H-MFI, FCC catalysts, transitional metals (Fe/Cr) and aluminas (γ, α) for biomass pyrolysis has been carried out in a fixed bed reactor [6]. It was concluded from this study that H-MFI is a promising catalyst for the selective production of aromatic hydrocarbons while transitional metal catalysts lead to the

selective production of phenol and light phenolics from biomass feedstock. De-oxygenation of glycerol or sorbitol, as model compounds representing bio-oil, has been reported over several catalysts (H-MFI, $\gamma$-$Al_2O_3$, H-FAU (USY), SiC and commercial FCC catalyst) [7] and it was concluded that, at high de-oxygenation levels, achieved with H-FAU (USY) catalyst, aromatic hydrocarbons (fossil fuel compatible) and coke were the major products.

Alkali and alkali earth metals e.g., Na, K, Ca have attracted attention as promising catalysts for upgrading of biomass vapours in recent years [8-11]. This is also because they are naturally present in the biomass. For instance, $Na^+$ found to be effective for the conversion of biomass by improving the bio-oil energy content [12, 13]. In the case of holo-celluloses, degradation is suggested to occur *via* depolymerisation to give compounds such as levoglucosan, or sugars which subsequently undergo ring opening degradation to give aliphatic acids, aldehydes, *etc*. It is suggested that choice of the type of alkali metal, its content and reaction temperature can influence yields of levoglucosan [11]. Levoglucosan can be further converted to aromatic components *via* oxygen removal as $H_2O$ [14]. Role for alkali metals on the decomposition of lignin is less discussed since in general these metals are less active to lignin conversion than to holo-cellulose conversion. The nature of working of alkali cations is not well established [3], but basicity of alkali and alkaline earth metals have been suggested to catalyse de-oxygenation, especially decarboxylation [15, 16].

In this chapter, influence of catalysts on the conversion of lignocellulosic biomass to various organic components is investigated with a view to establishing a catalytic pyrolysis process for a green refinery. Faujasite catalyst, which is the active ingredient in fluid catalytic cracking (FCC) catalyst, was employed because of its price, availability, mechanical/thermal stability, its ability to crack C-C, C-O bonds and regenarability from coke. H-FAU was further modified by $Na^+$ ion exchange to probe role for alkali in pyrolytic de-oxygenation. Advantages of using catalyst over the thermal pyrolysis (in absence of the catalysts) are discussed.

## 3.2. Experimental

### *3.2.1. Catalyst preparation and characterisation*

Faujasite materials: Na-FAU, $Na_{0.2}H_{0.8}$-FAU, and H-FAU were obtained from Zeolyst International and Albemarle and employed as the upgrading catalysts. Basic properties of these materials are shown in Table 3.1.

**Table 3.1.** Basic properties of Faujasite catalysts

| Catalyst | $SiO_2/Al_2O_3$ molar ratio | Nominal cation form | $Na_2O$ (mass fraction %) | Surface area ($m^2\ g^{-1}$) |
|---|---|---|---|---|
| Na-FAU | 5.1 | $Na^+$ | 13 | 900 |
| $Na_{0.2}H_{0.8}$-FAU | 5.1 | $H^+/Na^+$ | 2.8 | 730 |
| H-FAU | 7 | $H^+$ | 0.2 | 650 |

### *3.2.2. Catalytic test*

The pyrolysis and catalytic upgrading set-up, analysis techniques and definitions used in this chapter are described in detail in Chapter 2. In all experiments, 2 g of biomass (Canadian whitepine) and 0.2 g catalyst was packed inside the reactor. The pyrolysis bed was heated to 500 $^oC$ with a temperature ramp of 40 $^oC.sec^{-1}$. The catalyst bed was kept constantly at 500 $^oC$ throughout the experiments. Duration of all experiments was set at 10 min. The flow rate of Ar was 70 $mL.min^{-1}$, which gave an average vapour residence time of 4 sec.

## 3.3. Results and discussion

First, results of thermal pyrolysis experiments in the absence of catalysts are discussed. It is intended to use these results to establish the proper choice of laboratory experiments and determine the possibility to carry out catalytic pyrolysis experiments.

### *3.3.1. Thermal pyrolysis*

Yields of products in the thermal pyrolysis experiments were, based on mass fraction, 20.4 % of fast pyrolysis char, 10.3 % of gas and 61.2% of liquid which adds up to a total mass

balance of 92%. Liquid product contained 36.9% (in mass, based on initial weight of biomass) of organic fraction and 24.3% yield of water. The relatively high liquid yield and low gas and solid yield shows resemblance to those obtained from fast pyrolysis in bigger scale systems [17-20].

Obtained solid char (*i.e.*, excluding minerals/ash), contained carbon (78.7 mass fraction %), hydrogen (2.8 %) and oxygen (18.5%). Energy content of this char was measured to be 26 $MJ.kg^{-1}$. This, combined with the yield of 20.4%, provides more than enough energy (by burning the char in air) to drive the pyrolysis reaction without the necessity of external heat, which makes the whole process autothermal (Figure 1.2) *via* proper heat integration.

Carbon monoxide and carbon dioxide are major components in pyrolysis gas (total >90% selectivity) with yields of 4.66 and 4.75% (mass fraction, compared to biomass), respectively. There are smaller amounts of ($C_1$-$C_3$) hydrocarbons and hydrogen (yields of 0.83 and 0.02% respectively).

**Table 3.2.** Comparison of main characteristics of bio-oil with those of biomass and fuel-oil

| **Materials** | **C*** | **H*** | **O*** | **Energy density ($MJ\ kg^{-1}$)** | **pH** | **Water content*** |
|---|---|---|---|---|---|---|
| Biomass | 48.74 | 5.80 | 45.46 | 16 | - | 5.6 |
| Bio-oil | 52.11 | 5.70 | 42.34 | 19 | 2.4 | 30.5 |
| Fuel-oil | 85.30 | 11.47 | 1.05 | 40 | 5.7 | 0.1 |

*data are in mass fraction %

Table 3.2 lists the differences in the major properties of the obtained liquid (bio-oil) with those of the original biomass and a representative fossil fuel-oil. Compared to the parent biomass, bio-oil contains almost the same amount of hydrogen (~ 5.8 mass fraction %), slightly more carbon (52.11 % of bio-oil compared to 48.74% of biomass) and less oxygen (42.34% of bio-oil compared to 45.6% of biomass).

However, this difference is very small compared to the difference between bio-oil and fuel oil. Compared to bio-oil (H/C 1.3), fuel oil has much higher carbon and hydrogen content

(85.30% and 11.47%, respectively, H/C 1.6) and much less oxygen (1.05%). Higher [C], [H] content of fuel oil gives it higher energy content. Table 3.2 also summarises the problems when working with bio-oil. Presence of high [O] content in bio-oil results in a corrosive, acidic, viscous, unstable and particulates containing oil with a relatively low energy density compared to that of fossil fuels.

To have a better understanding of the undesired properties of bio-oil, and the factors that cause them, GC/MS was used to analyse the chemical composition of bio-oil.

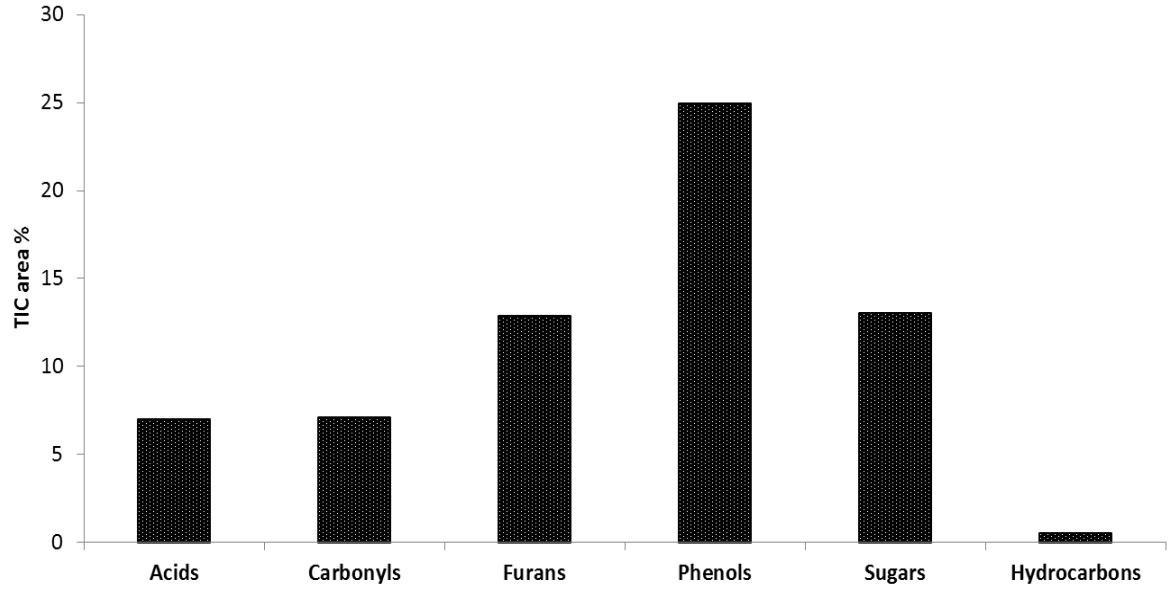


**Figure 3.1.** Distribution of different chemical groups in bio-oil

Since bio-oil is a complicated mixture of hundreds of different organic compounds, it is reasonable to classify them into different groups based on their chemical functionality. Such a classification of the components of bio oil is shown in Figure 3.1. In Figure 3.1, the vertical axis shows the relative proportions of different groups in the bio-oil calculated by summing the total ion chromatogram (TIC) area percentages of all the compounds belonging to these groups. This method, commonly used by other authors [21-23], generates semi-quantitative results. It can be used to compare the concentrations of a certain component in bio-oil obtained under different conditions.

Figure 3.2 shows the components of biomass and the possible products that can be formed from them by pyrolysis.

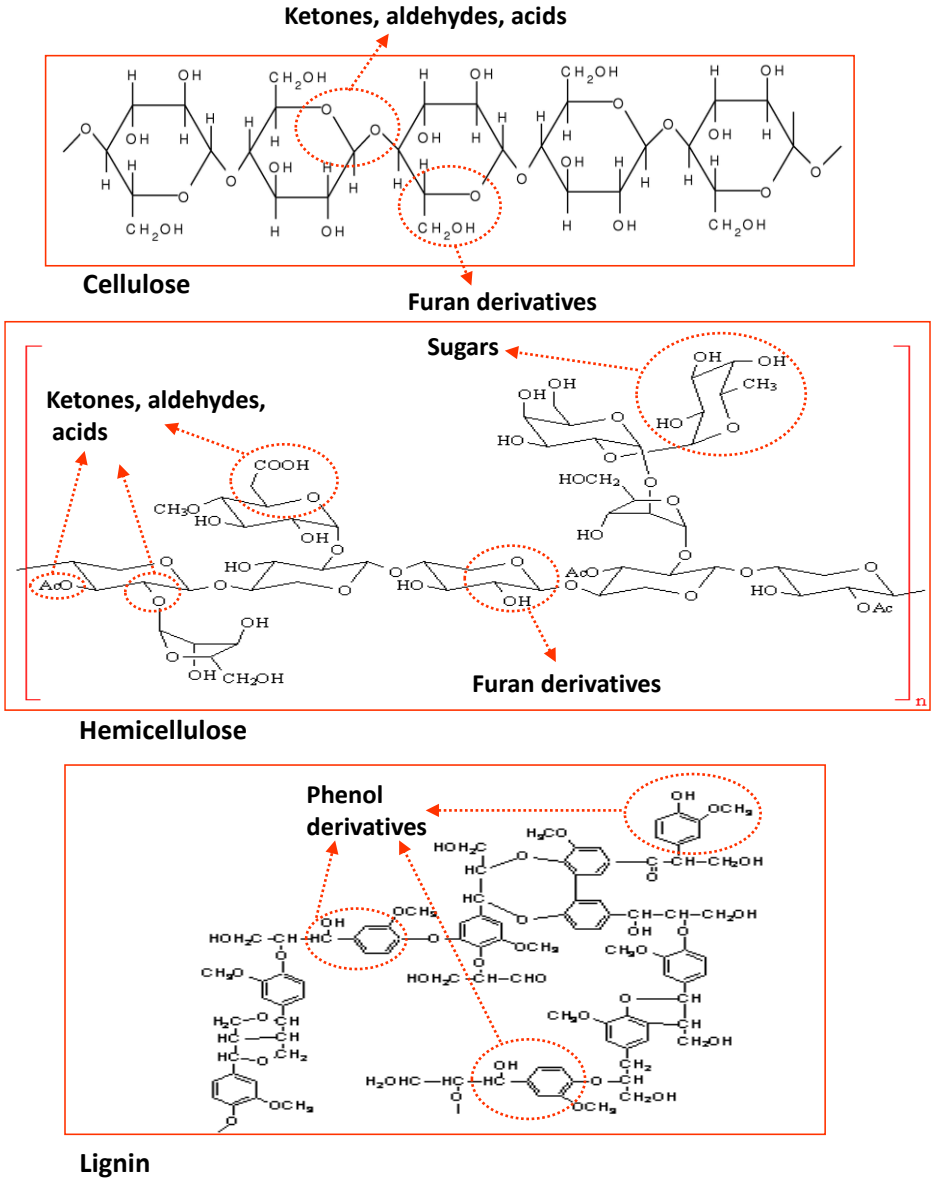


**Figure 3.2.** Chemical structure of cellulose, hemicellulose, lignin and the correlation to their products found in bio-oil

Bio-oil contains a variety of carboxylic acids e.g., formic, acetic acids, mainly formed by the decomposition of cellulose and hemicellulose fractions of biomass [24]. These are the main components that cause acidity of the bio oil [25]. Phenols which form by the decomposition of lignin also contribute to acidity but to a much lesser extent [25]. Carbonyl compounds such as aldehydes and ketones, have tendency to undergo condensation reactions causing viscosity increase make the oil unstable [24]. Hydrocarbons and furans (formed from holocelluloses) are the required components due to their high energy content [3].

In order to improve the properties of bio-oil, it is thus essential to remove / modify the problematic components during de-oxygenation. Essentially de-oxygenation of harmful components can be achieved by converting them to products such as $CO_2$, CO or $H_2O$. In order to illustrate how effective each route is, in an energy content point of view, glucose ($C_6H_{12}O_6$) was chosen as a model compound. From glucose, we can either remove one or more $CO_2$ or CO or $H_2O$ molecules and obtain corresponding products (Figure 3.3).

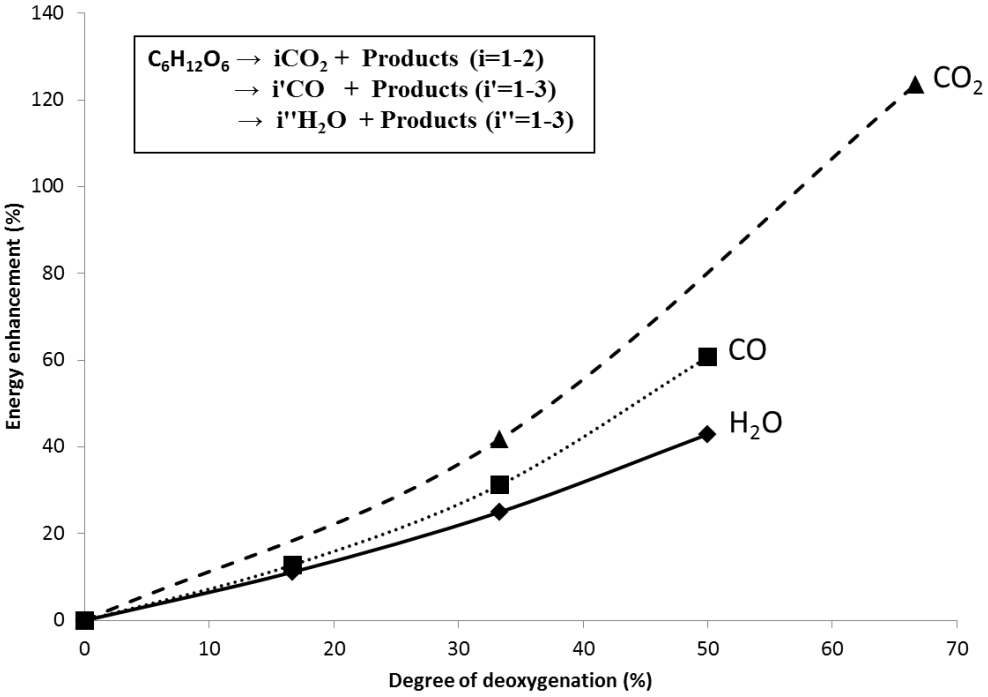


**Figure 3.3.** Efficiency of different oxygen removal routes, calculated using Dulong formula*

*HHV (MJ/kg) = (0.3388*[C])+(1.442*([H] -[O]/8))

The higher heating values (HHV) of these products can be estimated using Dulong formula, a widely-used model to estimate the HHV of a compound based on its elemental composition ([C], [H], [O]%, mass fraction) [26-28]. The higher heating values and oxygen contents of the products were then compared with those of the original glucose. These comparisons are represented by the energy enhancement (%) and the degree of deoxygenation (%), respectively (Figure 5). It is obvious from Figure 5 that selective de-oxygenation to $CO_2$ is the most beneficial. This is because per carbon atom lost, two oxygen atoms are removed and thus carbon loss is lower. For the same reason, de-oxygenation as CO is less efficient. Formation of water lowers hydrogen content of biomass, and is thus the least preferred.

Incorporation of a catalyst in the pyrolysis process must have the ability to selectively deoxygenate unwanted pyrolysis product oxygenates and form $CO_2$. Results of catalytic pyrolysis are discussed next.

### *3.3.2. Post-treatment vs. mixing catalytic pyrolysis modes*

Catalytic pyrolysis experiments were carried out with three faujasite catalysts, details of which are given in Table 3.2. Since both catalysts and biomass are solids, there are two ways to introduce the catalysts into the pyrolysis system, namely: (i) mixing mode and (ii) post-treatment mode. Details of these two modes can be found in section 2.1. The aim of applying catalysts in our work is to reduce the oxygen content of biomass to get a higher quality bio-oil. It is therefore reasonable to use degree of de-oxygenation to compare the efficiency of the two modes. The formula for the oxygen removal degree is shown below.

$$\text{Oxygen removal degree} = [1 - ([O]\%_{\text{bio-oil}} \times \text{Yield}_{\text{bio-oil}} / [O]\%_{\text{biomass}})] \times 100$$

In this formula [O]% represents the oxygen content (mass fraction) of a specific material. Oxygen removal degree can be used to judge the amount of oxygen that has been removed from the biomass and retained in the bio-oil. In non-catalytic experiment, the bio-oil contains 21% less oxygen than which was originally present in biomass. By using $Na_{0.2}H_{0.8}$-FAU catalyst in mixing mode, it is possible to remove 23% oxygen from biomass, which is slightly better compared to non-catalytic experiment. The same catalyst in post-treatment mode, however, shows much higher activity in terms of oxygen removal, which is 31%.

In post-treatment mode, the biomass vapours always have to travel through the catalyst bed and contact the catalytic sites at the required temperature. In the mixing mode the situation is different. The problems are (i) solid-solid contact between the catalyst and the biomass (particle size: 300-600 μm) is not ideal, and (ii) since catalyst and biomass are subjected to the temperature ramp simultaneously, biomass vapours that already form at lower temperatures (around 300$^{o}$C) pass the catalyst before it has reached pyrolysis temperature (500$^{o}$C). For these reasons, not surprisingly, post-treatment mode is superior to mixing mode in terms of oxygen removal, and hence this mode is chosen for further catalytic tests.

### *3.3.3. Catalytic experiments*

#### *3.3.3.1. Products distribution*

In this section the catalytic influences on the yields of pyrolysis products (gas, liquid and solid) and on the composition of solid and gas products are discussed. Influence of the catalysts on the composition of liquid phase is discussed separately in section 3.3.3.2. Figure 3.4 shows the yields of pyrolysis products obtained from catalytic and non-catalytic (thermal) experiments.

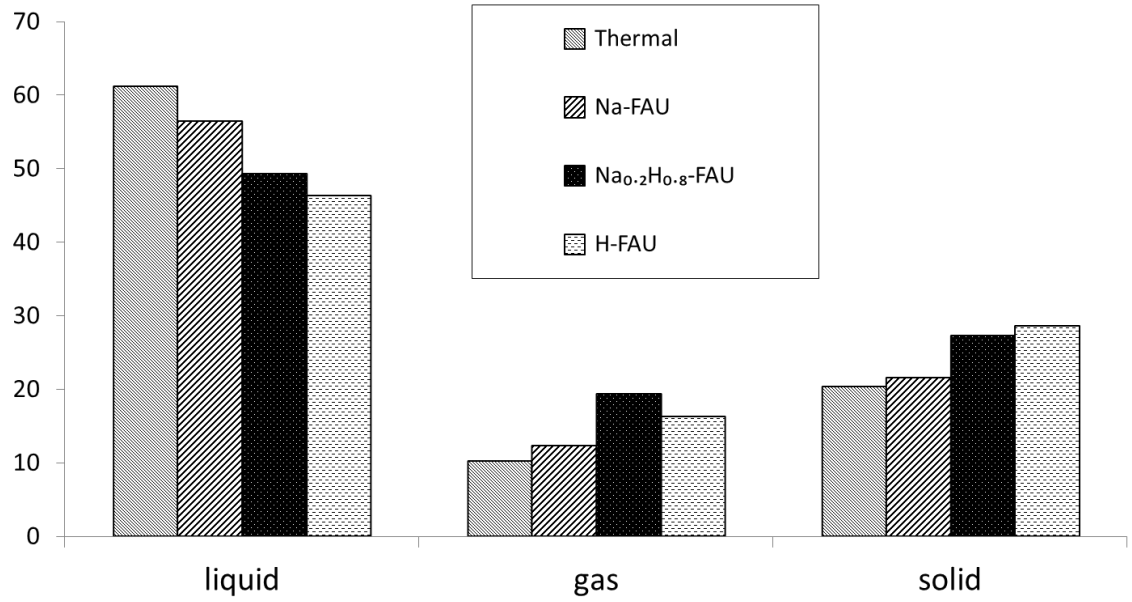


**Figure 3.4.** Product yields in catalytic and non-catalytic experiments

For all the experiments the mass balances are more than 90%. One can see from Figure 3.4 that the solid and gas yields increase while that of liquid decreases in presence of the catalysts. H-FAU gave the lowest liquid yield (46.3 mass fraction %, based on initial weight of biomass), highest solid yield (28.6%) and high gas yield (16.3%). In Figure 6, solid yields shown are the sum of solid char left in the pyrolysis compartment (>90 mass fraction % of total solid) plus the coke formed over the catalyst. Coke formed on the catalyst is maximised with H-FAU catalyst with the yield of 1.8% (mass fraction, based on initial weight of biomass) compared to that of 1.6% on $Na_{0.2}H_{0.8}$-FAU and 1.3% on Na-FAU. Among the catalysts, H-FAU also has the highest concentration of acid sites ($H^+$) and the highest cracking activity of C-C, C-H and C-O bonds and it is not surprising that it produces the maximum

amount of coke. Comparable experiment with inert material (quartz) in place of catalyst did not produce any coke. H-FAU also gave the maximum amount of water (yield of 22 mass fraction %, based on initial weight of biomass) as expected, since dehydration is strongly catalysed by acids.

For all the catalysts, elemental compositions and higher heat value (HHV) of the char and coke were analysed. All the results are based on ash-free calculations, which means that the compositions and heat values were only attributed to the organic fraction of the solid. Elemental composition of char formed in the pyrolysis chamber was, as expected, similar for all experiments (78.7 % carbon, 2.8 % hydrogen and 18.5 % oxygen, mass fraction). Surprisingly, compositions of coke formed on the catalysts were also similar, only the amount of coke varied and was maximised with H-FAU catalyst. This coke contains 87.5 % carbon, 6 % oxygen and 6.5 % hydrogen, mass fraction. As can be seen, the oxygen content of coke formed on the catalyst is much lower than that of char in the pyrolysis chamber, but it still contains 6 % of oxygen (mass fraction). This implies that it is not the classical hydrocarbon coke that is formed on the catalyst but oxygen-containing oligomeric species. Moreover, it can be seen that this coke is aromatic in nature (H/C ~ 1). Both acidic $H^+$ sites and sodium ions $Na^+$ seem to catalyse this oligomer formation since both H-FAU and Na-FAU resulted in coke formation.

**Table 3.4.** Composition of non-condensable gas yields; data are given in mass fraction %, based on initial weight of biomass

| Gas | Thermal | Na-Y | $Na_{0.2}H_{0.8}$-Y | H-Y |
|---|---|---|---|---|
| CO | 4.66 | 4.89 | 8.01 | 7.25 |
| $CO_2$ | 4.75 | 4.37 | 7.55 | 6.03 |
| HC | 0.83 | 1.10 | 3.66 | 2.91 |
| $H_2$ | 0.02 | 0.03 | 0.18 | 0.09 |

The gases formed during catalytic experiments are mainly composed of CO and $CO_2$, the rest being smaller hydrocarbons ($C_1$-$C_3$) and hydrogen. Details are shown in Table 3.4. As can be seen, the yields of CO and $CO_2$ increased in the presence of catalysts, especially in the cases of $Na_{0.2}H_{0.8}$-FAU and H-FAU. Using $Na_{0.2}H_{0.8}$-FAU, the yield of CO and $CO_2$ increased ~1.7 times compared to the non-catalytic experiment. $Na_{0.2}H_{0.8}$-FAU also shows

the maximum amount of hydrocarbon and hydrogen compared to all experiments. Consequence of these results on the properties of bio oil is discussed in the next section.

*3.3.3.2. Catalytic effects on the composition of bio-oil*

This section discusses the change in bio-oil composition, as analysed by GC-MS, for the various catalytic experiments and the correlations between the composition and properties, namely: acidity/corrosiveness, stability, and energy density of bio-oils.

*3.3.3.2.1. Acidity*

Pyrolysis of wood results in the formation of carboxylic acids and other acidic components which make the bio-oil corrosive and negatively affect its applicability as a fuel. It was shown that among the various components present in bio-oil, carboxylic acids contribute to the acidity of bio-oil the most (60-70%) [25]. Other components which contribute to the acidity of bio-oil are phenols (5-10%) and sugars (20%). For this reason, the acidity of bio-oil can be correlated to the amount of carboxylic acids determined by GC/MS. Validity of this correlation is shown in Figure 3.5 by plotting the acidity of several bio-oil samples determined by potassium hydroxide titration (TAN) *versus* the corresponding carboxylic acid concentrations determined by GC/MS.

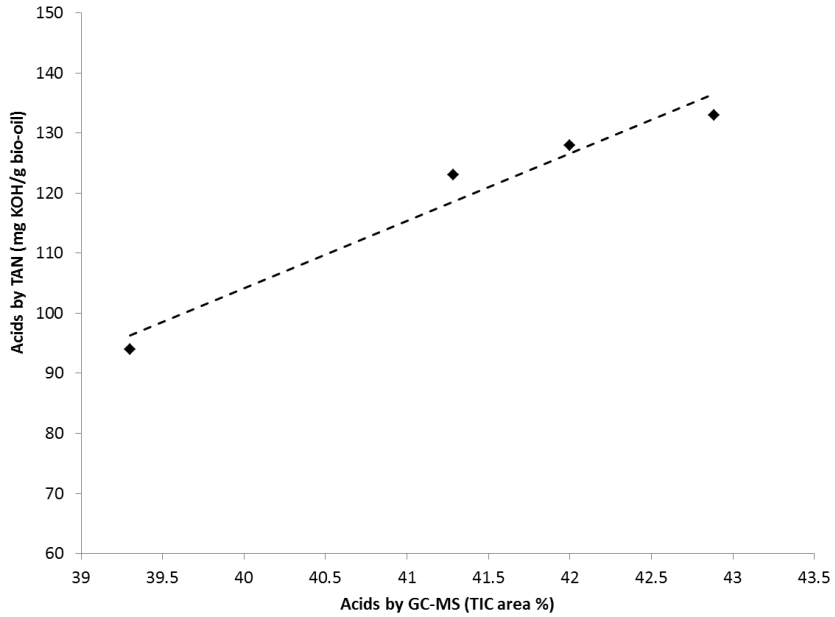


**Figure 3.5.** Correlation of TAN with total amount of acids in bio-oil; Measurement error of TAN analysis calculated to be 1.47% based on 95% confidence level

Figure 3.6 shows the influence of catalysts on the amounts of acids, phenols, and sugars formed.

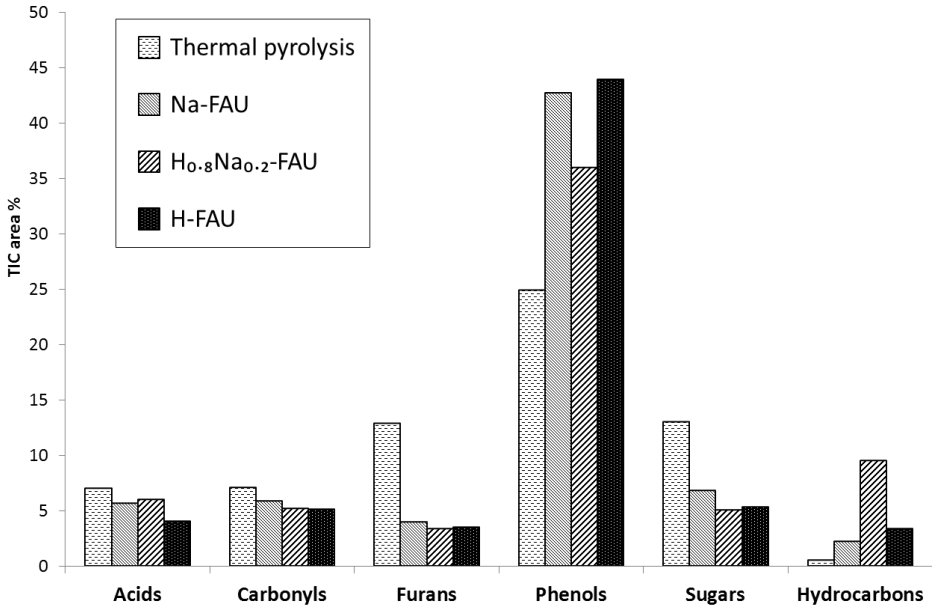


**Figure 3.6.** Distribution of chemical groups in bio-oils obtained from catalytic and non-catalytic experiments

All the catalysts reduced the amount of carboxylic acids compared to thermal experiment with H-FAU having the most influence. It is noteworthy to recall that the reduction in carboxylic acids is correlated to the increase in yield of $CO_2$ in gas stream (Table 3.4). Since the amount of acids and the acidity of bio-oils is well correlated, it is expected that H-FAU is a good catalyst to reduce the acidity of bio-oil. In the meantime, the amount of phenols increased drastically in the presence of catalysts (Figure 3.6). Phenolic components are less troublesome in terms of causing acidity and, together with their high energy content, are more desired than carboxylic acids. This increase also indicates the ability of FAU catalysts to decompose more lignin-derived vapour.

*3.3.3.2.2. Energy density*

Hydrocarbons are the most valuable fuel components from pyrolysis of biomass due to their high heating value. The amount of hydrocarbons formed in bio-oil using each catalyst is compared in Figure 3.6.. As can be seen from the figure, there is only a slight increase in hydrocarbon concentration when Na-FAU is used compared to thermal pyrolysis. However, when H-FAU and especially $Na_{0.2}H_{0.8}$-FAU were used, the area percentage of hydrocarbons

in bio-oil increased significantly from 0.5% (thermal) to 3.4% (H-FAU) and 9.5% ($Na_{0.2}H_{0.8}$-FAU). During catalytic deoxygenation of biomass, hydrocarbons are proposed to be formed from sugars through several reactions including dehydration of monomer sugars to dehydrated products, *i.e.* furans, and subsequent decarbonylation, decarboxylation and oligomerization of dehydrated products to aromatics [3]. Another possible pathway for hydrocarbon formation is decarboxylation of organic acids to $CO_2$ and hydrocarbons. Because the hydrogen content of biomass is very low, in the absence of external source of hydrogen most of the hydrocarbons in bio-oil can be found as aromatics. Moreover, aromatic hydrocarbons can also be produced from phenolic compounds by scission of all oxygenate substituents from phenol ring [16, 23]. It can be concluded that in the presence of $Na_{0.2}H_{0.8}$-FAU catalyst, hydrocarbons are most likely produced from deoxygenation of phenols and sugars because the amount of phenols and sugars obtained using this catalyst was the lowest (Figure 3.6).

*3.3.3.2.3. Stability*

Aging process of bio-oil results in an increase in molecular weight and viscosity of bio-oil due to the presence of reactive components, *i.e.* aldehydes and ketones. A number of possible reactions responsible for the instability of bio-oil was proposed [29], including reactions of (i) organic acids with alcohols forming ester and water, (ii) aldehydes and alcohols forming hemiacetals or acetals and water, (iii) aldehydes forming oligomers and resins, (iv) aldehydes and phenols forming resins and water, (v) and aldol type of condensation reaction between aldehydes and ketones. Reactions ii, iv and v consume aldehydes, phenols and form water and the fact that the amount of aldehydes and phenols in the old oil decreased and water increased compared to fresh oil supports this (Figure 3.7).

In order to have an overview of how the molecular weight distribution of the compounds in bio-oil has shifted during aging process, two bio-oil samples were analyzed using GPC technique: one is a sample of a fresh bio-oil and the other is the bio-oil which was produced in the same conditions but has been kept at laboratory conditions for 1 year. The results are shown in Figure 3.7. The GPC chromatogram can be divided into 2 regions: low molecular weight ($M<400$ g.mol$^{-1}$) and high molecular weight ($M> 400$ g.mol$^{-1}$). In the low molecular weight region, the curve corresponding to the old oil has similar shape compared to that of the fresh oil but with lower intensity.

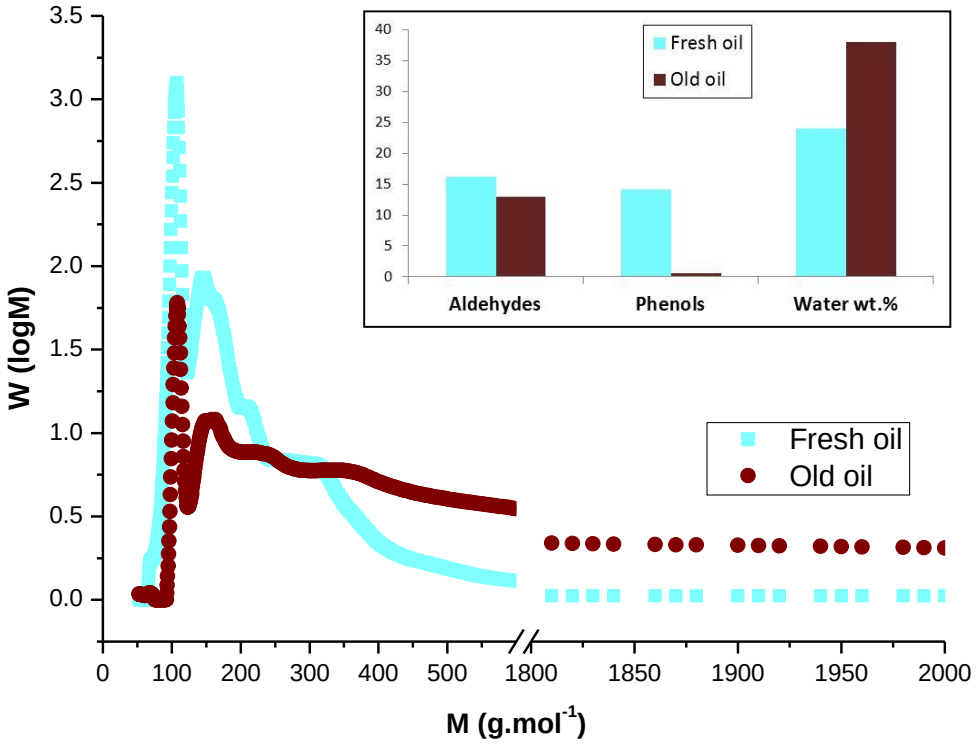


**Figure 3.7.** Molecular weight distribution of fresh and old bio-oils

The opposite occurs with the high molecular weight region (similar shape, higher intensity). From these results, it can be concluded that during storage process, the low-molecular-weight compounds in the fresh oil has reacted with each other to form heavier molecules and increase the viscosity of bio-oil. Figure 3.6 compares the effect of each catalyst on the formation of aldehydes/ketones (carbonyls) in bio-oil. It is obvious from the figure that all the catalysts reduce the amount of carbonyls in bio-oil compared to thermal reaction with H-FAU and $Na_{0.2}H_{0.8}$-FAU having the most influence. It can be concluded that the higher the proton concentration of the catalyst is, the more carbonyls are removed from bio-oil and the higher stability of bio-oils is expected.

Highest de-oxygenation extent obtained with $Na_{0.2}H_{0.8}$-FAU, accompanied by the highest amount of $CO_2$ formation, as expected, also results in bio-oil with higher energy content (24 MJ $kg^{-1}$, compared to 22 MJ $kg^{-1}$ for Na-FAU and H-FAU). $Na_{0.2}H_{0.8}$-FAU is a promising catalyst because it (i) decreases the acid content of the bio-oil, (ii) removes unstable components such as aldehydes and ketones, (iii) and by increasing the phenols and

hydrocarbon contents it not only improves the energy density of bio-oil but also makes it easier to blend with crude [30].

*3.3.4. Catalyst regeneration/Recycle*

In our proposed scheme, the catalyst/coke is burnt to generate heat for the process and recycled back to the reactor (Figure 1.2) similar to the FCC process. In order to investigate the regenerability of the catalysts, pyrolysis experiments were conducted with fresh and regenerated $Na_{0.2}H_{0.8}$-FAU catalyst.

Regeneration by coke combustion was probed in a TGA experiment which showed that complete removal of coke is achieved by 600ºC. Catalyst after one pyrolysis run was regenerated at 600ºC in flowing air (30 $cm^3$ $min^{-1}$) for 5 hours. XRD analyses of the two samples: fresh and regenerated are shown in Figure 3.8.

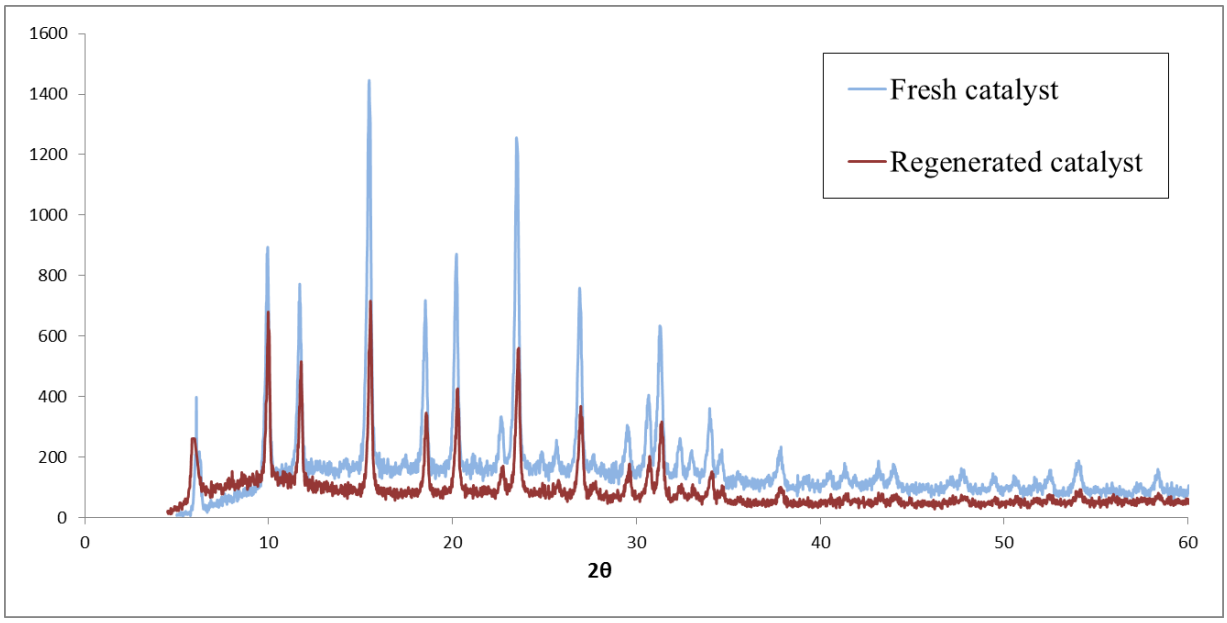


**Figure 3.8.** XRD analyses of fresh and regenerated catalysts

No appreciable differences were observed. Results of catalytic pyrolysis experiments for fresh and regenerated catalyst are shown together in Figure 3.9. As can be seen, the fresh and regenerated catalysts have almost the same performance in pyrolysis reaction. It can be concluded that the catalyst is regenerable. However, this conclusion is only valid for the catalyst which was regenerated after one cycle, while in industry (*e.g.* in FCC process)

catalysts were required to be functional after many cycles. Testing catalytic performance after multiple cycles is, nevertheless, out of scope of the study.

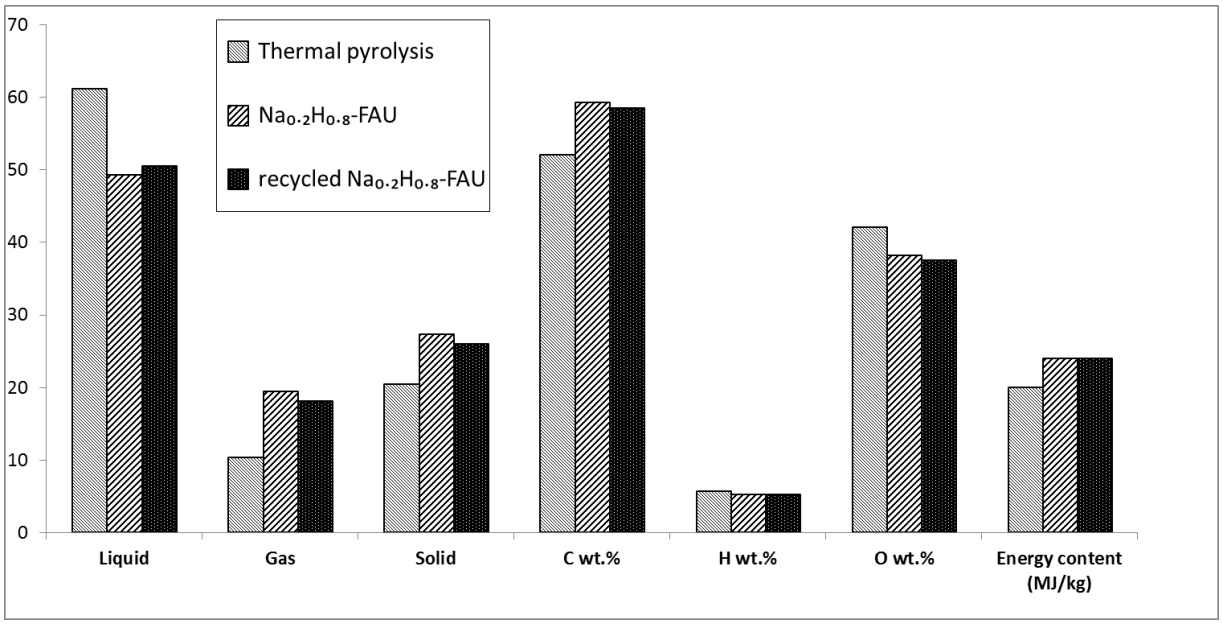


**Figure 3.9.** Comparing catalytic activity of fresh and recycled catalysts

## 3.3. Conclusion

In this chapter, catalytic upgrading of biomass pyrolysis vapours was studied in a lab-scale fix-bed reactor at 500°C. Three zeolite catalysts with different $H^+$ and $Na^+$ concentrations including H-FAU, $Na_{0.2}H_{0.8}$-FAU and Na-FAU were tested in the reaction. The results showed that the amount of $H^+$ and $Na^+$ of the catalyst plays an important role in the product yields and product distribution. The higher the concentration of $H^+$ of the catalyst is, the lower the liquid yield, and the higher the solid and gas yields are obtained. It was shown that two of major problems with bio-oil, namely the corrosiveness and instability, were mainly caused by carbonyl and carboxylic acid compounds, respectively. The best catalyst candidate is $Na_{0.2}H_{0.8}$-FAU, which reduced the most acid and carbonyl compounds while boosted the amount of the desirable phenolic and hydrocarbon compounds compared to non-catalytic experiment and to the other two catalysts. $Na_{0.2}H_{0.8}$-FAU also removed the most oxygen as $CO_2$, resulting in an oil with lowest oxygen content (38 mass fraction %) and highest energy content (24 $MJ.kg^{-1}$). It was shown possible to regenerate the spent catalyst without changing its crystalline structure and catalytic performance.

# References


[1] Bridgwater AV, Meier D, Radlein D. An overview of fast pyrolysis of biomass. Org Geochem 1999;30(12):1479-93.

[2] Czernik S, Bridgwater AV. Overview of applications of biomass fast pyrolysis oil. Energ Fuel 2004;18(2):590-8.

[3] Huber GW, Iborra S, Corma A. Synthesis of transportation fuels from biomass: Chemistry, catalysts, and engineering. Chem Rev 2006;106(9):4044-98.

[4] Bridgwater AV. Catalysis in Thermal Biomass Conversion. Appl Catal A-Gen 1994;116(1-2):5-47.

[5] Williams PT, Nugranad N. Comparison of products from the pyrolysis and catalytic pyrolysis of rice husks. Energy 2000;25(6):493-513.

[6] Samolada MC, Papafotica A, Vasalos IA. Catalyst Evaluation for Catalytic Biomass Pyrolysis. Energ Fuel 2000;14(6):1161-7.

[7] Corma A, Huber GW, Sauvanaud L, O'Connor P. Processing biomass-derived oxygenates in the oil refinery: Catalytic cracking (FCC) reaction pathways and role of catalyst. J Catal 2007;247(2):307-27.

[8] Fahmi R, Bridgwater AV, Darvell LI, Jones JM, Yates N, Thain S, et al. The effect of alkali metals on combustion and pyrolysis of Lolium and Festuca grasses, switchgrass and willow. Fuel 2007;86(10-11):1560-9.

[9] Mullen CA, Boateng AA. Chemical composition of bio-oils produced by fast pyrolysis of two energy crops. Energ Fuel 2008;22(3):2104-9.

[10] Nowakowski DJ, Woodbridge CR, Jones JM. Phosphorus catalysis in the pyrolysis behaviour of biomass. J Anal Appl Pyrol 2008;83(2):197-204.

[11] Patwardhan PR, Satrio JA, Brown RC, Shanks BH. Influence of inorganic salts on the primary pyrolysis products of cellulose. Bioresource Technol 2010;101(12):4646-55.

[12] Babich IV, van der Hulst M, Lefferts L, Moulijn JA, O'Connor P, Seshan K. Catalytic pyrolysis of microalgae to high-quality liquid bio-fuels. Biomass Bioenerg 2011;35(7):3199-207.

[13] Zabeti M, Nguyen TS, Lefferts L, Heeres HJ, Seshan K. In situ catalytic pyrolysis of lignocellulose using alkali-modified amorphous silica alumina. Bioresource Technol 2012;118(0):374-81.

[14] Vispute TP, Zhang HY, Sanna A, Xiao R, Huber GW. Renewable Chemical Commodity Feedstocks from Integrated Catalytic Processing of Pyrolysis Oils. Science 2010;330(6008):1222-7.

[15] Selva M, Fabris M, Perosa A. Decarboxylation of dialkyl carbonates to dialkyl ethers over alkali metal-exchanged faujasites. Green Chem 2011;13(4):863-72.

[16] Ding LH, Rahimi P, Hawkins R, Bhatt S, Shi Y. Naphthenic acid removal from heavy oils on alkaline earth-metal oxides and ZnO catalysts. Appl Catal A-Gen 2009;371(1-2):121-30.

[17] Choi HS, Choi YS, Park HC. Fast pyrolysis characteristics of lignocellulosic biomass with varying reaction conditions. Renew Energ 2012;42(0):131-5.

[18] Bridgwater AV. Review of fast pyrolysis of biomass and product upgrading. Biomass Bioenerg 2012;38:68-94.

[19] Zhang HY, Xiao R, Wang DH, He GY, Shao SS, Zhang JB, et al. Biomass fast pyrolysis in a fluidized bed reactor under N(2), CO(2), CO, CH(4) and H(2) atmospheres. Bioresource Technol 2011;102(5):4258-64.

[20] Pattiya A. Bio-oil production via fast pyrolysis of biomass residues from cassava plants in a fluidised-bed reactor. Bioresource Technol 2011;102(2):1959-67.

[21] Dominguez A, Menendez JA, Inguanzo M, Bernard PL, Pis JJ. Gas chromatographic-mass spectrometric study of the oil fractions produced by microwave-assisted pyrolysis of different sewage sludges. J Chromatogr A 2003;1012(2):193-206.

[22] Marin N, Collura S, Sharypov VI, Beregovtsova NG, Baryshnikov SV, Kutnetzov BN, et al. Copyrolysis of wood biomass and synthetic polymers mixtures. Part II: characterisation of the liquid phases. J Anal Appl Pyrol 2002;65(1):41-55.
[23] Goncalves AR, Schuchardt U, Meier D, Faix O. Pyrolysis gas chromatography of the macromolecular fractions of oxidized Organocell lignins. J Anal Appl Pyrol 1997;40-1:543-51.
[24] Bridgwater AV, Peacocke GVC. Fast pyrolysis processes for biomass. Renew Sust Energ Rev 2000;4(1):1-73.
[25] Oasmaa A, Elliott DC, Korhonen J. Acidity of Biomass Fast Pyrolysis Bio-oils. Energ Fuel 2010;24:6548-54.
[26] Mason DM, Gandhi KN. Formulas for calculating the calorific value of coal and coal chars: Development, tests, and uses. Fuel Process Technol 1983;7(1):11-22.
[27] Wanignon Ferdinand F, Van de Steene L, Kamenan Blaise K, Siaka T. Prediction of pyrolysis oils higher heating value with gas chromatography–mass spectrometry. Fuel 2012;96(0):141-5.
[28] Kathiravale S, Yunus MNM, Sopian K, Samsuddin AH, Rahman RA. Modeling the heating value of Municipal Solid Waste. Fuel 2003;82(9):1119-25.
[29] Diebold J. A review of the chemical and physical mechanisms of the storage stability of fast pyrolysis bio-oils. Subcontractor report. National Renewable Energy Laboratory, Golden, CO Energy Do; 2000 NREL/SR-570-27613.
[30] Anderson BD, Rytting JH, Higuchi T. Influence of self-association on the solubility of phenol in isooctane and cyclohexane. J Am Chem Soc 1979;101(18):5194-7.

# Chapter 4

## Conversion of lignocellulosic biomass to green fuel oil over sodium based catalysts

*T.S. Nguyen, M. Zabeti, L. Lefferts, G. Brem, K. Seshan, Bioresource Technology 142 (2013)353*

**Abstract.** This chapter studied the upgrading of biomass pyrolysis vapours over 20 wt.% $Na_2CO_3$/ γ-$Al_2O_3$ catalyst. Characterization of the catalyst using SEM and XRD has shown that sodium carbonate is well-dispersed on the support γ-$Al_2O_3$. TGA and $^{23}Na$ MAS NMR suggested the formation of new hydrated sodium phase, which is likely responsible for the high activity of the catalyst. It has been shown that catalytic oil has much lower oxygen content (12.3 wt.%) compared to non-catalytic oil (42.1 wt.%). This comes together with a tremendous increase in the energy density (37 compared to 19 $MJ.kg^{-1}$). Decarboxylation of carboxylic acids was favoured on the catalyst, resulting to an oil almost neutral (TAN= 3.8 mg KOH/g oil and pH=6.5). However, the mentioned decarboxylation also resulted in the formation of carbonyls, which correlates to low stability of the oil. Catalytic pyrolysis results in a bio-oil which resembles a fossil fuel oil in its properties.

## 4.1. Introduction

In Chapter 3, it has been shown that the presence of sodium ions in Faujasite matrix helped improve de-oxygenation of biomass pyrolysis vapours, reduced the amount of acids, aldehydes/ketones and enhanced the hydrocarbon content and thus the energy density of the oil. However, the de-oxygenation obtained with Na-FAU catalysts was still not optimal. Catalytic pyrolysis led to a bio-oil, with an oxygen content of 38 wt.% in comparison to non-catalytic case where it was 42 wt.%. However, it was also shown that, with $Na_2CO_3$, extensive de-oxygenation could be achieved during the catalytic pyrolysis of chlorella Algea, shown by the significant increase in the energy density of bio-oil from 21 MJ $kg^{-1}$(non-catalytic) to 32 MJ $kg^{-1}$(with $Na_2CO_3$) at 450 °C [1]. The incorporation of $Na_2CO_3$ to white pine during pyrolysis was reported to lead to a catalytic bio-oil with a significant degree of de-oxygenation [2]. Williams *et al.*[3] studied the influence of sodium salts on the kinetics of biomass pyrolysis. A clear acceleration in the pyrolysis reaction rate is observed for salt impregnated biomass and this acceleration is dependent upon the salt concentration. It is proposed that the sodium ions not only catalyse biomass decomposition *via* chelation to hydroxyl and ether groups in cellulose- the most abundant component in biomass, but also evolved during pyrolysis, forming new active sites by diffusion of the ions from salt particles to chelation complexes. It is speculated that changes in geometry upon chelation favours certain ring conformations which might enhance reactivity to cracking reactions [3].

Sodium carbonate has low surface area and has a tendency to form clusters in presence of water, and is susceptible to attrition due to low mechanical strength. For a typical fluidised bed pyrolysis process, anchoring sodium carbonate on a mechanically strong support would be beneficial. It has been reported [4] that in the presence of γ-$Al_2O_3$ oxygen content of bio-oil was 24 wt.% compared to that of 42 wt.% of non-catalytic oil, showing promise. γ-$Al_2O_3$ was also found to significantly increase the concentration of aliphatic and aromatic hydrocarbons in the bio-oil during the pyrolysis of *miscanthus x giganteus grass* compared to non-catalytic tests [5]. γ-$Al_2O_3$ is also mesoporous in nature, allow access to bulkier biomass oxygenates and the problem of coking/pore blockage may be less compared to microporous FAU zeolites.

Based on elemental composition, oxygen content of the bio-oil below 15 wt.% would be necessary to bring its heat content / energy density similar to that of fuel oil [6]. It is

important to achieve such levels of oxygen content, *via* selective de-oxygenation/eliminating oxygenates that cause properties, as discussed in Chapter 1, that are detrimental for the use of bio-oil as a fuel. In this chapter the influence of $Na_2CO_3/\gamma$-$Al_2O_3$ catalysts on the conversion of lignocellulosic biomass to various organic components is investigated with a view to establishing a catalytic pyrolysis process for a green refinery.

## 4.2. Experimental

### *4.2.1. Catalyst preparation and characterisation*

$\gamma$-$Al_2O_3$ was obtained from Akzo Nobel and $Na_2CO_3$ from Sigma-Aldrich. The catalyst 20 wt.% $Na_2CO_3/\gamma$-$Al_2O_3$ was prepared by wet impregnation, of which the detailed procedure was shown in section 2.2.2. Fresh and used catalysts were characterized by BET, XRD, TGA-MS, $^{23}$Na MAS NMR elemental analysis and SEM imaging. These techniques are further described in detail in section 2.3.1.

### *4.2.2. Catalytic testing*

The experimental set-up and applied definitions are described in detail in Chapter 2. In all experiments, 2 g of biomass and 1 g catalyst was packed inside the reactor. Temperature of the pyrolysis and catalyst bed was set at 500$^o$C. Duration of all experiments was 10 min. The flow rate of Ar was 70 mL.min$^{-1}$, which gave an average vapour residence time of 4 sec. Products of the catalytic pyrolysis process were subjected to GC, GC-MS, elemental analysis, bomb calorimetry, TGA, TAN and pH measurement. Details of these analyses were given in section 2.3.2.

Later in this chapter, it is shown that the nature of the coke formed on the catalyst during upgrade of pyrolysis vapour is different from traditional hydrocarbon coke. This coke is high in oxygen content and proposed to be formed by the oligomerization of oxygenates presenting in pyrolysis vapour. For that reason, we would like to introduce the term heterogeneous char, instead of coke, for this type of material. This term will be used throughout the chapter. The traditional homogeneous char formed directly in biomass pyrolysis will be mentioned as char.

## 4.3. Results and discussion

*4.3.1. Catalytic pyrolysis*

The mass balance for catalytic and non-catalytic (thermal) pyrolysis experiments is summarized in Table 4.1. All the yields are based on the initial weight of biomass. For calculation of the gas yield in catalytic pyrolysis of biomass, a blank experiment was carried out in which the same amount of catalyst was loaded in the catalytic compartment while the biomass compartment was left empty. The gas yield shown in Table 4.1 was obtained by subtracting the amount of gas obtained in the blank experiment from that of the real catalytic test. This approach will eliminate all possible interference resulted from the decomposition of $Na_2CO_3$ to gas yields.

**Table 4.1.** Mass balance of catalytic and non-catalytic pyrolysis of biomass

| Sample | Yield wt.% | | | | |
|---|---|---|---|---|---|
| | Liquid | Char[3] | Hetero. char[4] | Gas | Total |
| Thermal | 61[1] | 19 | 0 | 13 | 93 |
| 20 wt.% $Na_2CO_3$/ γ-$Al_2O_3$ | 37[2] | 19 | 15 | 23 | 94 |

[1]Consists of 20 wt.% yield of water and 41 wt% of non-separable organic+aqueous phases

[2]Consists of 22 wt.% yield of water, 9 wt.% of organic phase and 6 wt.% of aqueous phase

[3] Homogeneous char left in the pyrolysis chamber

[4] Heterogeneous char formed on the catalyst

For all experiments, the mass balances are more than 90 wt.%. The thermal (non-catalytic) pyrolysis resulted in a single-phase bio-oil. Phase separation (organic & aqueous phases) was observed in the bio-oil when pyrolysis experiments were carried out in the presence of sodium-based catalyst. These two phases were separated physically easily using a micro-syringe. The aqueous phase is composed of compounds with high polarity, for *e.g.* acids, ketones, which originated from the cellulose and hemicellulose components of biomass [7]. Organic phase mostly contains phenolic compounds originating from lignin, as phenols have low solubilities in water. As can be seen in Table 4.1, the total liquid yield (organic + aqueous) of 37 wt.% in the catalytic experiment is lower than that of thermal pyrolysis (61 wt.%). This is due to (i) the increased loss of carbon *via* cracking of the pyrolysis vapors on the surface of the catalysts to heterogeneous char and (ii) the formation of more gaseous products.

Since the catalysts and biomass are physically separated, catalyst is not expected to interfere with the primary decomposition of biomass. All pyrolysis experiments were carried out at the same conditions, thus the yields of char formed in the pyrolysis chamber are the same in all cases. The mass balance shown in Table 4.1 supports this (char yield of 19 wt.% for both experiments). As mentioned previously, the catalyst additionally converts part of the pyrolysis vapour into heterogeneous char (yield of 15 wt.%) and more gas (nearly double in yield compared to thermal pyrolysis). In the sections below we discuss the details of de-oxygenation and the relevance to other characteristics of bio-oil.

Influence of the catalyst on the de-oxygenation of biomass vapours can be inferred from Table 4.2. The interference caused by $Na_2CO_3$ decomposition to $CO_2$ yield is eliminated by carrying out a blank experiment, as mentioned previously. During de-oxygenation of biomass, oxygen cannot be removed as $O_2$ because of thermodynamics. Instead, it is released *via* the formation of either $H_2O$, CO or $CO_2$. Removal of oxygen *via* $H_2O$ should be avoided to retain higher H/C ratio and energy content of bio-oil. Oxygen removal *via* COx formation is preferred [8], particularly, formation of $CO_2$ is optimal because this route removes two oxygen atoms per carbon atom, and hence allows for (i) a higher oxygen removal efficiency and (ii) lower carbon loss.

**Table 4.2.** Influence of the catalysts on the de-oxygenation of bio-oil

| Sample | Yield (wt.%) | | | Oxygen content (wt%) | |
|---|---|---|---|---|---|
| | $CO_2$ | CO | $H_2O$ | In char | In hetero. char |
| Thermal | 5.1 | 5 | 20 | 18.5 | -- |
| 20 wt.% $Na_2CO_3$/ $\gamma$-$Al_2O_3$ | 12.2 | 7.2 | 22 | 18.5 | 41.5 |

It can be seen from Table 4.2 that the formation of $CO_2$ was favoured on the sodium-based catalysts. CO yields also increased but to a smaller extent. The formation of water was only slightly enhanced with the catalyst compared to thermal experiment. It is known that both Lewis and Bronsted acid sites exists on the surface of $\gamma$-$Al_2O_3$, which can be responsible for the dehydration of organic compounds in pyrolysis vapours enhancing water formation [9].

Oxygen content of heterogeneous and homogeneous char formed during pyrolysis is also shown in Table 4.2. Besides the increase in the yields of $H_2O$ and $CO_x$, the catalyst also influenced the de-oxygenation of biomass in the nature of heterogeneous char that was formed. As has been mentioned, the char formation in the pyrolysis chamber cannot be

influenced by catalysts. The char in all cases has, within experimental error, identical elemental composition of 78.7 wt.% C, 2,8 wt.% H and 18.8 wt.% O (ash free basis). This is also similar to the composition of char obtained from fast pyrolysis as reported in literature [10, 11], which confirms that IR heating is a reasonable mimic of actual fast pyrolysis. The catalyst, on the other hand, caused formation of heterogeneous char which is different in composition to that of the char formed homogeneously (Table 4.2). The oxygen content of the heterogeneous char obtained is 41.5 wt.%. The high oxygen content of this heterogeneous char, together with its relatively high yield of 15 wt.% (Table 4.1), makes heterogeneous char formation on sodium-based catalysts an important de-oxygenation route. Significantly, the de-oxygenation obtained is very high with only 6.9 wt.% [O] from the biomass ending up in bio-oil, the rest distributed in water (43.1 %), COx (28.6%), heterogeneous char (13.7 %) and char (7.7%). Compared to non-catalytic experiment, there is 14 wt.% more of [O] from biomass removed *via* $CO_x$ and 13.7 wt.% [O] *via* heterogeneous char in catalytic upgrading. This shows that de-oxygenation *via* heterogeneous char and gas formation are equally important in achieving high-quality oil.

So far the influence of the catalyst on the de-oxygenation of pyrolysis vapours into different products has been discussed. To summarize, the sodium supported on alumina catalyst, showed improved performance compared to non-catalytic test, as shown by: (i) only a slight increase in water formation (from 20 to 22 wt.%), (ii) a significant increase in $CO_2$ yield (from 5.1 to 12.2 wt.%), and (iii) a significant de-oxygenation *via* the formation of oxygen-containing heterogeneous char compared to non-catalytic pyrolysis. These factors all reflect in the quality of the desired product bio-oil, as shown in Table 4.3.

**Table 4.3.** Influence of the catalyst on the properties of bio-oil

| Sample | [O] content bio-oil (wt.%) | HHV (MJ $kg^{-1}$) |
|---|---|---|
| Thermal[1] | 42.1 | 19 |
| 20 wt.% $Na_2CO_3$/ γ-$Al_2O_3$[2] | 12.3 | 37 |

[1]Values obtained with the non-separable organic+aqueous phase, dry basis

[2]Values obtained with the organic phase, dry basis

Results shown in Table 4.3, indicate that the $Na_2CO_3$/ γ-$Al_2O_3$ is very promising for the de-oxygenation of pyrolysis vapours. Oxygen content of the catalytic bio-oil is about 12 wt.% compared to 42% in the case of thermal pyrolysis oil. This is a significant level of de-oxygenation. Remarkably, the resulting bio-oil (organic phase) has an energy content (37

$MJ.kg^{-1}$) which is close to that of traditional fuel oil [6]. This result shows that the 20 wt.% $Na_2CO_3$/ γ-$Al_2O_3$ is a potential catalyst for the upgrading of biomass vapours with reference to energy content.

To understand better how the catalysts influences the chemistry of biomass pyrolysis, GC-MS technique was employed to analyse the chemical composition of bio-oils. The results of GC-MS analyses show that bio-oil is a complex mixture of hundreds of different organic components, which in turn reflect the decomposition of different components of the parental biomass (cellulose, hemicellulose and lignin). The organic compounds are classified into different families, based on their functionalities, for *e.g.* carboxylic acids(R-COOH), (substituted-)phenols, carbonyls (ketones and aldehydes), (substituted-)furans, sugars (glucose), and hydrocarbons (aliphatic and aromatic). Such classification is shown in Table 4.4.

**Table 4.4**. GC-MS analysis of bio-oil and its componental classification based on functionalities

| Sample | Acid | Carbonyl | Furan | Phenol | Sugar | Hydrocarbon[1] | Others |
|---|---|---|---|---|---|---|---|
| Thermal[2] | 12.0 | 14.1 | 12.9 | 25.0 | 14.0 | 0.5 | 1.7 |
| 20 wt. % $Na_2CO_3$ /γ-$Al_2O_3$[3] | 0.0 | 35.8 | 0.37 | 31.6 | 0.0 | 17.8 | 0.33 |

[1]Selectivity: 95% aromatic, 5% aliphatic HC
[2]Values obtained with the non-separable organic+aqueous phase
[3]Values obtained with the organic phase

Table 4.4 also shows the relative proportions of different families in the bio-oil calculated by summing the total ion chromatogram (TIC) area percentages of all the compounds belonging to these families. This method, commonly used by other authors [12-14], generates semi-quantitative results. However, it can be used to compare the concentrations of a certain component in bio-oil obtained under different conditions. All GC-MS analyses were carried out using the whole liquid phase (organic and aqueous) in order to have a better overview of the change in composition from non-catalytic to catalytic bio-oil.

In the following sections the influence of the catalyst on the decomposition of holocellulose and lignin fractions of biomass and the correlation between the chemical composition of bio-oil and its critical properties, such as energy density, acidity, and stability are discussed.

*4.3.1.1. Energy density*

Among the desired compounds in bio-oil, hydrocarbons are the most valuable fuel component because of their high heating value. It can be seen in Table 4.4 that the catalyst has significantly enhanced the formation of hydrocarbons, which is shown by an increase in the TIC area % of HCs from 0.5% (non-catalytic oil) to 17.8% (catalytic oil). This increase in HC concentration is correlated to the tremendous increase in energy density of bio-oil, as shown in Table 4.3. Hydrocarbons can be formed during biomass pyrolysis *via* one of the three possible routes: (i) decarbonylation, decarboxylation and oligomerization of dehydrated products of sugars, *i.e.* furans into aromatic hydrocarbons, (ii) decarboxylation of carboxylic acids into aliphatic hydrocarbons and $CO_2$ and (iii) hydrogenation/hydrogenolysis of phenols into aromatic hydrocarbons [15]. It can be seen from Table 4.4 that both acids and sugars have been completely removed and the content of phenols has increased in the catalytic bio-oil compared to non-catalytic one. This suggests that route (i) and (ii) contribute more than route (iii). Moreover, since the aromatic HCs are the dominant among all HCs (Table 4.4) it can be concluded that sugars are the main precursor for HCs in our study.

*4.3.1.2. Acidity*

Pyrolysis of wood results in the formation of carboxylic acids and other acidic components which make the bio-oil corrosive and negatively affect its applicability as a fuel. It has been shown [16] that, among the various components present in bio-oil, carboxylic acids contribute to the acidity of bio-oil the most (60-70%). Other components which contribute to the acidity of bio-oil are phenols (5-10%) and sugars (20%). Carboxylic acids and sugars are unwanted components since they greatly contribute to the acidity of bio-oil. Phenolic compounds, on the other hand, are desirable since they have less contribution to the acidity and are of high added value. As can be seen in Table 4.4, the catalyst has completely removed carboxylic acids from bio-oil. The two carboxylic acids originally present in non-catalytic oil, namely acetic acid and propionic acid, with the contents of 6.8 and 5.1 %, respectively were not observed at all in the catalytic oil. The same trend occurs to the sugars in bio-oil. The main sugar component observed in non-catalytic oil is D-Allose with the TIC area % of 12% was also completely removed in catalytic oil.

In the presence of catalyst, carboxylic acid and sugar components in the pyrolysis vapour have been completely removed and hence it can be expected that the bio-oil obtained

from this catalyst has lower acidity than non-catalytic oil. The acid measurements, shown in Table 4.5, supported this.

**Table 4.5.** Acidity of bio-oil

| Sample | TAN[1] (mg KOH/g oil) | pH |
|---|---|---|
| Thermal[2] | 119 | 2.6 |
| 20 wt. % $Na_2CO_3/\gamma$-$Al_2O_3$[3] | 3.8 | 6.5 |

[1]Total acid number based on standard ASTM 664
[2]Values obtained with the non-separable organic+aqueous phase
[3]Values obtained with the organic phase

In TAN measurement, per gram of catalytic bio-oil needs only 3.8 mg of KOH to titrate compared to 119 mg for non-catalytic oil. The pH measurement correlated well with this result, in which catalytic bio-oil showed to be almost neutral with pH = 6.5 while non-catalytic bio-oil is acidic (pH = 2.6). The oil obtained from this catalyst, therefore, will be much less corrosive and safer to transport in metal tanks and pipes.

Carboxylic acids can have only minimal contribution to the formation of HCs because very low amounts of aliphatic hydrocarbons ($C_1$-$C_4$) were observed in the liquid or gas phases. Thus it is necessary to establish a chemical pathway which can explain the elimination of acids in the catalytic bio-oil. It was observed in our GC-MS analysis that the mentioned removal of acids (acetic and propionic) was accompanied by the formation of ketones, namely acetone, 2-butanone and 3-pentanone; which were absent in the non-catalytic oil. Moreover, it has been shown [17] that acetic acid can be converted into acetone with very high conversion and selectivity (>99%) on a basic catalyst $CeO_2$/1% $K_2O/TiO_2$. Thus, the following mechanism is suggested for the conversion of carboxylic acids on $Na_2CO_3/\gamma$-$Al_2O_3$ catalyst:

$$R_1COOH + R_2COOH \rightarrow R_1COR_2 + CO_2 + H_2O$$

Removal of carboxylic acids according to this route is still a problem because (i) the de-oxygenation of acids occurs through both decarboxylation and dehydration reactions and (ii) the formation of ketones, which are the precursors of the instability of bio-oil as discussed next.

*4.3.1.3. Stability*

In general, presence of ketones and aldehydes cause problems for the stability of the bio-oil by undergoing condensation reactions which enhance the formation of higher molecular weight components and increase viscosity [18]. As mentioned in the previous section, presence of the catalyst has increased the amount of carbonyls formed in bio-oil, making it more susceptible to polymerization. The aging process of the catalytic (20 wt. % $Na_2CO_3/\gamma$-$Al_2O_3$) bio-oil is shown in Figure 4.1.

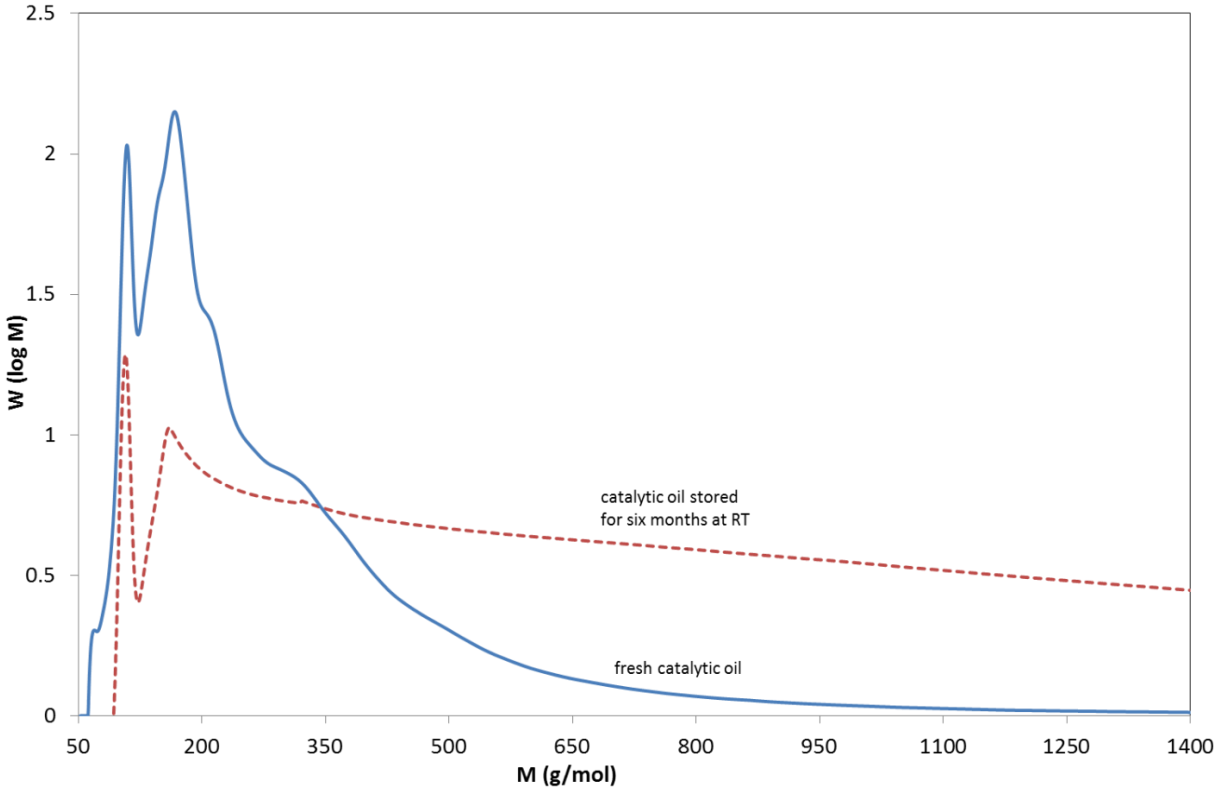


**Figure 4.1.** Molecular weight distribution of the fresh and old catalytic bio-oils analysed by GPC

Using gel permeation chromatogram, it is possible to observe the change in the molecular weight distribution of bio-oil upon storage. In Figure 4.1, the freshly generated bio-oil is compared to the oil generated using the same catalyst and conditions but stored at laboratory conditions for 6 months. As can be seen, comparing fresh to old oil, the amount of low molecular weight (<400) decreased while that of the higher molecular weight (>400) increased. This, in fact, reflects the aging process of bio-oils, in which low molecular weight compounds react with each other to form high molecular weight compounds and increase the

viscosity of bio-oil. It has been shown [19, 20] that ketones and aldehydes can undergo Aldol condensation and hydrogenation to yield liquid alkanes. Thus, a post pyrolysis hydrogenation of bio-oil or an *in situ* hydropyrolysis are possible steps. The former is often reported and the latter in the early stages of research in our group.

Results discussed so far show that, presence of $Na_2CO_3/\gamma\text{-}Al_2O_3$ during pyrolysis allows extensive de-oxygenation and the resulting bio-oil has excellent characteristics to be suitable for fuel applications. In the following section an analysis of the catalyst and its properties in relation to its performance is discussed.

*4.3.2. State of the catalyst*

The BET surface area of the prepared 20 wt.% $Na_2CO_3/\gamma\text{-}Al_2O_3$ catalyst was 196 $m^2.g^{-1}$, compared to the 249 $m^2.g^{-1}$ of the support $\gamma\text{-}Al_2O_3$.

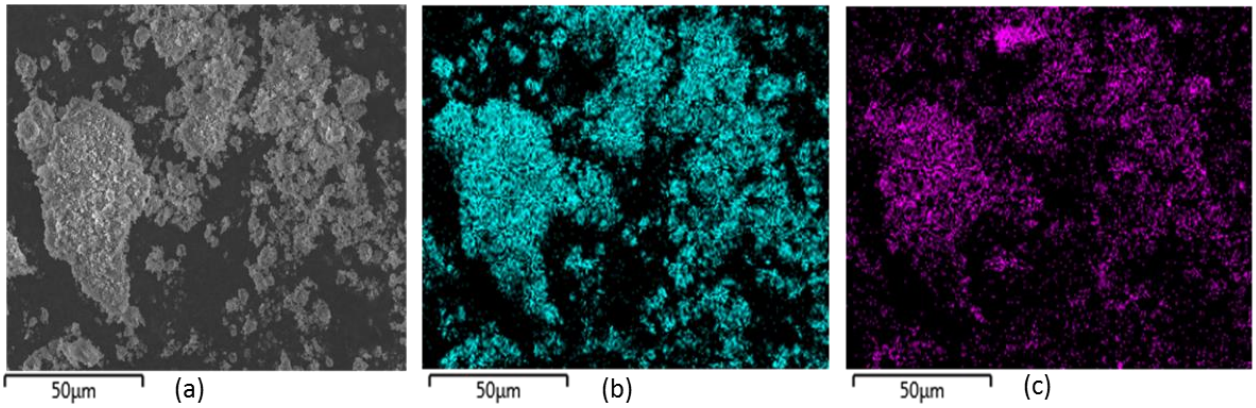


**Figure 4.2.** (a) SEM photograph, with EDX corresponding to (b) Al mapping and (c) Na mapping of the 20 wt.% $Na_2CO_3/\gamma\text{-}Al_2O_3$ catalyst

Figure 4.2(a) shows a SEM photograph of the catalyst area used for detailed elemental mapping (EDX). The dots as shown in Figures 4.2(b) and 4.2(c) represent the position of the detected aluminum and sodium particles, correspondingly. As can be seen, sodium and aluminum are thoroughly mixed. Thus, it can be concluded that $Na_2CO_3$ is homogeneously dispersed on the support $\gamma\text{-}Al_2O_3$ on micron length scale.

XRD patterns of the samples are shown in Figure 4.3. In the case of $\gamma\text{-}Al_2O_3$ three broad peaks at 2θ of 38°, 46° and $66^0$ which correspond to the [311], [400] and [440] planes [21], respectively, are seen. Diffractogram of the catalyst resembles that of the $\gamma\text{-}Al_2O_3$. No sharp crystalline peaks corresponding to any of the sodium compounds were observed. It can be concluded from XRD that sodium carbonate is well dispersed as small clusters on $\gamma\text{-}Al_2O_3$.

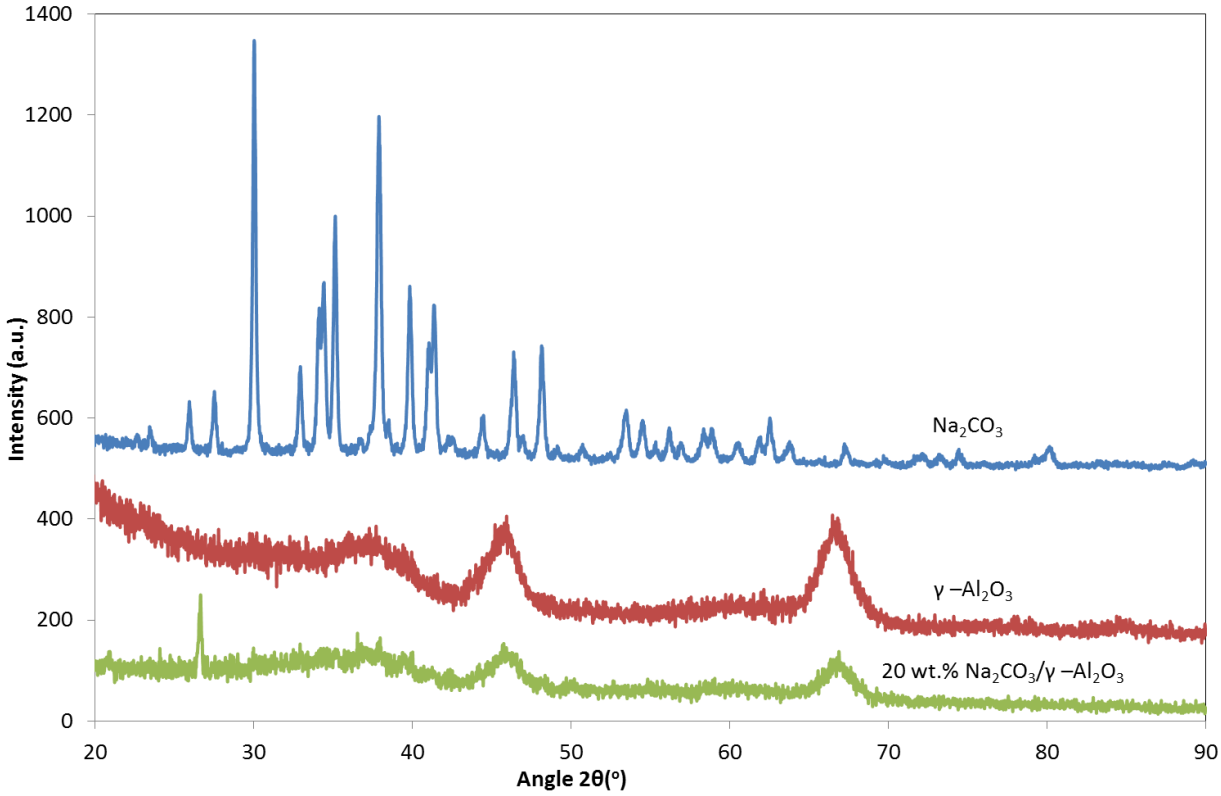


**Figure 4.3.** Comparison of XRD analyses of the catalyst and its two components

The TGA analyses of the catalyst and its two components are shown in Figure 4.4. It is known that when heated, the metastable γ-$Al_2O_3$ transforms into the thermally stable α-$Al_2O_3$ *via* the formation of 2 transitional phases δ- and θ-$Al_2O_3$ [22-24]. These phase changes are often accompanied by the removal of hydroxyl groups, which explains the decrease in weight of the γ-$Al_2O_3$ when heated (Figure 4.4). Moreover, the weight loss of 2.8 wt.% of this material up to 800°C completely agrees with what reported in literature about the amount of chemisorbed water removed when a γ-$Al_2O_3$ sample, with similar surface area, was heated to 800°C [9].

$Na_2CO_3$, on the other hand, shows to be very stable until 850°C, which follows by a sharp decrease in weight related to the decomposition of the material into $Na_2O$ and $CO_2$. The reaction is shown below:

$Na_2CO_3 \rightarrow Na_2O + CO_2$ (Reaction 1)

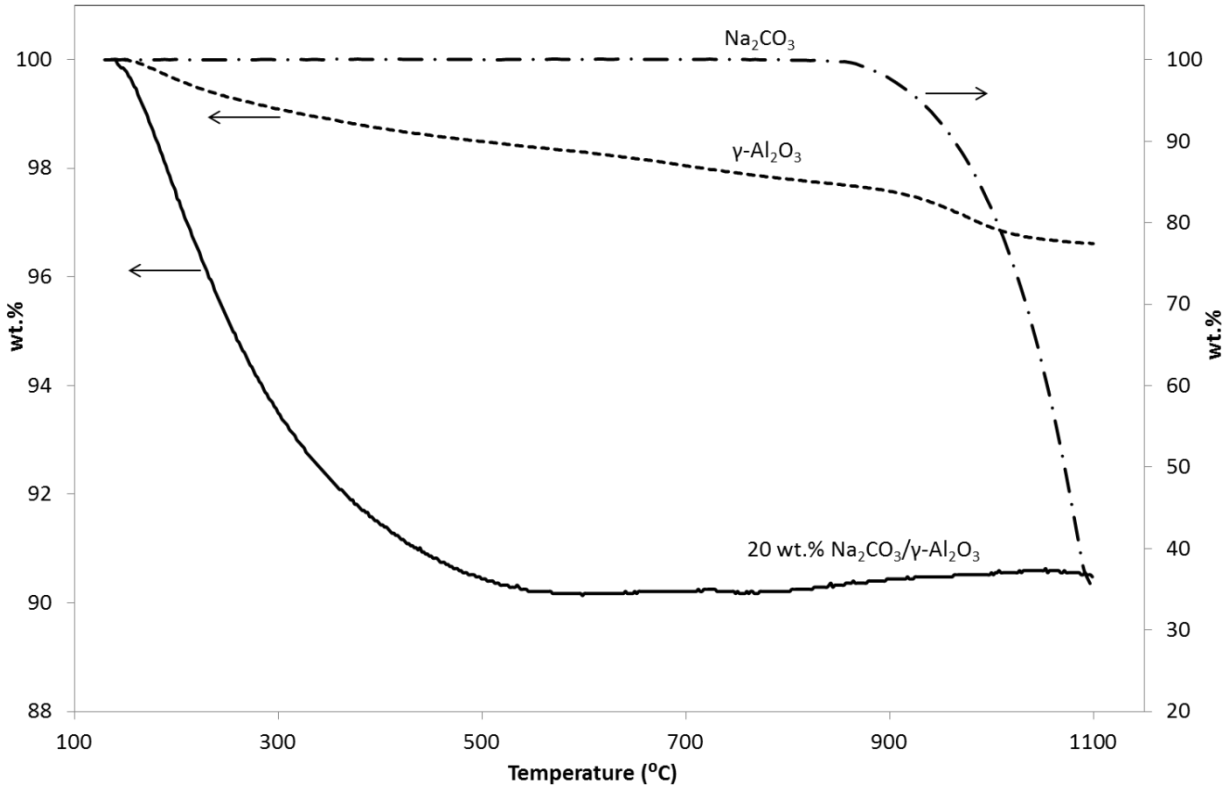


**Figure 4.4.** TGA analyses of the catalyst and its components

Based on the stoichiometry of reaction 1, it is possible to calculate the weight loss to be 41.5 wt.% if we assume 100% conversion of sodium carbonate. However, it can be seen from Figure 4.4 that the weight loss of $Na_2CO_3$ at 1100°C is 62.6 wt.%, which is significantly higher than the theoretical maximum weight loss above. This can be explained by the fact that at high temperature there are 3 processes occurring almost simultaneously in the $Na_2CO_3$ sample, which are: decomposition (reaction 1), melting and vaporization. Vaporization of $Na_2CO_3$ is responsible for this extra weight loss. However, these changes in $Na_2CO_3$ hardly influence the activity of the catalyst since all catalytic experiments were carried out at 500°C, which is well below the 900°C in the TG analysis.

The decomposition of the 20 wt.% $Na_2CO_3$/ γ-$Al_2O_3$ catalyst occurs quite differently. The catalyst showed weight decrease already at 134°C. This weight loss has a faster rate and also is larger than the maximum possible weight loss due to that of the γ-$Al_2O_3$ present (1.2 wt.% dehydration up to 500°C). This is very interesting since the pure $Na_2CO_3$, as mentioned previously, does not decompose until 850°C. This also suggests that $Na_2CO_3$ is modified in the presence of γ-$Al_2O_3$ and is present as a different chemical species in the catalyst. Any additional effect of $Na_2CO_3$ particle size will be subject of a future study.

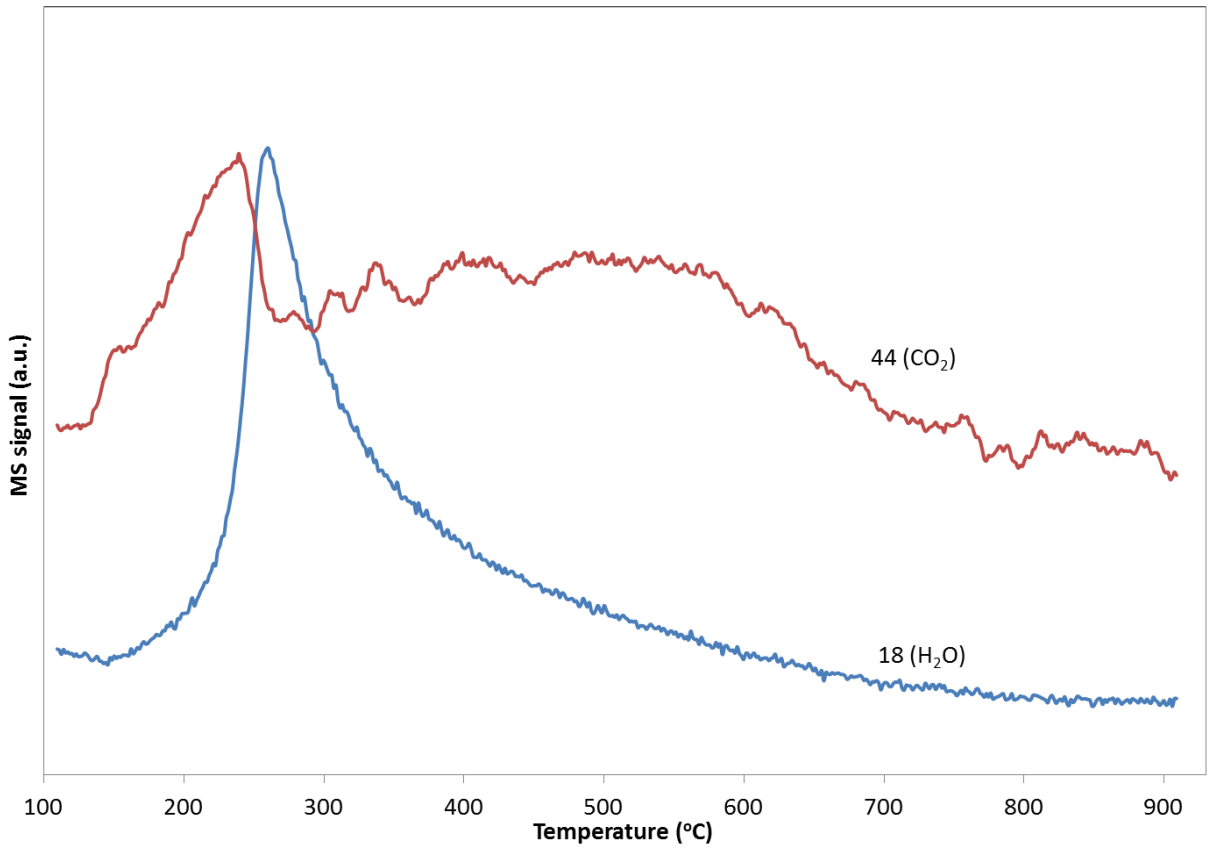


**Figure 4.5.** MS analysis of the exhaust from TGA experiment

In Figure 4.4 the weight loss for the catalyst up to 500°C, where pyrolysis experiments are carried out, is 9.6 wt.%. Taking into account its mass fraction of 80 wt.% in the catalyst, the weight loss corresponding to water removal from γ-$Al_2O_3$ is 1.2 wt.%. Thus there is an extra weight loss of 8.4 wt.%. Taking into account that $Na_2CO_3$ loading is 20 wt.%, the weight loss corresponding to its decomposition to $Na_2O$ would be 8.3 wt.%. An MS was used to analyse the volatiles coming out of the TGA and the results are shown in Figure 4.5. It can be seen that there is both $CO_2$ and water are released during the weight loss. This suggests that Na is probably present in the catalyst as a hydrated carbonate phase.

The $^{23}Na$ MAS NMR analyses of the catalyst together with that of $Na_2CO_3$ is shown in Figure S3. The $^{23}Na$ spectrum of pure $Na_2CO_3$ is characterized typically [25] by a sharp peak at 5.5 ppm a broad one around -8.5 ppm and a small peak at -1 ppm. The peaks at -1 and -8.5 are usually associated with Na ions interacting with hydroxyl groups, i.e., hydrated species [26].

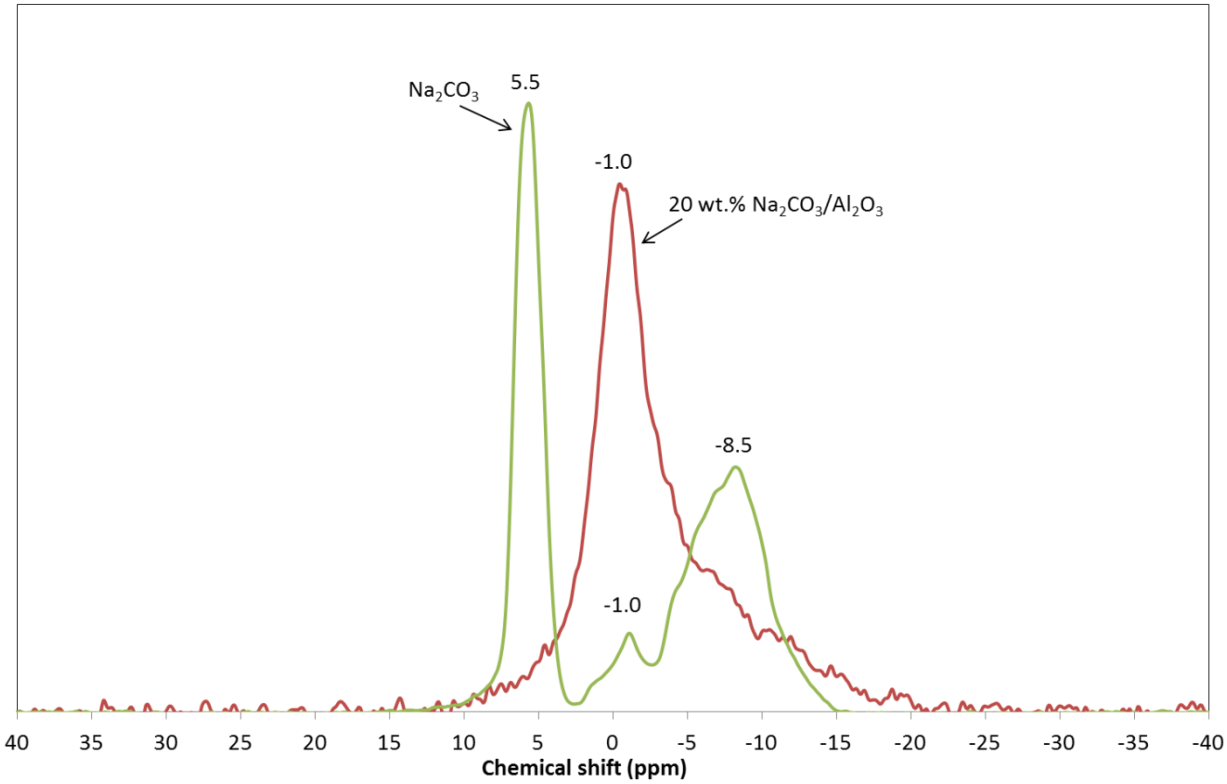


**Figure 4.4.** $^{23}$Na MAS NMR spectra of pure $Na_2CO_3$ and of the catalyst sample

Interestingly, in the case of $Na_2CO_3$/ γ-$Al_2O_3$, the two dominating peaks have either almost disappeared (5.5 ppm) or reduced in intensity and became a shoulder (-8.5 ppm). In the meantime the (relative) intensity of the peak at -1 ppm has significantly increased. NMR analyses of 5-20 wt.% $Na_2CO_3$/ γ-$Al_2O_3$ samples were carried out [26] and the peak around -1 ppm was tentatively assign to the formation $Na^+$ ions coordinating with hydroxyl group of alumina as shown below. It is possible that such an interaction is responsible for the formation of a hydrated sodium carbonate species which decomposes at lower temperatures.

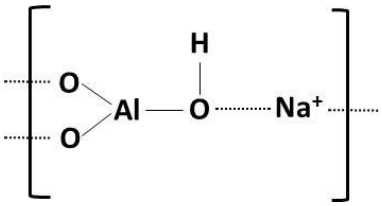


Interestingly, in the TGA experiments we see weight loss corresponding to that of sodium carbonate decomposition to sodium oxide (reaction 1). We also see MS signals corresponding to both $CO_2$ and water during this transition. This also implies that sodium is present in the catalyst as a hydrated, sodium carbonate. The catalytically active species under the pyrolysis temperatures, thus, could be sodium cations coordinated with the hydroxyl

groups of alumina in equilibrium with water and carbon dioxide present in the vapor phase. A detailed NMR study about the nature of this phase is currently in progress.

Biomass pyrolysis involves C-C, C-H and C-O bond scission and acid base properties of the catalyst plays an important role in this. Interaction of sodium ions with the hydroxyl groups of alumina probably changes the acid base properties of $\gamma$-$Al_2O_3$. The improved performance of the catalyst may be attributed to this.

*4.3.3. Catalytic bio-oil vs. fossil fuel oil*

**Table 4.6.** Comparison of key properties of non-catalytic, catalytic bio-oil and those of fuel oil

| Characteristic | Non-catalytic oil[1] | Catalytic bio-oil[2] | Fuel oil |
|---|---|---|---|
| Water content (wt.%) | 34 | 3 | 0.1 |
| C (wt.%, dry) | 52 | 78.2 | 85.3 |
| H (wt.%, dry) | 5.7 | 8.7 | 11.5 |
| O (wt.%, dry) | 42 | 12.3 | 1 |
| HHV ($MJ.kg^{-1}$) | 19 | 37 | 40 |
| pH | 2.6 | 6.5 | 5.7 |

[1]Values obtained with the non-separable organic+aqueous phase
[2]Values obtained with the organic phase

The key properties of non-catalytic and catalytic bio-oil and those of fuel oils are compared in the Table 4.6. As can be seen, with the 20 wt.% $Na_2CO_3$/ $\gamma$-$Al_2O_3$ it is possible to make a bio-oil which is by far superior to non-catalytic oil and very similar in properties to that of traditional fuel oil. The catalytic bio-oil has low oxygen content (12.3 wt.%), almost neutral (pH=6.5) and high energy density (37 MJ $kg^{-1}$). In order to reduce the oxygen content of this catalytic bio-oil to the same level as in fuel oil, a mild hydrogenation is required. Hydrogenation is also necessary to minimize the amount of carbonyls in this bio-oil as discussed previously, and to increase the yield of bio-oil.

The biggest drawback of the catalytic upgrading process is the low yield (9 wt.%) of the desired product, the catalytic bio-oil. Because of this low yield, only 21% of the initial energy in biomass was transferred into this catalytic bio-oil, compared to 48% in non-catalytic experiment, even though the energy density and other properties of the catalytic oil are much more suitable for fuel applications. The above difference in energy recovery of bio-oil resulted from the redistribution of the initial biomass energy into: (i) heterogeneous char and (ii) aqueous phase of the catalytic liquid. Thus, to overcome this problem and to increase the

energy efficiency of the process, it is necessary to extract the energy from the two mentioned side products, for *e.g.* by burning the heterogeneous char to generate process heat and reforming the aqueous phase to produce hydrogen. In short, despite of the high de-oxygenation achieved with $Na/Al_2O_3$ catalyst, the extremely high amount of heterogeneous char formed on the catalyst not only makes the process less efficient by reducing the yield of bio-oil and the energy recovery but also poses a huge problem in catalyst handling. Intensive research therefore should be carried out to inhibit heterogeneous char formation on the catalyst and taken into account in the catalyst design before it can be applied in real life.

It can be seen from Table 4.1 that the liquid product obtained from our catalytic pyrolysis experiment consists of 22 wt.% yield of water, 9 wt.% of organic phase (bio-oil) and 6 wt.% of aqueous phase (oxygenates). This organic phase contains 12.3 wt.% of oxygen. Thus, complete de-oxygenation by hydrogenation of the phase will require 1.86 moles of hydrogen per 1 kg of the total liquid. $H_2$ can be generated by reforming of the oxygenates in the aqueous phase of bio-oil [27]. It was shown recently by us that [27] the maximum amount of hydrogen that can be generated from these oxygenates *via* a combination of steam reforming and water gas shift reactions is 15.6 moles per 1 kg of the total liquid. These calculations show that the amount of hydrogen obtained from the aqueous phase is more than enough for de-oxygenation of the organic phase to achieve similar oxygen content as in fuel oil. Hence, the integration of reforming of the aqueous phase to generate hydrogen to the upgrading of the organic phase shows very promising in an economical point of view.

## 4.4. Conclusions

Compared to non-catalytic pyrolysis, catalytic upgrading in the presence of $Na_2CO_3$/ $\gamma$-$Al_2O_3$ results in higher level of selective de-oxygenation with the oxygen ending up in heterogeneous char or removed as COx. Interaction between sodium and alumina present in the catalyst leads to the emerge of a new sodium phase, in which Na ions likely coordinates with hydroxyl group of alumina. The bio-oil obtained from catalytic experiment has comparable properties to those of fuel oil, for *e.g.* neutral in terms of acidity/basicity (pH=6.5) and possesses high energy density (37 MJ $kg^{-1}$ of bio-oil compared to 40 MJ $kg^{-1}$ of fuel oil).

# References


[1] I.V. Babich, M. van der Hulst, L. Lefferts, J.A. Moulijn, P. O'Connor, K. Seshan, Biomass and Bioenergy 35 (2011) 3199-3207.

[2] P. O'Connor, D. Stamires, S. Daamen, Process for the conversion of biomass to liquid fuels and specialty chemicals, KiOR, Inc, 2012.

[3] A. Saddawi, J.M. Jones, A. Williams, Fuel Processing Technology 104 (2012) 189-197.

[4] S.D. Stefanidis, K.G. Kalogiannis, E.F. Iliopoulou, A.A. Lappas, P.A. Pilavachi, Bioresour. Technol. 102 (2011) 8261-8267.

[5] S. Yorgun, Y.E. Şimşek, Bioresour. Technol. 99 (2008) 8095-8100.

[6] G.W. Huber, S. Iborra, A. Corma, Chem. Rev. 106 (2006) 4044-4098.

[7] J. Xu, J. Jiang, W. Lv, W. Dai, Y. Sun, Biomass Bioenergy 34 (2010) 1059-1063.

[8] T.S. Nguyen, M. Zabeti, L. Lefferts, G. Brem, K. Seshan, Biomass Bioenergy 48 (2013) 100-110.

[9] J. Medema, J.J.G.M. Van Bokhoven, A.E.T. Kuiper, J. Catal. 25 (1972) 238-244.

[10] E. Henrich, S. Bürkle, Z.I. Meza-Renken, S. Rumpel, J. Anal. Appl. Pyrolysis 49 (1999) 221-241.

[11] M. Stals, R. Carleer, G. Reggers, S. Schreurs, J. Yperman, J. Anal. Appl. Pyrolysis 89 (2010) 22-29.

[12] A. Dominguez, J.A. Menendez, M. Inguanzo, P.L. Bernard, J.J. Pis, J. Chromatogr. A 1012 (2003) 193-206.

[13] A.R. Goncalves, U. Schuchardt, D. Meier, O. Faix, J. Anal. Appl. Pyrolysis 40-1 (1997) 543-551.

[14] N. Marin, S. Collura, V.I. Sharypov, N.G. Beregovtsova, S.V. Baryshnikov, B.N. Kutnetzov, V. Cebolla, J.V. Weber, J. Anal. Appl. Pyrolysis 65 (2002) 41-55.

[15] G.W. Huber, S. Iborra, A. Corma, Chem. Rev. 106 (2006) 4044-4098.

[16] A. Oasmaa, D.C. Elliott, J. Korhonen, Energy Fuels 24 (2010) 6548-6554.

[17] L. Deng, Y. Fu, Q. Guo, Energy Fuels 23 (2008) 564-568.

[18] J. Diebold, A review of the chemical and physical mechanisms of the storage stability of fast pyrolysis bio-oils, National Renewable Energy Laboratory, Golden, Colorado, 2000, p. 60.

[19] C.J. Barrett, J.N. Chheda, G.W. Huber, J.A. Dumesic, Appl. Catal. B 66 (2006) 111-118.

[20] G.W. Huber, J.N. Chheda, C.J. Barrett, J.A. Dumesic, Science 308 (2005) 1446-1450.

[21] A. Khaleel, S. Al-Mansouri, Colloids Surf. A 369 (2010) 272-280.

[22] R.S. Zhou, R.L. Snyder, Acta Crystallogr. B 47 (1991) 617-630.

[23] H.D. Santos, P.D. Santos, Mater. Lett. 13 (1992) 175-179.

[24] M. Bodaghi, A.R. Mirhabibi, H. Zolfonun, M. Tahriri, M. Karimi, Phase Transit. 81 (2008) 571-580.

[25] A.R. Jones, R. Winter, G.N. Greaves, I.H. Smith, J. Phys. Chem. B 109 (2005) 23154-23161.

[26] F. Deng, Y. Du, C. Ye, Y. Kong, Solid State Nucl. Magn. Reson. 2 (1993) 317-324.

[27] D. de Vlieger, Design of efficient catalysts for gasification of biomass-derived waste streams in hot compressed water- Towards industrial applicability, PhD thesis, Univ Twente ISBN 978–90–365–3492–5, 2012.

# Chapter 5

## Catalytic conversion of biomass pyrolysis vapours over sodium-based catalyst: A study on the state of sodium on the catalyst

*To be submitted to ChemCatChem*

**Abstract.** Study using TGA-MS and $^{23}Na$ and $^{1}H$ MAS NMR techniques reveal the formation of a new sodium specie in the catalyst, which is responsible for the high catalytic activity. This specie is later proposed to be formed by the coordination of $Na^{+}$ ions and the hydroxyl groups on the surface of $\gamma$-$Al_2O_3$. Regeneration of the catalyst was carried out in air at 600$^{o}$C and the regenerated material shows to have lower activity towards de-oxygenation compared to fresh catalyst. This deactivation is likely attributed to the change in the active sodium specie during regeneration.

## 5.1. Introduction

Faujasite materials with various concentrations of ion $Na^+$ was used as the de-oxygenation catalyst in Chapter 3. It was shown that sodium ions positively influenced the de-oxygenation of bio-oil, reduced the amount of acids, aldehydes/ketones and enhanced the hydrocarbon content and thus the energy density of the oil. $Na_2CO_3$ was shown to promote the de-oxygenation of bio-oil during pyrolysis of chlorella algae, shown by the significant increase in the energy density of bio-oil from 21 $MJ.kg^{-1}$ (non-catalytic) to 32 $MJ.kg^{-1}$ (with $Na_2CO_3$) at 450°C [1]. It was shown that a bio-crude oil with energy density close to that of petroleum crude oil (30 MJ $kg^{-1}$) could be produced by liquefaction of microalgae, and a high yield of 51.6 wt.% of bio-crude oil was obtained with $Na_2CO_3$ catalyst [2]. Additionally, $Na_2CO_3$ resulted in higher selectivity to mono-aromatic components in the bio-crude oil.

Despite being a very promising catalyst for the conversion of biomass, $Na_2CO_3$ itself has low surface area and has a tendency to form clusters in presence of water, and is susceptible to attrition due to low mechanical strength. For a typical fluidised bed pyrolysis process, anchoring sodium carbonate on a mechanically strong support would be essential. For this reason, γ-$Al_2O_3$ was employed as the support for $Na_2CO_3$. The upgrade of pyrolysis vapour over $Na_2CO_3$/γ-$Al_2O_3$ catalyst was studied in Chapter 4. The advantages of this support compared to H-FAU are: (i) being lower in acidity lowered conversion of bio-oil into unwanted coke *via* oligomerisation reactions and water formation *via* dehydration, both of which are acid catalysed reactions and (ii) possessing bigger pores (mesoporous) which grant access to the larger molecules formed during pyrolysis. Moreover, γ-$Al_2O_3$ possesses a defect lattice structure that is terminated by surface hydroxyl groups [3], which play an important role in the acidity and hence the catalytic activity of this oxide [4]. It was concluded that at high calcination temperature of 800 $^oC$, the concentration of –OH groups on the surface of alumina was lower than those at lower temperatures and this was shown to correlate to the acidity and catalytic activity of this material [4].

It was shown in Chapter 4 that the bio-oil obtained by applying $Na_2CO_3$/γ-$Al_2O_3$ catalyst possessed superior quality compared to that from non-catalytic experiment. This catalytic bio-oil is almost neutral in term of acidity, has much lower oxygen content (~12 wt.%) than that of non-catalytic oil (~42 wt.%) and approaches the energy density of fuel oil

(37 $MJ.kg^{-1}$). One aspect of the catalyst was that it generated higher amounts of carbonyl components in the bio-oil, which can cause stability problems due to condensation reaction with alcohols, e.g. phenols.

The purpose of this present chapter is to gain an insight to the state of sodium in the catalyst, interaction between sodium and alumina support and identify the active catalytic site involved in the de-oxygenation of bio-oil. Such a study is aimed at looking at the possibility to improve the efficiency of the catalyst also with further modification.

## 5.2. Experimental

### *5.2.1. Catalyst preparation and characterisation*

$Na_2CO_3/\gamma$-$Al_2O_3$ catalysts with different $Na_2CO_3$ concentrations were prepared as described in section 2.2.2. Catalysts were characterized by XRF, BET, XRD, TGA-MS, $^{23}Na$ $^{1}H$ and $^{27}Al$ MAS NMR. These techniques are further described in section 2.3.1.

### *5.2.2. Catalytic testing*

The experimental set-up and applied definitions are described in detail in Chapter 2. For each experiment 2 g of biomass and 1 g of catalyst were used. Temperature of the pyrolysis and catalyst bed was set at 500$^{o}$C. Duration of all experiments was 10 min. The flow rate of Ar was 70 $mL.min^{-1}$, which gave an average vapour residence time of 4 sec. Products of the catalytic pyrolysis process were subjected to GC, elemental analysis and bomb calorimetry. Details of these analyses were given in section 2.3.2.

## 5.3. Results and discussion

### *5.3.1. Catalytic upgrading of bio-oil*

Results of the catalytic and non-catalytic pyrolysis experiments with pine wood, are summarised in Table 5.1. Compared to thermal pyrolysis, catalytic experiments resulted in higher yields of gas and solid and lower yields of liquid bio-oil product. The fact that more gas and solid products formed in catalytic experiments can be attributed to secondary reactions of organic components present in the pyrolysis vapours, involving C-C, C-O, and C-H bond cleavages, in presence of the catalysts. It can be seen that the two $Na_2CO_3/\ \gamma$-$Al_2O_3$ materials were the most active for de-oxygenation of bio-oil. The oxygen contents of bio-oils

obtained in presence of these two catalysts are in the range of 12 wt.%, which is about a half of those from other materials (22 wt.%) and a fourth of that from non-catalytic pyrolysis (42 wt.%).

**Table 5.1.** Summary of pyrolysis of biomass over different catalytic materials

| | Product yields (wt.%) | | | Bio-oil's properties | | $CO_2$ yields (wt.%) |
|---|---|---|---|---|---|---|
| | Liquid | Solid | Gas | Oxygen content (wt.%) | HHV (MJ $kg^{-1}$) | |
| Thermal (No catalyst) | 61 | 19 | 13 | 42.1 | 19 | 5.1 |
| γ-$Al_2O_3$ | 44 | 28 | 18 | 22.8 | 31 | 8.3 |
| $Na_2CO_3$ | 40 | 35 | 16 | 23.3 | 30 | 10.4 |
| 20 wt.% $Na_2CO_3$/ γ-$Al_2O_3$ | 37 | 34 | 23 | 12.3 | 37 | 12.1 |
| 33 wt.% $Na_2CO_3$/ γ-$Al_2O_3$ | 39 | 30 | 22 | 13.1 | 37 | 12.2 |

This decrease in oxygen content was accompanied by a tremendous increase in the energy content of bio-oil to 37 MJ $kg^{-1}$, approaching that of fossil fuel oil (42 MJ $kg^{-1}$). In addition, it can be seen that the two $Na_2CO_3$/γ-$Al_2O_3$ catalysts are the most selective among the tested materials for the de-oxygenation of pyrolysis vapour into $CO_2$, shown by the highest $CO_2$ yield of 12 wt.% (Table 5.1). This selectivity towards $CO_2$ is desirable in biomass de-oxygenation in order to minimize carbon loss. $CO_2$ yields reported are not influenced by the $CO_2$ formed from the decomposition of $Na_2CO_3$ at the pyrolysis experimental temperature. This is because, (i) the catalysts were activated *in-situ* at 500$^oC$ under Ar flow for 30 min before each experiment and (ii) as will be shown later (section 5.3.2.2) $Na_2CO_3$ fraction in the supported catalysts readily decompose at 500$^oC$ into $CO_2$ and $Na_2O$.

The properties of bio-oil reported in Table 5.1, for the $Na_2CO_3$/ γ-$Al_2O_3$ catalyst are very promising while considering its application as a fossil fuel additive/substitutes [5]. Detailed characterisation of this catalyst is discussed in the section below, to enable understanding of its catalytic function.

*5.3.2. Characterization of the catalysts*

*5.3.2.1. X-ray diffraction (XRD)*

X-ray diffractograms of the supported catalyst and related materials are shown in Figure 5.1. As already shown in Chapter 4, $Na_2CO_3$ is very crystalline, illustrated by multiple sharp peaks in the 2θ = 20-90$^o$ range. In the diffractogram of γ-$Al_2O_3$ three broad peaks were observed at 2θ of 38$^o$, 46$^o$ and 66$^0$ which is correlated to three different planes in the oxide's crystal [6].

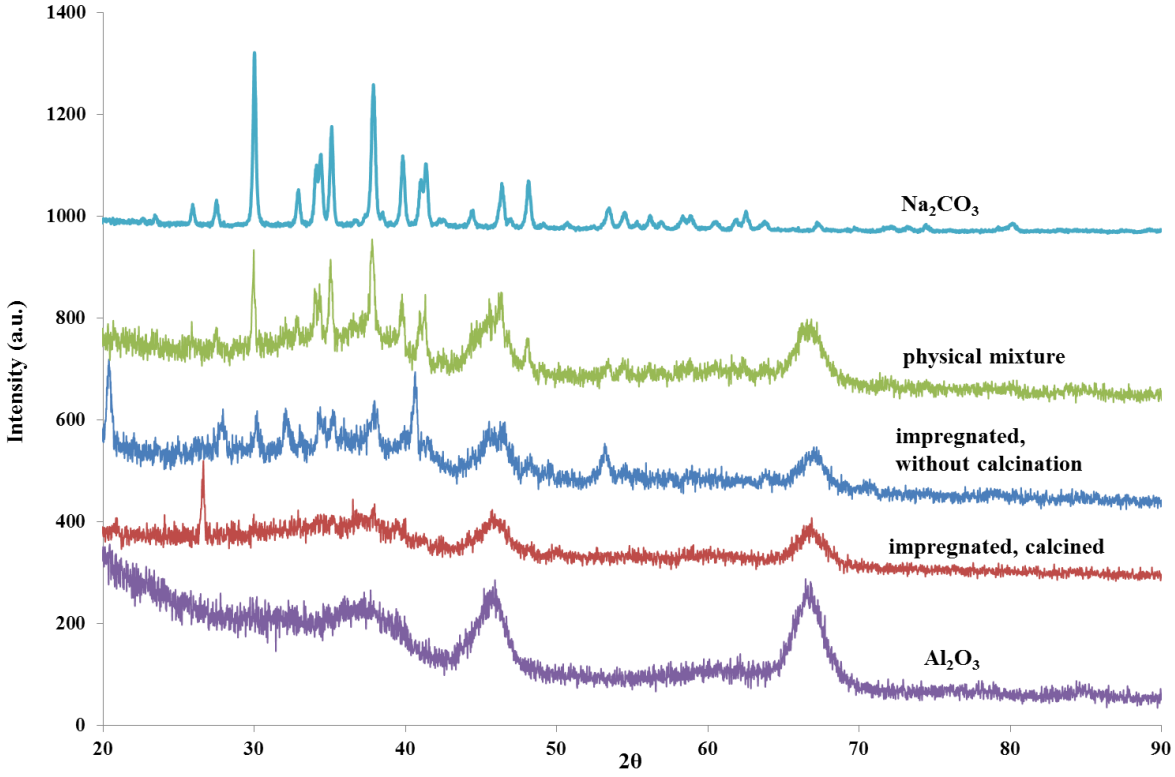


**Figure 5.1.** Comparison of different sodium carbonate dispersion shown by XRD diffractograms

In our study, $Na_2CO_3$ was brought into contact with the support using different methods, which are: (i) mixing the salt and support physically, or (ii) impregnation of $Na_2CO_3$ onto γ-$Al_2O_3$ followed by calcination. It can be seen that there is almost no separate phase of sodium detected in the material prepared using wet impregnation followed by calcination. This is completely different compared to the X-ray diffractogram of the sample in which $Na_2CO_3$ and γ-$Al_2O_3$ was physically mixed. The peaks belonging to both $Na_2CO_3$ and γ-$Al_2O_3$ components were all detected in the physically-mixed sample. Absence of sharp peaks for the

calcined catalyst indicates that sodium is present as well-dispersed small crystallites of $Na_2CO_3$ or as another amorphous phase interacting with alumina support.

*5.3.2.2. TGA analyses*

The TGA analyses of the calcined catalysts are shown in Figure 5.2. It is known that, when heated, the metastable γ-$Al_2O_3$ transforms into the thermally stable α-$Al_2O_3$ *via* the formation of two transitional phases δ- and θ-$Al_2O_3$ [7-9].

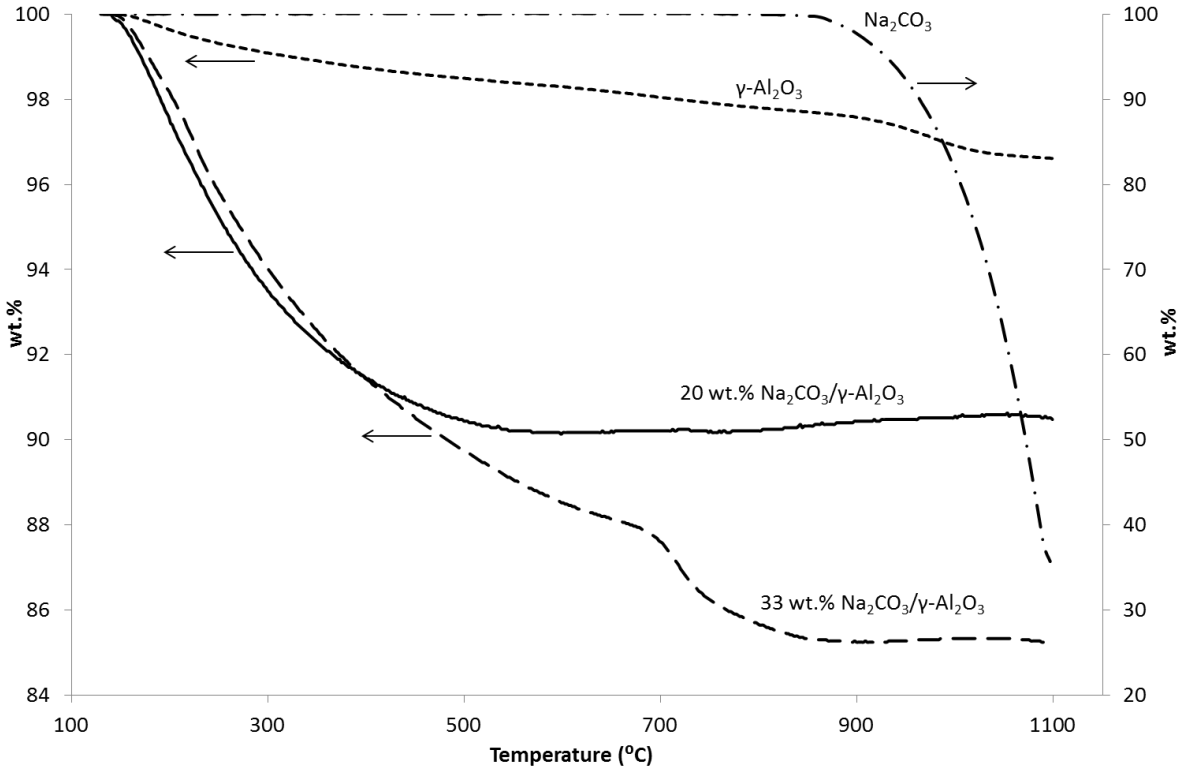


**Figure 5.2.** TGA analyses of the catalysts

These phase changes are often accompanied by condensation involving hydroxyl groups (dehydration) forming water, which explains the decrease in weight of the γ-$Al_2O_3$ when heated (Figure 5.2). Pure $Na_2CO_3$, on the other hand, showed to be very stable until 850 $^oC$, followed by a sharp weight loss which corresponded to the decomposition to $Na_2O$ and $CO_2$. This decomposition was further confirmed by the detection of $CO_2$ signal (m/e = 44) using a mass spectrometer connected to the outlet of the TGA. The total weight loss of $Na_2CO_3$ observed up to 1100 °C in Figure 5.2 is 20% higher than the maximum weight loss due to decomposition alone. We have shown recently that this is due to the fact that the

decomposition of $Na_2CO_3$ can be accompanied by reported vaporization and/or sublimation of $Na_2O$ at these high temperatures (*ca.*1000$^oC$) [10, 11], which caused a further mass loss compared to that calculated from stoichiometry of the decomposition reaction to sodium oxide. This is not an issue in the current work as the pyrolysis experiments were carried out at the lower temperature of 500 $^oC$.

The decomposition of the 20 and 33 wt.% $Na_2CO_3$/ γ-$Al_2O_3$ catalysts occurred quite differently. Both of the materials showed weight decrease already at 135 $^oC$. This weight loss cannot be solely attributed to the dehydration of γ-$Al_2O_3$ since both the rate of decrease and the total weight loss are much higher than those observed during γ-$Al_2O_3$ dehydration. Therefore it can be deduced that not only γ-$Al_2O_3$ but also decomposition of $Na_2CO_3$ have contributed to this weight loss. To confirm this further, a MS was connected to the outlet of the TGA in order to identify volatiles released during the TGA experiments. It was found that two MS peaks corresponding to $CO_2$ and $H_2O$ emerged at the same temperature region as the weight loss. Comparing the profile and decomposition temperature of $Na_2CO_3$ in its pure form (850 $^oC$) to those in the supported catalysts (135 $^oC$), it can be concluded that $Na_2CO_3$ is present in the supported catalysts in a different state. This new specie is likely formed due to the interaction between $Na_2CO_3$ and γ-$Al_2O_3$

From Figure 5.2, it can be seen that the total observed weight losses of the 20 and 33 wt.% $Na_2CO_3$/ γ-$Al_2O_3$ catalysts up to 900 $^oC$ are 10 and 15%, respectively. The corresponding contributions of γ-$Al_2O_3$ to the above weight losses are 2.02 and 1.69%, respectively. These values were calculated based on the observed weight loss of γ-$Al_2O_3$ and its corresponding concentrations in the supported materials (80 and 77 wt.%). Thus the contributions from $Na_2CO_3$ fraction in the two supported catalysts can then be calculated and are both shown to correspond to the decomposition of $Na_2CO_3$ into $Na_2O$ and $CO_2$. Interestingly, there seem to be two different weight loss regions in the TGA curve of the 33 wt.% $Na_2CO_3$/ γ-$Al_2O_3$ observed in Figure 5.2, separated by a small plateau at *ca.* 700 $^oC$. This should correspond to two different sodium species co-existing in this catalyst, which will be discussed in the next section.

*5.3.2.3. MAS NMR analyses*

The $^{23}Na$ MAS NMR spectra of $Na_2CO_3$/γ-$Al_2O_3$ samples with different $Na_2CO_3$ concentrations were compared with each other and with other sodium-containing compounds,

of which the results are summarized in Figure 5.3. It can be seen in Figure 5.3a that spectrum of the 100% $Na_2CO_3$ sample (pure $Na_2CO_3$) is characterized by two high-intensity peaks at 5.6 and -8.3 ppm, and a shoulder with much lower intensity at -1.6 ppm. Base on the literature work [12-18], these three resonances can be unambiguously assigned to the $^{23}Na$ ions located at three different sites; the chemical shifts are slightly changed because of different local environments.

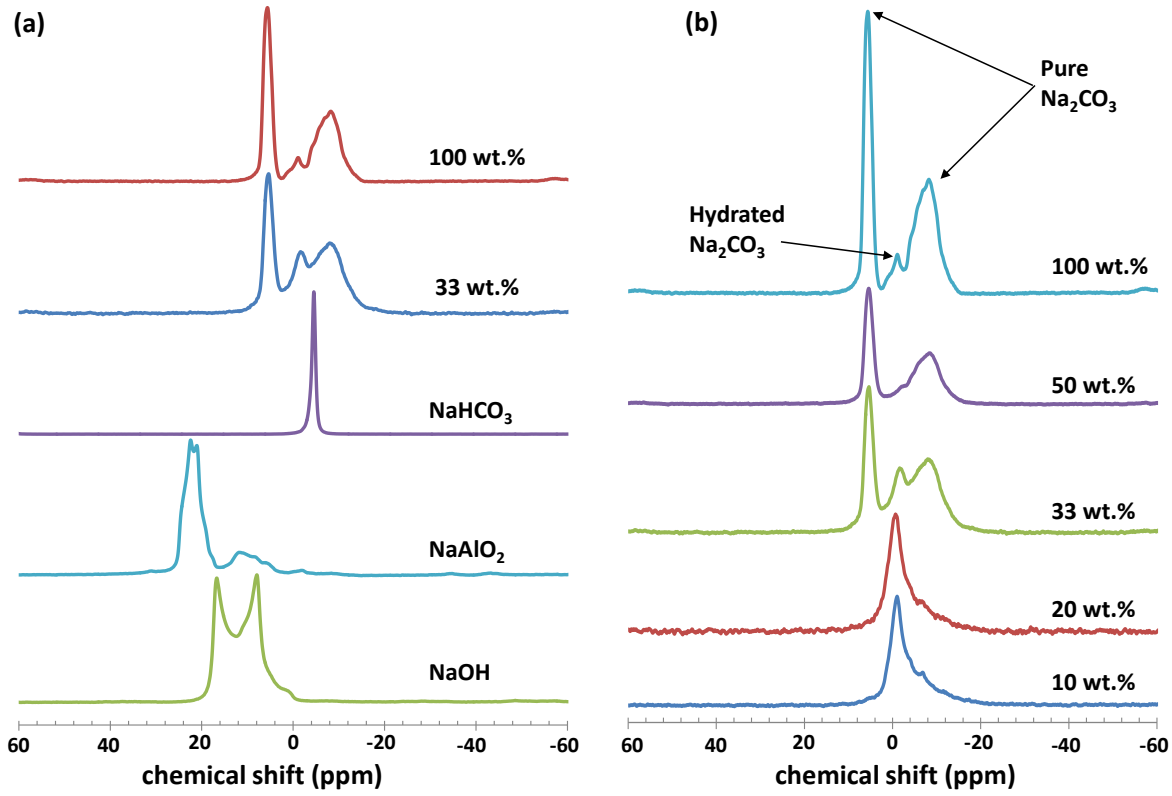


**Figure 5.3.** $^{23}Na$ MAS NMR spectra of (a) pure $Na_2CO_3$, 33 wt.% $Na_2CO_3$/ γ-$Al_2O_3$ and several sodium-containing candidates and (b) $Na_2CO_3$/ γ-$Al_2O_3$ with different mass concentrations of $Na_2CO_3$

Jones *et al.* [19] studied glass-forming reactions between $Na_2CO_3$ and $SiO_2$ using MAS NMR technique and observed two peaks in the $^{23}Na$ spectrum of $Na_2CO_3$ sample. These peaks were later assigned to the two crystallographic $Na^+$ sites in $Na_2CO_3$ structure [19]. However, details of the nature of these two sites were not discussed. The crystal structure of $Na_2CO_3$ has been investigated previously by others [20, 21]. Symmetrically independent cations (labelled 1,2,3) $Na^+_1$, $Na^+_2$ and $Na^+_3$ were shown to be present in $Na_2CO_3$ (Figure 5.4). The structure of sodium carbonate can be described as containing graphite-like layers formed

by $Na^{+}_3$ cations and $CO_3^{2-}$ anions, which are stacked along the hexagonal axis [21]. Additional $Na^{+}_1$, $Na^{+}_2$ cations are located in the hexagonal channels. Intuitively, it can be seen that the environment surrounding $Na^{+}_1$, $Na^{+}_2$ are very similar to each other while that of $Na^{+}_3$ is different (Figure 5.4). It is thus expected that the $^{23}Na$ MAS NMR signal corresponding to $Na^{+}_1$ and $Na^{+}_2$ will evolve at the same or very similar chemical shift. The average $Na_1$-O, $Na_2$-O and $Na_3$-O distances in $Na_2CO_3$ were shown to be 2.36, 2.38 and 2.70 $A^o$ , respectively [20]. It is interesting to note that the $Na_1$-O and $Na_2$-O distances are very similar to the sum of individual ionic radii for $Na^+$ (1.02 $A^o$) and $O^{2-}$ (1.40 $A^o$).

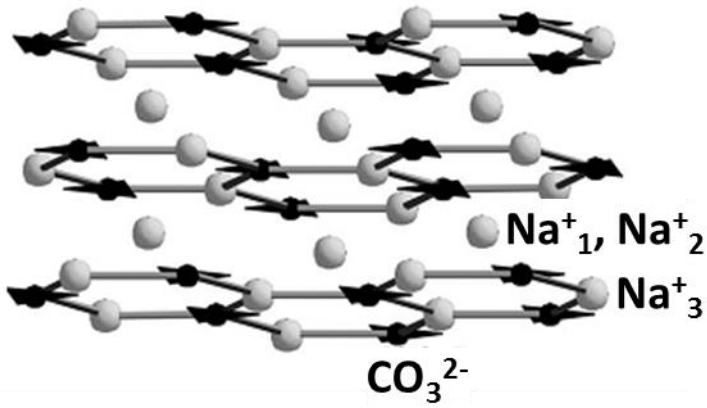


**Figure 5.4.** The crystal structure of $Na_2CO_3$ showing positions of sodium cations and carbonate anions according to Arakcheeva and Chapuis [21]

This strong sodium-oxygen interaction has been explained to cause sufficient electron transfer from the oxygen anion to the 3p orbital of the sodium ion, increasing the paramagnetic shielding contribution to the $^{23}Na$ chemical shift [22]. Consequently, the $^{23}Na$ NMR signal corresponding to $Na^{+}_1$ and $Na^{+}_2$ is expected to be more deshielded, *i.e.* moving to higher chemical shift, compared to that of $Na^{+}_3$. For this reason, it is likely that the peak that emerges at 5.6 ppm corresponds to $Na^{+}_1$ and $Na^{+}_2$ and that at -8.3 ppm to $Na^{+}_3$. The shoulder appearing at -1.6 ppm might be attributed a different sodium phase presenting in small amounts in $Na_2CO_3$ material.

Interestingly, the three peaks at -8.3, -1.6 and 5.6 ppm were also observed in the 33 wt.% $Na_2CO_3$/ $\gamma$-$Al_2O_3$ sample (Figure 3a). However, the intensity of the shoulder at -1.6 ppm has increased significantly compared to that in pure $Na_2CO_3$. An investigation has been carried out in order to identify this phase. $^{23}Na$ NMR spectra of sodium-containing compounds which might exist in $Na_2CO_3$ and $Na_2CO_3/Al_2O_3$ materials, namely sodium

aluminate [23], sodium bicarbonate [24] and sodium hydroxide [23, 25], were recorded and shown in Figure 3a. However, none of their chemical shift matches with the shoulder at -1.6 ppm.

It was shown previously with TGA-MS analysis of the 33 wt.% $Na_2CO_3/Al_2O_3$ that there are 2 regions of weight loss possibly corresponding to two phases of sodium in this material: one starts at as low as 135 $^oC$ and the other at around 700 $^oC$. Both of those weight losses were accompanied by the formation of $CO_2$ and, in the case of the weight loss at 135$^oC$, also by the formation of $H_2O$. Thus the sodium phase decomposed at 700 $^oC$ might be assigned to pure $Na_2CO_3$ and the one at 135 $^oC$ to a hydrated phase of sodium. This hydrated specie can be responsible for the shoulder at -1.6 ppm mentioned previously. The higher intensity of the -1.6 ppm shoulder in the 33 wt.% $Na_2CO_3/Al_2O_3$ sample shows that the hydrated specie is more abundant in the supported sodium material than in the pure $Na_2CO_3$. This can be attributed to the known availability of hydroxyl groups of the surface of $\gamma$-$Al_2O_3$ [26, 27] and is described in details in the next paragraph.

To further confirm the nature of this sodium specie, $^{23}Na$ NMR spectra of $Na_2CO_3/Al_2O_3$ samples with different $Na_2CO_3$ mass concentration were recorded and shown in Figure 3b. It can be seen that only one resonance line at -1.0 ppm was observed in the samples with low concentrations of $Na_2CO_3$ (10 and 20 wt.%). Two extra peaks at 5.6 and -8.3 ppm emerged in the sample with 33 wt.% $Na_2CO_3$. Further increase in $Na_2CO_3$ concentration resulted in the increase in intensity of these two peaks relatively to the one at -1.0 ppm. One can also observe that the peak at -1.0 ppm in the samples with 10 and 20 wt.% $Na_2CO_3$ has been shifted to -1.6 and -1.8 ppm in the 33, 100 and 50 wt.% samples, respectively. It is known that hydroxyl groups presenting on the surface of alumina possesses both acidic and basic properties [28]. At low coverage of $Na_2CO_3$ (10 and 20 wt.%), the sodium salt can interact with the hydroxyl groups on the surface of the support to form a surface hydrated specie as can be seen below:

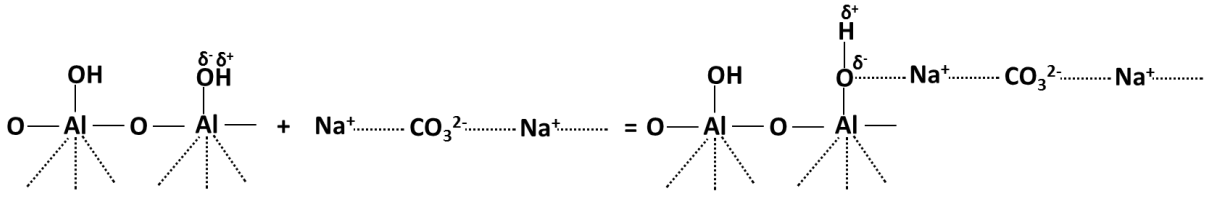

Similarly, the pure $Na_2CO_3$ sample (100 wt.%) is able to absorb moisture during storage, resulting in the formation of a hydrated specie:

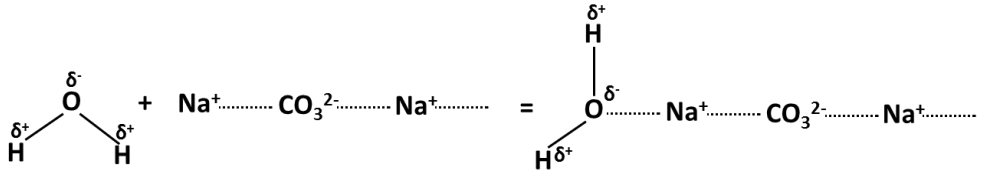


The electronic environment surrounding $Na^+$ ions in these two hydrated species are very similar and thus we propose that they resulted in two close peaks at -1.0 and -1.6 ppm in the $^{23}Na$ NMR spectra. $^1H$ MAS NMR measurements of the 10 wt.% $Na_2CO_3/Al_2O_3$ and pure $Na_2CO_3$ samples have provided us with additional insights into the local environments of H in those materials (Figure 5.5).

It can be observed in Figure 5.5 that there is one sharp peak at *ca.* 5 ppm in the proton NMR spectrum of the10 wt.% $Na_2CO_3/\gamma$-$Al_2O_3$ sample. In Fig 3(b), we attributed for the same sample a peak at -1 ppm to hydrated sodium specie. We propose that the $^1H$ MAS NMR peak at 5 ppm (Figure 5.5) corresponds to the same hydrated sodium specie discussed earlier. On the other hand, the formation of two distinct peaks was witnessed in the proton NMR spectrum of the pure (100 wt.%) $Na_2CO_3$ sample. The first sharp peak at *ca.* 18 ppm can be attributed to the proton of an acid, likely the carbonic acid formed by the interaction of $CO_3^{2-}$ ion and the physisorbed $H_2O$. The second peak is very broad and found in the same chemical shift region as of the peak in the10 wt.% $Na_2CO_3/\gamma$-$Al_2O_3$ sample (Figure 5.5). Thus this broad peak and the peak observed in the 10 wt.% $Na_2CO_3/\gamma$-$Al_2O_3$ sample should correspond to the proton in sodium species hydrated by (i) the physisorbed $H_2O$ and (ii) the –OH groups of $Al_2O_3$, respectively. Additionally, it can be seen that the peak obtained with pure $Na_2CO_3$ sample is much broader compared to the peak of the 10 wt.% sample. This suggests the high availability and widely spreading of physisorbed $H_2O$ in the hygroscopic $Na_2CO_3$ sample; which is contrasted to the limited presence only at the sodium-alumina interface of the –OH groups in the 10 wt.% $Na_2CO_3/\gamma$-$Al_2O_3$ sample. Number of hydroxyl groups on the surface of alumina is limited and hence increasing the $Na_2CO_3$ concentration lead to the saturation of $Na^+$ ions interacting with the hydroxyl group on the surface of the support.

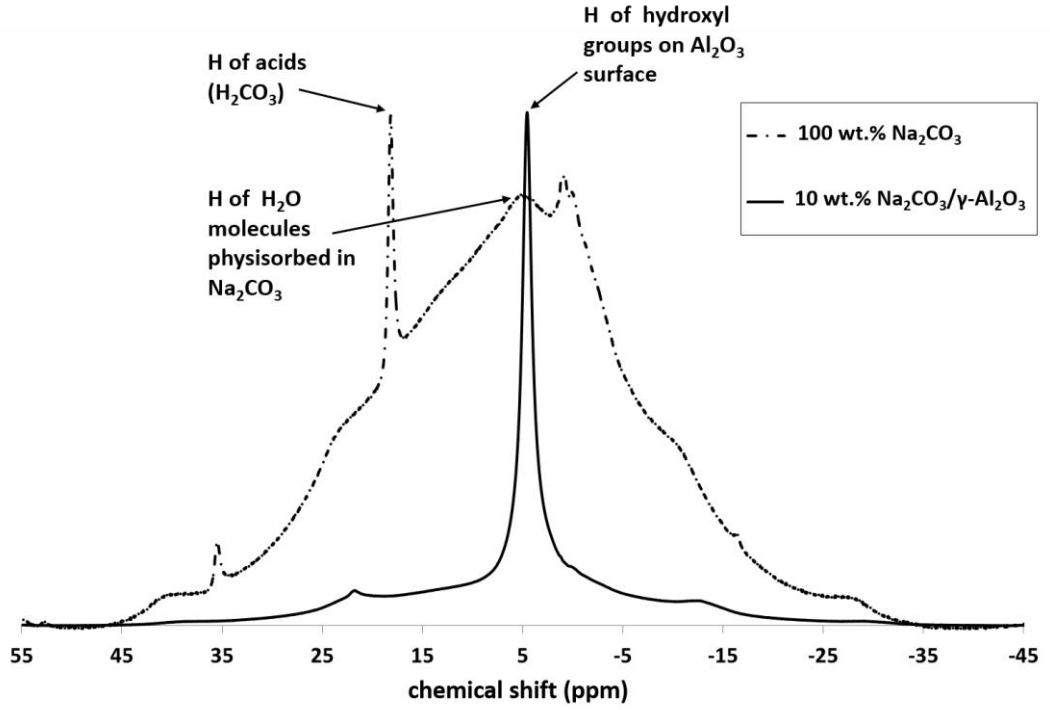


**Figure 5.5.** Comparison between $^{1}H$ MAS NMR spectra of 10% $Na_2CO_3$/γ-$Al_2O_3$ and pure $Na_2CO_3$ samples

To estimate the concentration corresponding to $Na^+$ saturation, a monolayer coverage model was computed. As the ionic radius of $O^{2-}$ (1.40 Å) is much larger than that of $Al^{3+}$ (0.51 Å), it can be considered that the surface of γ-$Al_2O_3$ is mainly covered by oxygen atoms [29]. The surface area of γ-$Al_2O_3$ used in our study was measured at 249 $m^2$ per gram. The area covered by each oxygen atom is $2\pi R_o^2$ ($R_o$ is the ionic radius of oxygen), so an area of 249 $m^2$ is covered by $249/2\pi R_o^2$ oxygen atoms. Assuming that each atom is associated with one $Na^+$ ion, one can easily calculate the concentration of $Na_2CO_3$ corresponding to a monolayer coverage, which is 19.9 wt.%. Thus the observed change in $^{23}Na$ NMR spectra when the loading was increased from 10 to 50 wt.% could be explained as follows: During impregnation, sodium ions are homogenously distributed over the alumina surface (see section 3.2.1) and closely coordinated with the surface hydroxyl groups. The formed surface hydrated specie resulted in a peak at -1.0 ppm in the chemical shift. When the amount of $Na_2CO_3$ was increased to 20 wt.%, all oxygen atoms of γ-alumina are coordinated with $Na^+$ ions, forming a monolayer of the surface hydrated specie. The additional $Na_2CO_3$ will be deposited on top of this monolayer and begins to form clusters, *i.e.* the surface $Na_2CO_3$ aggregates, which corresponds to the two peaks at 5.6 and -8.3 ppm. By increasing the

loading of $Na_2CO_3$ from 33 to 50 wt.%, only the amount of surface $Na_2CO_3$ cluster increases while the amount of hydrated specie remains unchanged, and this resulted in an increase in the relative intensity of the two peaks at 5.6 and -8.3 ppm. The deposition of the surface $Na_2CO_3$ cluster changes the environment of $Na^+$ in the form of hydrated specie and causes a shift in the peak corresponding to this specie, from -1.0 to -1.6 and -1.8 ppm, as mentioned previously.

The NMR study is also correlated to the weight loss observed in TGA experiments. It has been shown that the 20 wt.% $Na_2CO_3/\gamma$-$Al_2O_3$ catalyst started decomposing/losing weight at a much lower temperature compared to that of the pure $Na_2CO_3$ sample. It can be suggested that the coordination between $Na^+$ ions and the surface hydroxyl groups has weakened the ionic bonds in between $Na^+$ and $CO_3^{2-}$. Consequently, the amount of energy required to cleave these ionic bonds is much less compared to that in pure $Na_2CO_3$, resulting in a lower decomposition temperature (135 $^oC$). The two weight loss regions observed in the 33 wt.% $Na_2CO_3$ sample correspond to the two sodium species presenting in this sample, *i.e.* the hydrated and the surface $Na_2CO_3$ clusters. One may wonder why the decomposition temperature of the surface cluster in the 33 wt.% $Na_2CO_3$ sample is lower than that of pure $Na_2CO_3$ (Figure 5.2), even though they are supposed to be the same pure $Na_2CO_3$ specie. The former started to decompose at *ca.* 700 $^oC$ while the latter is shown to be stable until 850 $^oC$. During impregnation, sodium carbonate is dissolved in water and this salt is recrystallized on the alumina support during drying and calcination treatments. The recrystallization of sodium carbonate might differ, depending on the factors involved (for *e.g.* amount of water used, impregnation time, drying and calcination rate and temperature, *etc.*). This might result in sodium carbonate crystals with different crystallite size which explains the difference in decomposition temperature between the two. It is difficult to to estimate the cluster sizes of $Na_2CO_3$, thus, further study is necessary to confirm this statement.

Figure 5.6 summarizes the $^{27}Al$ MAS spectra of $\gamma$-$Al_2O_3$ and the supported catalysts with different $Na_2CO_3$ loadings. Two resonance signals, one at *ca.* 70 ppm and the other at 11 ppm, were observed. These two peaks are similar to those reported in other studies [30, 31]. The resonance at 70 ppm corresponds to the tetrahedral Al and the other to the octahedral Al [30]. It can be observed that there is a downshift in the resonance signal of the tetrahedral Al in the supported catalysts compared to that of $\gamma$-$Al_2O_3$. This can be a result of the interaction between absorbed $Na^+$ ions and oxygen atoms of the hydroxyl groups of $\gamma$-alumina, as

discussed previously, which causes a deshielding effect on $Al^{3+}$ ions. The chemical shifts of the octahedral Al also varied depending on the loading of sodium carbonate, but to a lesser extent.

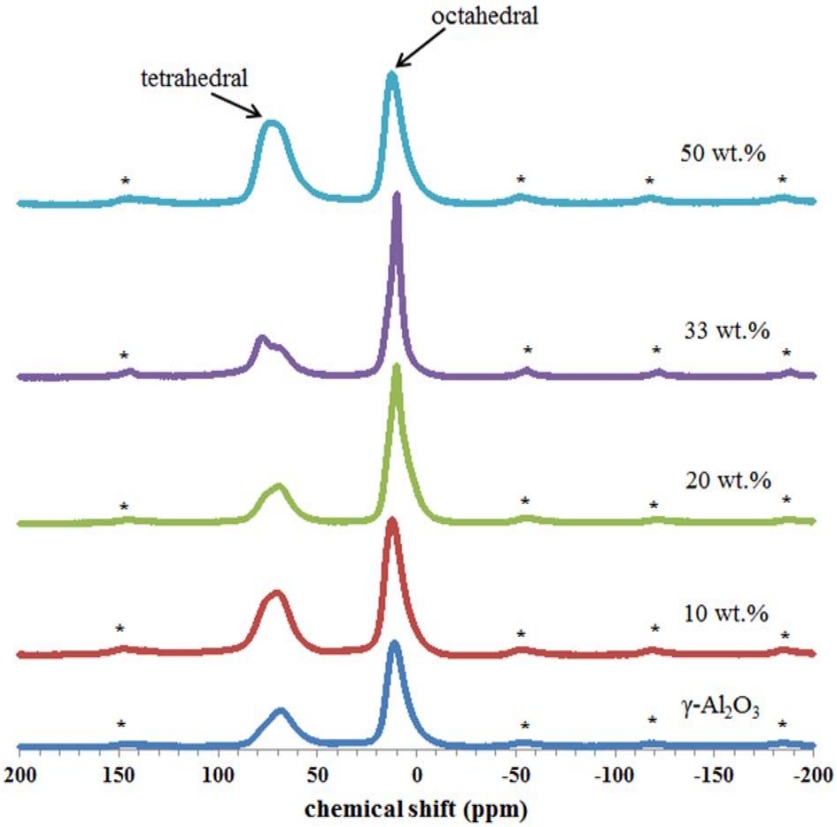


**Figure 5.6.** $^{27}Al$ MAS NMR spectra of $\gamma$-$Al_2O_3$ and of $Na_2CO_3$/ $\gamma$-$Al_2O_3$ samples with different $Na_2CO_3$ loadings. Asterisks denote spinning sidebands

NMR results shows that only hydrated sodium specie, thus interacting with the alumina support, is present in the 20 wt.% $Na_2CO_3$ sample. Based on the fact that this catalyst is also the most active catalyst in the de-oxygenation of bio-oil (Table 5.1), it is suggested that this specie is the one responsible for this superior activity of the catalyst. The reaction pathway of the pyrolysis vapour in presence of the sodium catalyst is discussed next.

It is shown in this chapter and also in Chapter 4 that the catalytic upgrading of pyrolysis vapours in presence of sodium catalyst resulted in a selective de-oxygenation into $CO_2$. This was accompanied by a sharp reduction in carboxylic acid content and a significant

increase in ketone content in the obtained pyrolysis oil. The proposed ketonization leading to this is shown in equilibrium (Eq.1) in the following scheme:


(Eq.1)

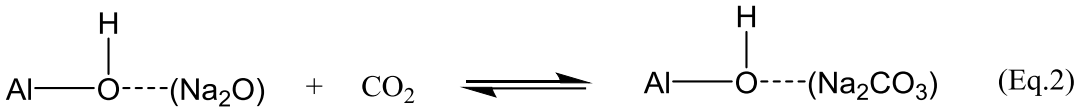


(Eq.2)

As shown previously, the hydrated $Na_2CO_3$ in the supported catalysts decomposes readily at low temperature (135 $^oC$) to sodium oxide and $CO_2$. Since all catalysts were activated *in situ* at 500 $^oC$ prior to experiments, the hydrated sodium likely exists in the form of sodium oxide during the upgrading of pyrolysis vapour. During catalytic experiments, this basic sodium oxide can capture the $CO_2$ formed in (Eq.1) and thus shift the equilibrium to the right, resulting in a higher degree of de-oxygenation. The sodium oxide and the captured $CO_2$ is also in equilibrium with the carbonate form, as shown in (Eq.2). In the proposed scheme the role of sodium-based material is not a catalyst in the traditional definition, but rather as means to capture and release $CO_2$ and thus facilitate carboxylic acid conversion *via* ketonisation or decomposition.

*5.3.3. Regeneration of catalyst*

After one catalytic cycle, the 20 wt.% $Na_2CO_3$/ $\gamma$-$Al_2O_3$ material was recovered and regenerated by calcination in air at 600$^oC$. The properties of fresh and regenerated catalysts and the corresponding bio-oil products were compared in Table 5.2.

**Table 5.2.** Properties of fresh and regenerated catalysts and the obtained bio-oils

| **Catalyst** | **BET surface area ($m^2$ $g^{-1}$)** | **Pore volume ($cm^3$ $g^{-1}$)** | **Na content [a] (wt.%)** | **Bio-oil[b]** | |
|---|---|---|---|---|---|
| | | | | **Yield (wt.%)** | **wt.% [O]** |
| Fresh catalyst | 196 | 0.47 | 4.5 | 9 | 12.3 |
| Regenerated catalyst | 188 | 0.46 | 4.7 | 10 | 19.5 |

[a]content of sodium element in the catalysts, measured by XRF

[b]bio-oil obtained from the corresponding catalysts

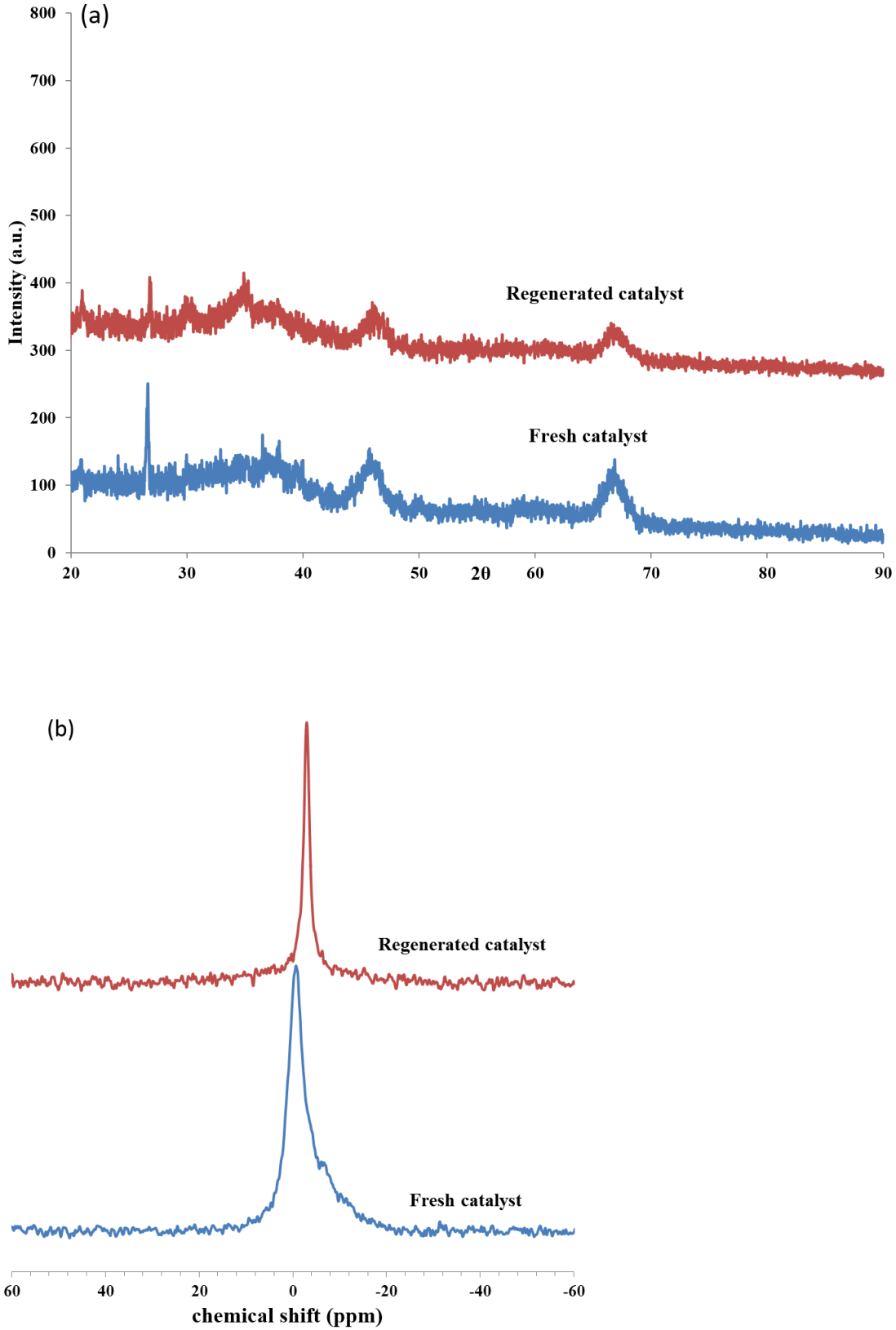


**Figure 5.7.** Comparison of properties of fresh and regenerated catalysts, shown by (a) XRD and (b) $^{23}$Na MAS NMR analyses

As can be seen, the regeneration procedure did not significantly affect the properties of the alumina support. The surface area and pore volume of the material were slightly reduced after this treatment. XRD analyses of the fresh and regenerated catalysts also confirm this (Figure 5.7a). The diffractograms of fresh and regenerated materials are almost identical, with the three characteristic peaks of gamma alumina observed at 2θ of $38^o$, $46^o$ and $66^0$.

From the MAS NMR spectra, it can be seen that there is a 2 ppm shift, from -1 ppm to – 3ppm, in the regenerated material compared to the fresh one (Figure 5.7b), which suggests that the hydrated sodium specie may have been modified. Additionally, one may notice there is a slight increase in the sodium content going from fresh to regenerated materials (Table 5.2), which is possibly caused by the deposition of the inorganic minerals (*i.e.* ash) from biomass feed onto the catalyst .

Table 5.2 also shows the difference in the catalytic performance of the two materials in the de-oxygenation of pyrolysis vapour. It can be seen that the yields of bio-oil in the two cases are similar but there is a noticeable difference in the quality of these bio-oil products. Upgrading of pyrolysis vapour over regenerated catalyst resulted in a bio-oil with higher oxygen content compared to the fresh catalyst. As mentioned previously, while the support is hardly affected by biomass upgrading and subsequent regeneration processes, there is change observed in the hydrated specie during this process. It is likely that this change is responsible for the changed performance of the catalyst, which is consistent with the proposal of the hydrated sodium oxide being the active site for de-oxygenation.

## 5.4. Conclusion

It has been shown in this chapter that sodium carbonate supported on gamma-alumina catalysts were shown to possess excellent activity in the de-oxygenation of biomass-derived vapour. XRD analyses confirmed the presence of sodium carbonate in those catalysts as well-dispersed small crystallites or as another amorphous phase interacting with alumina support. TGA-MS analyses suggested that sodium carbonate presented in the catalysts in a different state compared to that in pure sodium carbonate. $^{23}$Na MAS NMR analyses confirmed the presence of 3 peaks in the supported catalysts which were attributed to pure sodium carbonate and an unknown sodium specie. The specie is later proposed to be formed by the interaction between sodium ions and the hydroxyl groups on the surface of alumina support. Results from

$^{1}H$, $^{23}Na$ MAS NMR, TGA-MS analyses and a theoretical calculation agree well with each other and all support the above proposal. A reaction scheme explaining the high activity of those catalysts in de-oxygenation is proposed, in which the role of sodium-based material is not a catalyst in the traditional definition, but rather as means to capture and release $CO_2$ and thus facilitate the de-carboxylation of carboxylic acids. There is a certain level of deactivation in the regenerated catalyst after one catalytic cycle. While the alumina support was shown to be intact, change is observed in the sodium specie which is the reason for the above deactivation of the catalyst.

## References

[1] I.V. Babich, M. van der Hulst, L. Lefferts, J.A. Moulijn, P. O'Connor, K. Seshan, Biomass and Bioenergy 35 (2011) 3199-3207.
[2] U. Jena, K.C. Das, J.R. Kastner, Applied Energy 98 (2012) 368-375.
[3] T.H. Ballinger, J.T. Yates, Langmuir 7 (1991) 3041-3045.
[4] J.B. Peri, R.B. Hannan, The Journal of Physical Chemistry 64 (1960) 1526-1530.
[5] T.S. Nguyen, M. Zabeti, L. Lefferts, G. Brem, K. Seshan, Bioresource Technology 142 (2013) 353-360.
[6] A. Khaleel, S. Al-Mansouri, Colloids and Surfaces A: Physicochemical and Engineering Aspects 369 (2010) 272-280.
[7] M. Bodaghi, A.R. Mirhabibi, H. Zolfonun, M. Tahriri, M. Karimi, Phase Transit. 81 (2008) 571-580.
[8] H. de Souza Santos, P. de Souza Santos, Mater. Lett. 13 (1992) 175-179.
[9] R.-S. Zhou, R.L. Snyder, Acta Crystallogr B 47 (1991) 617-630.
[10] K. Nagase, T. Shimodaira, M. Itoh, Y. Zheng, PCCP 1 (1999) 5659-5664.
[11] T.M.C. Hoang, L. Lefferts, K. Seshan, ChemSusChem 6 (2013) 1651-1658.
[12] C.P. Grey, F.I. Poshni, A.F. Gualtieri, P. Norby, J.C. Hanson, D.R. Corbin, J. Am. Chem. Soc. 119 (1997) 1981-1989.
[13] P. Norby, F.I. Poshni, A.F. Gualtieri, J.C. Hanson, C.P. Grey, J. Phys. Chem B 102 (1998) 839-856.
[14] K.H. Lim, C.P. Grey, J. Am. Chem. Soc. 122 (2000) 9768-9780.
[15] M. Sánchez-Sánchez, T. Blasco, J. Am. Chem. Soc. 124 (2002) 3443-3456.
[16] S. Caldarelli, A. Buchholz, M. Hunger, J. Am. Chem. Soc. 123 (2001) 7118-7123.
[17] J. Zhu, N. Trefiak, T. Woo, Y. Huang, Microporous Mesoporous Mater. 114 (2008) 474-484.
[18] K.J.D. MacKenzie, E. Smith, Multinuclear Solid-State Nuclear Magnetic Resonance of Inorganic Materials, Elsevier Science, 2002.
[19] A.R. Jones, R. Winter, G.N. Greaves, I.H. Smith, J. Phys. Chem B 109 (2005) 23154-23161.
[20] M. Dusek, G. Chapuis, M. Meyer, V. Petricek, Acta Crystallogr B 59 (2003) 337-352.
[21] A. Arakcheeva, G. Chapuis, Acta Crystallogr B 61 (2005) 601-607.
[22] A. Wong, G. Wu, The Journal of Physical Chemistry A 104 (2000) 11844-11852.
[23] H. Koller, G. Engelhardt, A.P.M. Kentgens, J. Sauer, J. Phys. Chem. 98 (1994) 1544-1551.
[24] R. Tabeta, H. Saito, Chem. Lett. (1984) 293-296.
[25] S.F. Dec, G.E. Maciel, J.J. Fitzgerald, J. Am. Chem. Soc. 112 (1990) 9069-9077.
[26] M. Zamora, A. Cordoba, J. Phys. Chem. 82 (1978) 584-588.
[27] W.K. Hall, F.E. Lutinski, H.R. Gerberich, J. Catal. 3 (1964) 512-527.

[28] E. Santacesaria, D. Gelosa, S. Carrà, Product R&D 16 (1977) 45-47.
[29] P. Grange, Catalysis Reviews 21 (1980) 135-181.
[30] M.H. Lee, C.-F. Cheng, V. Heine, J. Klinowski, Chem. Phys. Lett. 265 (1997) 673-676.
[31] E.R.H. Van Eck, A.P.M. Kentgens, H. Kraus, R. Prins, J. Phys. Chem. 99 (1995) 16080-16086.

# Chapter 6

## Study on the catalytic conversion of lignin-derived components in pyrolysis vapours using model component

*To be submitted to Catalysis Today*

**Abstract.** Vanillyl alcohol was chosen as a model component for lignin-derived components in the pyrolysis vapours. The catalytic conversion of vanillyl alcohol over different catalysts was studied and it has been shown that this model component has undergoes consecutive reactions to form methoxy phenols, phenols, and eventually hydrocarbons with increasing degree of de-oxygenation. The degree of de-oxygenation of vanillyl alcohol was shown to increase with the increase in number of acid sites in catalysts. $\gamma$-$Al_2O_3$ material with the highest number of acid sites has resulted in the highest yield of aromatic hydrocarbons, accompanied by the highest yields of coke and gas compared to other materials used in this study. Two pathways have been shown leading to the formation of hydrocarbons from vanillyl alcohol, which are: (i) decomposition of vanillyl alcohol into small olefinic hydrocarbon fragments and the subsequent aromatization into final products and (ii) direct de-oxygenation of this model component over catalysts.

**Chapter 6**

## 6.1. Introduction

The pyrolysis of biomass is receiving tremendous interest as a potential method for converting solid biomass into liquid transportation fuels [1-8]. Lignocellulosic biomass is one of the most promising renewable resources because it is cheap and abundant [9-11]. Our work so far has been dedicated to finding an efficient catalyst for the pyrolytic conversion of lignocellulosic biomass, *via* de-polymerisation and simultaneous de-oxygenation, into a high quality fuel/fuel precursor. Different catalysts have been tested and a catalytic system of sodium carbonate supported on $\gamma$-$Al_2O_3$ was shown to have excellent de-oxygenation activity (Chapter 4). Detailed characterisation of this catalyst with a variety of techniques with an aim to understand the active catalytic site in this catalyst was discussed in Chapter 5.

Lignocellulosic biomass is mainly composed of cellulose, hemicellulose, and lignin. Cellulose (a crystalline polymer of glucose) and hemicellulose (an amorphous polymer, whose major component is a xylose monomer unit) make up 60-90 wt % of terrestrial biomass [1]. Lignin, a large polyaromatic matrix made up of alkoxy substituted phenyl propyl units, is the other major component of biomass and occupies about 15%-30% by dry weight [12].

During pyrolysis, decomposition of cellulose and hemicellulose results in a variety of components such as (substituted) furans, carboxylic acids, aldehydes, ketones. Catalytic pyrolysis of cellulose and hemicellulose carried out in the presence of the 20 wt.% $Na_2CO_3$/ $\gamma$-$Al_2O_3$ catalyst resulted in the formation of mainly aliphatic hydrocarbons, furans and carbonyls. The results of such experiments carried out by us are summerised in Table 6.1 Among those products, aliphatic hydrocarbons and furans are desirable as fuel precursors because of their high energy content, very low oxygen content and neutrality in acid/base scale. It can be seen in Table 6.1 that there is hardly any carboxylic acid present in the product formed in the catalytic pyrolysis of cellulose, hemicellulose or lignin. This acid removal function of the sodium-based catalyst is already discussed in Chapter 4 and 5. Carboxylic acids are either decomposed to $CO_2$, which occurs to a large extent, or to form carbonyls *via* condensation, acetone from acetic acid is one such example. It will be shown in Chapter 7 that carbonyls can be reduced significantly combining catalytic de-oxygenation and hydrogenation over a dual-bed catalyst system. In short, among the 5 groups of components shown in Table

6.1 two are desirable (aliphatic hydrocarbons, furans) and two are undesired but can be catalytically treated (carboxylic acids, carbonyls) to desirable components.

The sharp increase in aromatic products in the case of lignin pyrolysis reflects the structure of this component, which is a three dimensional amorphous polymer containing methoxylated phenyl propyl matrix made up of p-coumaryl, coniferyl and sinapyl alcohols [13]. Aromatics, possess high energy content and they are often allowed in limited concentration in fuels to increase their octane number. However, they are also known to be carcinogenic and can be corrosive (for *e.g.* phenols). Moreover, biomass pyrolysis oil contains up to 30 wt.% of lignin-derived aromatic components, mainly in phenolic form [14, 15]. Formation of various phenols during catalytic pyrolysis and their further conversion is thus of great interest while considering the need to form fuel compatible components.

**Table 6.1.** Selectivities based on TIC area % of main groups of products formed in the catalytic pyrolysis of cellulose, hemicellulose and lignin

| Component of biomass | Aliphatic HCs | Furans | Carbonyls | Acids | Aromatics* |
|---|---|---|---|---|---|
| Cellulose | 20.2 | 33.3 | 36.9 | 1.9 | 1.6 |
| Hemicellulose | 25.9 | 63.6 | 6.6 | 0.0 | 3.9 |
| Lignin | 11.8 | 52.4 | 1.3 | 0.0 | 32.3 |

*consists of substituted phenols and aromatic hydrocarbons

Over eight types of linkages have been identified in lignin structure [16]. Some of the common linkages in the structure of lignin are shown in Figure 6.1. The β-O-4 bond is the major type of linkage which occupies 46%–60% of the total linkages depending on the type of wood [17].

Pyrolysis of lignin has been studied by a few of people over the decades. In 1970s, Iatridis *et al.* pyrolyzed lignin in a "captive sample" reactor at temperature of 400 °C–700 °C and only identified a limited number of components by gas chromatography which included hydrocarbons, methanol, acetone, phenol and guaiacol due to the limitation in analytical technology [18]. Recently, Guozhan Jiang *et al.* identified~50 components from lignin pyrolysis at a temperature range of 400 °C – 800 °C [19]. The phenolic components yield was 16.2 wt.% for Alcell lignin and individual yield of most of the components were less than 1 wt.%. The thermal decomposition and weight loss of various lignin sources were studied by D. J. Nowakowski [20]. He found out that the major decomposition of lignin occurred at a temperature range of 350 °C to 450 °C and that the heating rate affected the amount of volatile products.

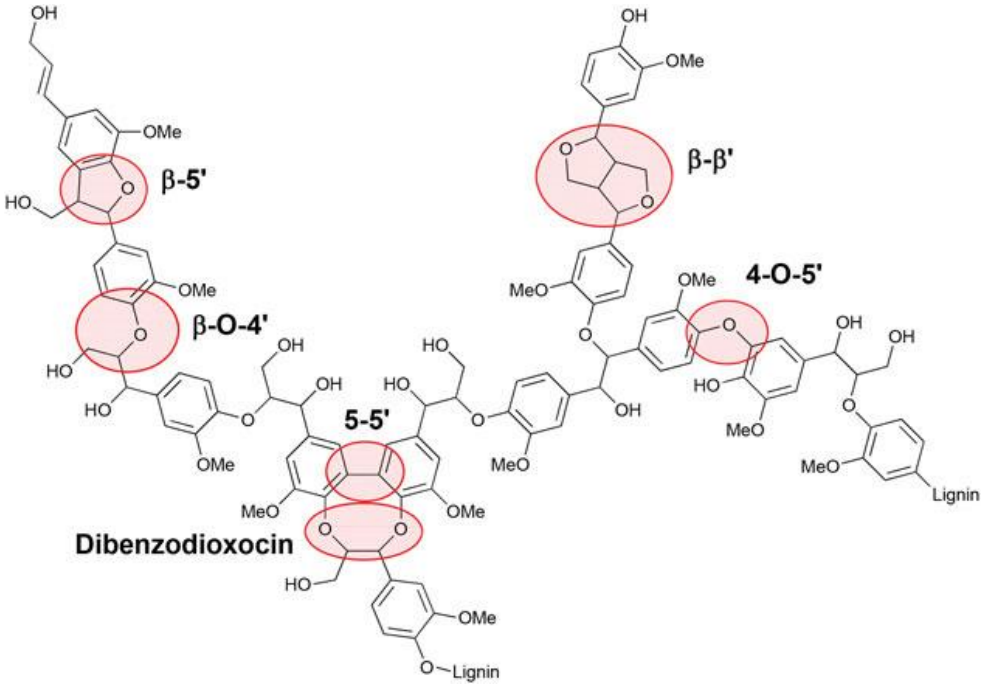


**Figure 6.1.** Representative structure of lignin with some highlighted common linkages

Several so called "lignin model components" have also been studied to avoid complexity. These lignin model components have simple structures and product distributions compared to real lignin. Guaiacol is the simplest monomeric model component and its pyrolysis behaviour was studied by Bredenberg in 1987 [21]. Catechol and phenol were shown to be the dominant products at 400 °C. A free radical reaction combined with a concerted reaction mechanism were suggested to explain guaiacol pyrolysis. Other substituted monomeric phenolic components such as syringol, isoeugenol, vanillin, anisole and dimethoxy-phenols were tested by Klein in 1981 [22]. It was concluded that the principal reactions of those compounds during pyrolysis are de-methylation, isomerisation and de-methoxylation. A free radical mechanism has been proposed by Schlosberg [23] and Masuku [24] to explain the pyrolysis of monomeric lignin components.

In this chapter, the pyrolysis conversion of vanillyl alcohol (VA) as a model component is studied. The structure of vanillyl alcohol is compared to those of the three building blocks of lignin and illustrated in Figure 6.2.

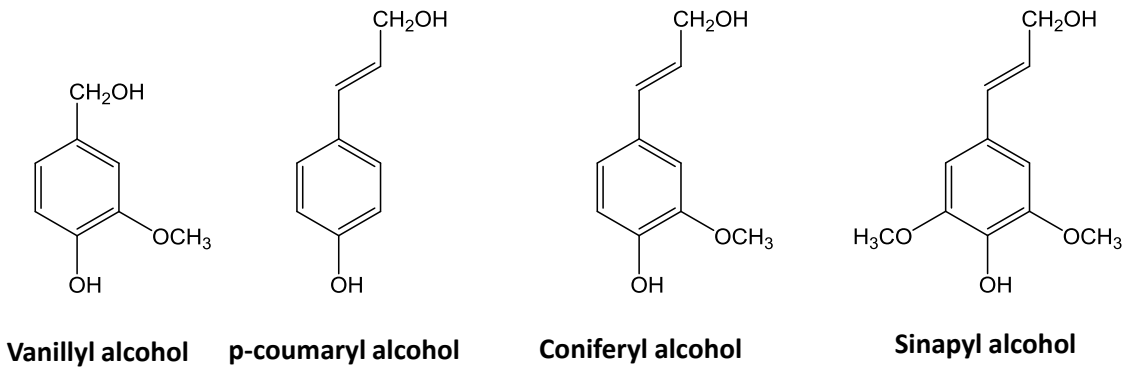


**Figure 6.2.** Structures of the model compound vanillyl alcohol and the three building blocks of lignin, namely p-coumaryl, coniferyl and sinapyl alcohols

The catalysts applied in this chapter are the same materials which were used in the catalytic upgrading of lignocellulose (pine wood) in the previous chapters. Vanillyl alcohol was chosen in this study since it contains all three types of functional groups attached to the aromatic ring as in lignin derivatives, namely: (i) alkyl group, via C-C bonds (ii) alkoxy group, C-O bonds and (iii) hydroxyl group, C-O bonds. The object of such a model component study is to (i) investigate the chemistry of the catalytic upgrading of lignin-derived components, (ii) comparing the effectiveness of different catalytic materials to cleave different bonds and (iii) determine the possible correlations between the conversion of lignin model component, vanillyl alcohol, and the conversion the lignocelluosic biomass, *i.e.* lignin in the presence of cellulose and hemicellulose, over those catalysts.

## 6.2. Experimental

### *6.2.1. Catalyst preparation and characterisation*

$\gamma$-$Al_2O_3$ (catalyst support) was obtained from Akzo Nobel, $Na_2CO_3$ (reagent grade >99.5%) and quartz reference material from Sigma Aldrich. $Na_2CO_3$/ $\gamma$-$Al_2O_3$ catalyst was prepared applying wet impregnation. Details of the catalyst preparation steps were described in section 2.2.2. Vanillyl alcohol (>98%), cellulose (microcrystalline, colloidal, >90%), hemicellulose (as xylan from beechwood, >90%), lignin (organosolv, >90%) were purchased from Sigma Aldrich.

### *6.2.2. Catalytic testing*

The experimental set-up and applied definitions are described in detail in Chapter 2. In each experiment, 1 g of vanillyl alcohol and 1 g of catalyst were loaded into the pyrolysis

and catalyst chambers, respectively. Temperature of the catalyst bed was maintained at 500 $^{o}$C for all experiments. The flow of Ar carrier gas was 70 mL min$^{-1}$. At the beginning of each experiment, vanillyl alcohol was quickly brought to its boiling point (*ca.* 293 $^{o}$C) in less than 5 sec. The formed vapour was then pushed by the Ar flow into the catalyst bed. The condensable products were collected in two consecutives condensers kept at -40 $^{o}$C. The condensable products were dissolved in acetone with the mass ratio of acetone : products of 95 : 5 and was subjected to GC-MS analyses. Components were identified comparing their mass spectra with the NIST mass spectral data library NIST08. Information about the database can be found in the NIST website [25]. In order to determine the distribution of these components, a semi-quantitative study was made by means of the percentage area of the total ion chromatogram (TIC) peaks. Detected components in the condensable phase were classified into five main groups based on their functionalities, namely: aromatic hydrocarbons, methoxy aromatic hydrocarbons, phenols, methoxy phenols, and cyclic pentenones. TIC area % of these groups were used to compare the differences in composition of the condensable fraction and calculated by summing up the area % of all corresponding members in those groups. The yield of the condensable phase is determined by the change in weight of the condensers before and after experiment. The yield of coke formed on catalysts was determined by carrying out TGA experiment of the catalyst-coke mixture in air. The gas yield was calculated by difference, assuming that the yields of the condensable phase, coke and gas make up to 100% of the original mass of VA. Details of these analyses were given in section 2.3.2.

## 6.3. Results and discussion

*6.3.1. Reference experiment*

In the reference experiment, 1 g of an inert material, *i.e.* quartz, was used. The detected components in the condensable (liquid) phase are shown in Table S6.1 along with their structures, group, and TIC area %. As can be seen, most of the starting material VA was not converted during the reference experiment, shown by the highest area % of this component (*ca.* 85 %). The two components with the second and third highest area % were vanillin and 2-methoxy-4-methylphenol (8.4 % and 4.8 %, respectively). They are likely the products from the self-oxidation of VA. There are other products presenting in small area %, resulted from the thermal decomposition of VA over quartz (Table S6.1).

The yields of the three products. *i.e.* condensable, coke and gas, from the thermal and catalytic conversion of vanillyl alcohol are summarised in Figure 6.3(a) It can be seen that only minor amount of coke (4 wt.%) and gas (2 wt.%) were formed in the reference experiment, which correlates to the low conversion of this model component as mentioned previously.

Previous studies on non-catalytic, thermal pyrolysis of monomeric model components of lignin showed them to occur *via* a free radical mechanism [23, 24]. The mechanism of vanillin pyrolysis was studied by Shin *et al.* using mass spectrometer and multivariate analysis at the pyrolysis temperatures of 500, 650 and 800 $^{o}$C [26]. It was shown by Shin that at 500 $^{o}$C vanillin was hardly converted, which agrees well with our result of the reference experiment. The low conversion of vanillyl alcohol observed in the non-catalytic experiment can be explained by the fact that the formation of free radicals requires the homolytic cleavage of chemical bonds; and at 500 $^{o}$C there is not enough thermal energy for the necessary for the necessary bond scission to occur.

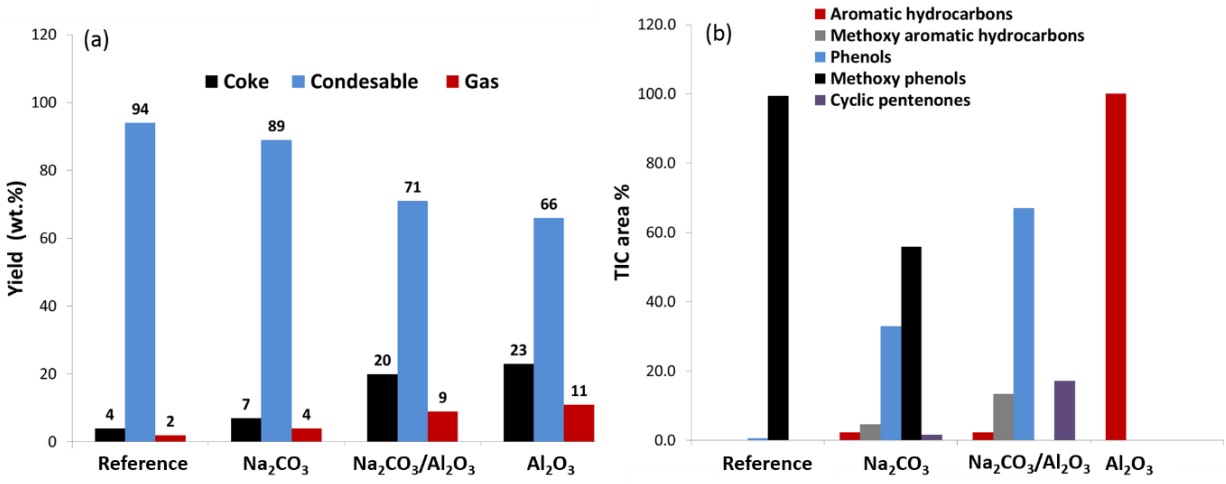


**Figure 6.3.** The effect of different catalysts to: (a) yields of coke, condensable, gas products, wt.% and (b) TIC area % of different groups in the condensable fraction. Reaction conditions: 500 $^{o}$C, 2 s, 1 g of VA and 1 g of catalyst.

Figure 6.3(b) illustrates the change in TIC area % of different groups of components in the condensable phase under the influence of different catalytic materials. It can be seen that there is hardly any de-oxygenation occurring on the quartz material and almost all products obtained in the reference experiment are methoxy phenols. This is expected because of the inertness of quartz material and de-oxygenation requires the presence of an acid catalyst.

Typically thermal pyrolysis of lignocellulosic biomass results in a bio-oil which has similar oxygen content (~42 wt%) as that in the starting material [2].

*6.3.2. Catalytic experiments*

In catalytic experiments, quartz material was replaced with different catalysts. All reaction conditions were the same as those in the reference experiment. Compositions of the condensable fractions obtained with $Na_2CO_3$, $Na_2CO_3$/ γ-$Al_2O_3$ and γ-$Al_2O_3$ catalysts are shown in Table S6.2, S6.3 and S6.4, respectively. TIC area % of the five groups of components are compared in Figure 6.3(b) and the mass balances shown in Figure 6.3(a). It can be seen in Tables S6.2-S6.4 that vanillyl alcohol was not detected in any of the catalytic experiments, which suggests that it was fully converted in presence of the catalysts.

Similar to the reference experiment, methoxy phenols are the most abundant in the condensable fraction obtained with $Na_2CO_3$ catalyst, as can be seen in Figure 6.3(b). However, the amount of phenols has increased significantly, along with the formation of other groups of components, for *e.g.* cyclic pentenones, aromatic hydrocarbons, *etc.* which were not present in the reference experiment. This trend continues with $Na_2CO_3$/ γ-$Al_2O_3$ catalyst, with which methoxy phenols were not detected in the condensable phase and instead phenols became the dominant group in terms of TIC area (67%). Moreover, compared to $Na_2CO_3$ catalyst, the area % of aromatic hydrocarbons in presence of $Na_2CO_3$/γ-$Al_2O_3$ is similar but those of methoxy aromatic hydrocarbons and cyclic pentenones have increased as shown in Figure 6.3(b). Finally, there is a tremendous change in the composition of the condensable phase obtained with γ-$Al_2O_3$, which separates this catalyst from the rest of the materials used in this study (Table S6.4 and Figure 6.3(b)). As can be seen, there is no oxygenates detected in the condensable phase in presence of γ-$Al_2O_3$. Detected components all fall into the aromatic hydrocarbons category. It can be seen in Figure 6.3(a) that compared to the reference case, there is more coke and gas and less condensable products obtained in all of the catalytic experiments; and the coke and gas yield was maximized on γ-$Al_2O_3$ catalyst.

*6.3.3. Proposed pathways for the conversion of vanillyl alcohol*

Earlier studies in which γ-$Al_2O_3$ was placed in contact with a series of indicator dyes of varying basicity suggest that the surface has modest acidity [27]. $^{13}C$ NMR studies of n-butylamine adsorbed on γ-$Al_2O_3$ demonstrate that both Lewis and Bronsted

acid sites co-exist on the surface [28]. These two types of acid sites are illustrated in Figure 6.4.

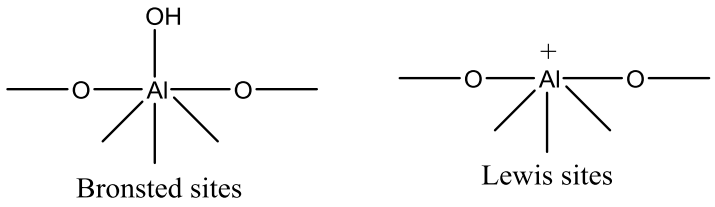


**Figure 6.4.** Illustration of Bronsted and Lewis acid sites in γ-$Al_2O_3$ [29]

A trend that can be easily seen in Figure 6.3(b) that the more acidic the catalyst is, the more deoxygenated products were obtained. As discussed previously, with the non-acidic quartz and $Na_2CO_3$, methoxy phenols were the dominant products. The lack of acid function in the two materials prevented the catalytic conversion into phenols and aromatic hydrocarbons. On the catalysts with acid sites, such as $Na_2CO_3$/γ-$Al_2O_3$ and γ-$Al_2O_3$, VA was deoxygenated into phenols and aromatic hydrocarbons, thus decreasing the yield of the condensable phase and increasing the yield of the coke and gas, as can be seen in Figure 6.3(a). As already shown in Chapter 5, there is an interaction between $Na_2CO_3$ and the acid sites on the surface of alumina, thus the number of acid sites in $Na_2CO_3$/γ-$Al_2O_3$ is expected to be less than that in $Al_2O_3$. This explains the higher aromatic hydrocarbon and coke yields in the presence of pure alumina. It was proposed by Ma *et al.*, that acid sites in zeolites cause dehydration, decarboxylation, dealkylation, cracking, isomerization, oligomerization, *etc.* of lignin into aromatic hydrocarbons [30]. Mullen and Boateng also proposed two pathways to explain the formation of aromatic hydrocarbons in the catalytic pyrolysis of lignin over H-ZSM5 catalyst [31]. Both pathways begin with the de-polymerization of lignin over HZSM-5 to form: (i) small olefins from the aliphatic linkers of the lignin matrix and (ii) alkoxy phenolic monomers. In the first pathway, aromatic hydrocarbons were formed *via* the aromatization of the olefins over HZSM-5. The second pathway involves the direct de-oxygenation of the alkoxy phenols over the zeolite into the corresponding aromatic hydrocarbons. However, we never detected significant amounts of olefins in our experiments, which suggests that either: (i) the catalytic conversion of VA occurred *via* the second pathway or (ii) the olefins were rapidly converted into aromatics.

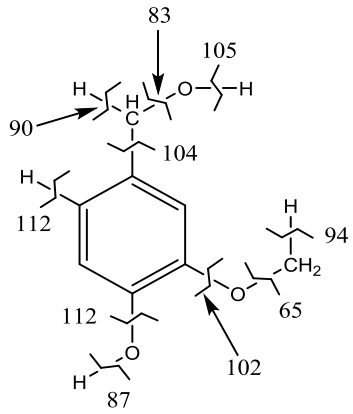


**Figure 6.5.** Estimated bond disassociation energies in vanillyl alcohol molecule by Shin [26] and Blanksby *et al.* [32], shown in kCal $mol^{-1}$

As mentioned previously the pyrolysis of vanillyl alcohol likely occurs *via* a free radical mechanism, initialized by the homolytic cleavage of C-C and C-O bonds in this molecule. Thus an important consideration to have is the corresponding bond disassociation energies. Although these bond disassociation energies have not been measured directly, one can approximate their values as being close to anisole ($C_6H_5CH_3$), phenol ($C_6H_5OH$) and benzyl alcohol ($C_6H_5CH_2OH$) and are summarized in Figure 6.5.

As can be seen, the disassociation energy of the C-O bond between a C atom of the aromatic ring and an O atom of the hydroxyl group is the highest (112 kCal $mol^{-1}$). It thus requires a large amount of thermal energy or a proper catalyst to facilitate the scission of this bond. For this reason most of the catalysts except for $\gamma$-$Al_2O_3$ resulted in a condensable phase which is rich in phenol derivatives (methoxy phenols and phenols).

Shin *et al.* has carried out a study on the mechanism of vanillin pyrolysis using mass spectrometry and multivariate analysis [26]. He showed that the weakest bond in vanillin is the C-O bond on the methoxy group and suggested that the unimolecular decomposition of vanillin would be dominated by the scission of this bond, forming a substituted phenoxy radicals (Figure 6.6, step 1). Further unimolecular rupture could result in an expulsion of CO (de-carbonylation) to form a cyclopenta-di-enyl radical (step 2). The cyclopenta-di-enyl radical formed in step 2 can undergo different pathways to form aromatic hydrocarbon and cyclopenta-di-en products (step 3-6). Step 3 involves the decomposition of cyclopenta-di-enyl radical into small hydrocarbon fragments and molecules, *i.e.* $C_3H_3$, $C_2H_2$, *etc.*, followed by

aromatization of these fragments into aromatic hydrocarbons (step 4). The cyclopenta-di-enyl can also be deoxygenated directly to form the corresponding aromatic hydrocarbons (step 5).

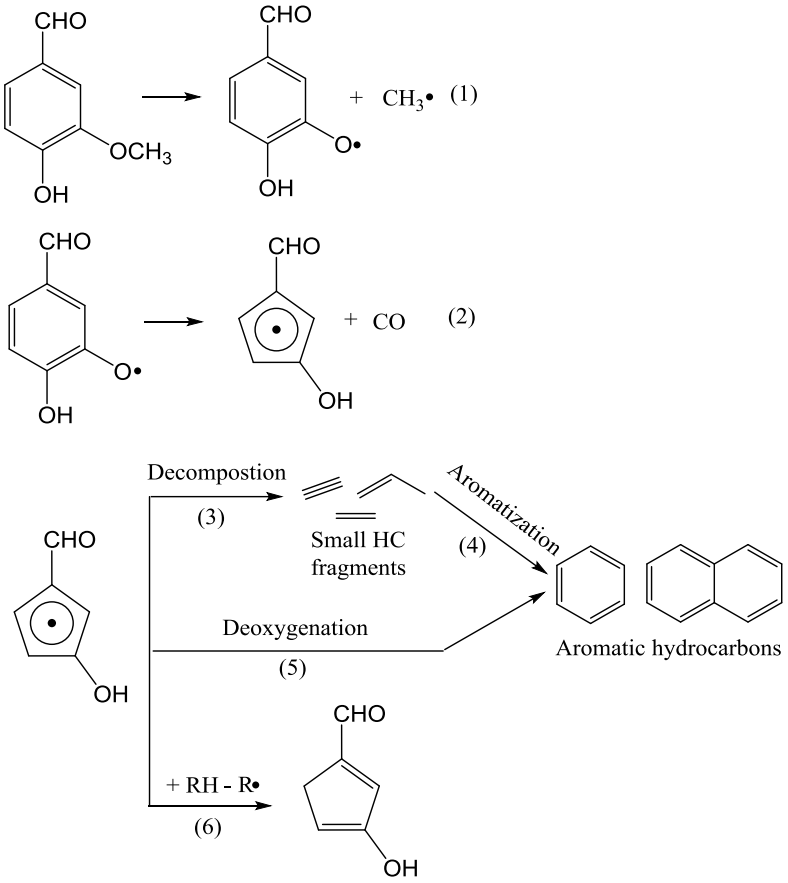


**Figure 6.6.** Multiple steps in the unimolecular decomposition of vanillin, proposed by Shin *et al. [26]*

Despite working with different feedstocks, i.e., lignin or a monomeric model component of lignin (vanillin), both Mullen [31] (shown previously) and Shin [26] *et al.* arrived at a very similar conclusion regarding the pathways to aromatic hydrocarbons: either *via* the aromatization of small unsaturated fragments or the direct de-oxygenation of monomeric species. Finally, the cyclopenta-di-enyl radical formed in step 2 can also abstract a H atom from other hydrocarbons to form a cyclopenta-di-ene (step 6). All the pathways described above can also be correlated to our study because of the similarities in: (i) the acidic nature of the catalysts, *i.e.* γ-$Al_2O_3$ and HZSM-5 even though they possess different strengths, and (ii) the starting material, *i.e.* vanillyl alcohol, lignin, vanillin possess similar structures. The formation of the above-mentioned cyclopenta-di-enyl radical is likely the foundation for the generation of the cyclic pentenones detected in our study (Table S6.2 and S6.3)

*6.3.4. Correlation with the catalytic pyrolysis of biomass*

So far in this chapter we have discussed the conversion of vanillyl alcohol as a model component of lignin-derived components over $Na_2CO_3$, $Na_2CO_3$/ γ-$Al_2O_3$, and γ-$Al_2O_3$ catalysts.

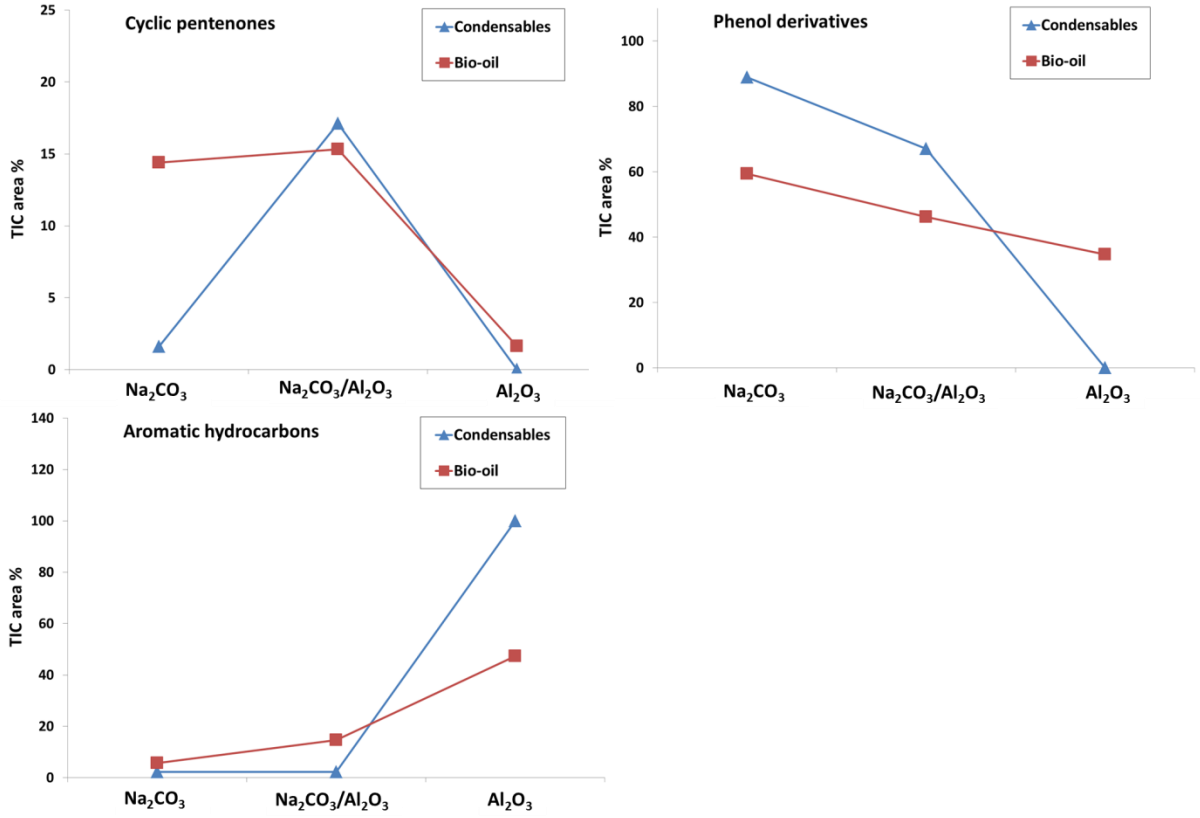


**Figure 6.7.** The change in composition of bio-oil from biomass pyrolysis and condensable (liquid) phase from VA conversion over different catalytic materials

The same catalysts have also been employed in the upgrading of biomass pyrolysis vapour into bio-oil, of which the results were discussed thoroughly in Chapters 4 and 5. Thus it is useful to establish if a correlation between the chemical profiles of the main products in biomass conversion, *i.e.* bio-oil, and that in model component conversion, *i.e.* the condensable phase, exists. The three chemical groups which were detected in both the bio-oil and the condensable phase are cyclic pentenones, phenol derivatives and aromatic hydrocarbons. The abundance of these 3 groups in bio-oil and condensable phase in presence of different catalysts, represented by the corresponding TIC area %, are illustrated in Figure 6.7.

Various cyclic pentenones have been detected in both bio-oil and the condensable fraction from VA pyrolysis. The cyclic pentenones found in bio-oil can be the decomposition products of both the carbohydrate fraction (cellulose, hemicellulose) and the lignin fraction of biomass. On the other hand, the possible pathway leading to the formation of cyclic pentenones from VA has been discussed previously. One interesting trend observed in Figure 6.7 is that the change in TIC area % of cyclic pentenones in both bio-oil and condensable phase are similar. The area % begins with an average value for $Na_2CO_3$, maximized with $Na_2CO_3/Al_2O_3$ catalyst and becoming minimal with $Al_2O_3$. The only difference is, in bio-oil, the gap between the area % of cyclic pentenones obtained with $Na_2CO_3$ and $Na_2CO_3/Al_2O_3$ catalysts is small while that in the condensable phase obtained from the conversion of VA is much bigger. This suggests that $Na_2CO_3$ might be more efficient in converting the carbohydrate part of biomass into cyclic pentenones compared to the lignin part.

The change in area % of phenol derivatives and aromatic hydrocarbons in bio-oil and condensable phase also have similar trend. However, the rates of change in the two cases are different. The rate of change of both phenol derivatives and aromatic hydrocarbons with the condensable phase is always faster, especially when $\gamma$-$Al_2O_3$ is applied. Again, this can be attributed to the difference in catalytic efficiency of $\gamma$-$Al_2O_3$ towards the conversion of carbohydrate and lignin fractions of biomass.

There are two conclusions that can be drawn based on the above discussion, which are: (i) lignin plays an important role in the chemistry of biomass pyrolysis and thus in determining the chemical profile and properties of the obtained bio-oil and (ii) vanillyl alcohol is a promising model component to study the behaviour of lignin in catalytic pyrolysis. However, more study should be carried out to gain deeper insight into this field, for *e.g.* comparison of lignin and vanillin alcohol pyrolysis over the catalysts.

## 6.4. Conclusions

Extent of de-oxygenation of vanilyl alcohol increased with the increase in number of acid sites in the catalyst. Consequently, $\gamma$-$Al_2O_3$, the most acidic among the catalysts studied, was an efficient de-oxygenation catalyst, resulting in mostly aromatic hydrocarbon products. Two pathways have been shown leading to the formation of aromatic hydrocarbons from vanillyl alcohol, which are: (i) the decomposition of vanillyl alcohol in to small olefinic

hydrocarbon fragments and the subsequent aromatization into final products and (ii) the direct de-oxygenation of vanillyl alcohol over the catalysts. Comparison of the chemical profiles between biomass and vanillyl alcohol pyrolysis has shown similarities between the two cases in terms of the trend of change. However, there are differences in the rate of change which can be attributed to difference in the catalytic efficiency towards different components of biomass (cellulose, hemicellulose, lignin).

## Supplementary

**Table S6.1.** Components identified in the condensable phase of the reference experiment

| Name | Structure | Group | Area % |
|---|---|---|---|
| Phenol, 2-methoxy- | 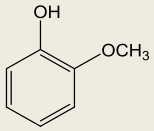 | Methoxy phenols | 0.51 |
| Vanillyl alcohol | 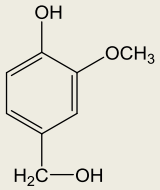 | Methoxy phenols | 84.93 |
| Phenol, 2-methoxy-4-methyl- | 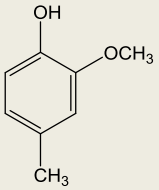 | Methoxy phenols | 4.81 |
| Vanillin | 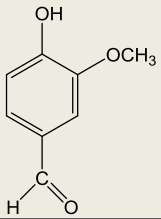 | Methoxy phenols | 8.37 |
| Phenol, 4-ethyl-2-methoxy- | 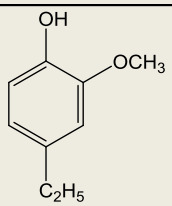 | Methoxy phenols | 0.40 |
| Benzene, 1-ethyl-4-methoxy- | 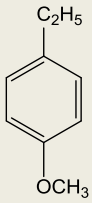 | Methoxy phenols | 0.23 |
| Phenol, 2,4-dimethyl- | 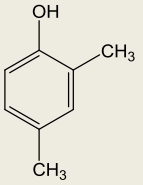 | Phenols | 0.43 |
| Phenol, 2-methyl- | 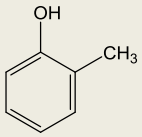 | Phenols | 0.21 |

**Table S6.2.** Identified components in the condensable phase with $Na_2CO_3$ material

| Name | Structure | Group | Area% |
|---|---|---|---|
| Phenol, 2-methoxy-3-methyl- | 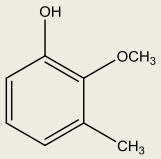 | Methoxy phenols | 0.32 |
| 2-Methoxy-5-methylphenol | 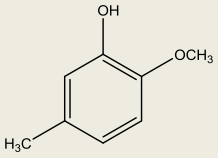 | Methoxy phenols | 1.21 |
| Phenol, 2-methoxy-4-methyl- | 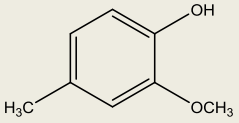 | Methoxy phenols | 32.58 |
| Phenol, 4-ethyl-2-methoxy- | 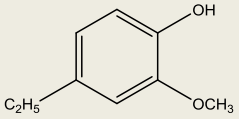 | Methoxy phenols | 6.17 |
| Ethanone, 1-(2-hydroxy-6-methoxyphenyl)- | 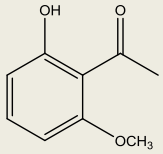 | Methoxy phenols | 0.41 |

**Table S6.2.** (continue)

| Name | Structure | Group | Area% |
|---|---|---|---|
| Benzene |  | Aromatic hydrocarbons | 0.33 |
| Toluene | 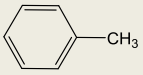 | Aromatic hydrocarbons | 0.51 |
| Bicyclo[4.2.0] octa-1,3,5-triene | 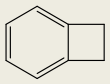 | Aromatic hydrocarbons | 0.25 |
| Indene | 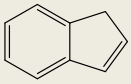 | Aromatic hydrocarbons | 0.37 |
| 1H-Indene, 1-methyl- | 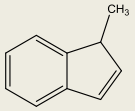 | Aromatic hydrocarbons | 0.27 |
| Naphthalene | 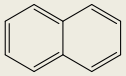 | Aromatic hydrocarbons | 0.31 |
| Naphthalene, 1-methyl- | 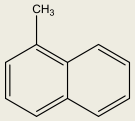 | Aromatic hydrocarbons | 0.26 |
| Benzofuran | 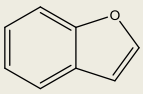 | Methoxy aromatic hydrocarbons | 0.34 |
| Benzofuran, 2-methyl- | 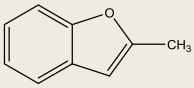 | Methoxy aromatic hydrocarbons | 0.55 |
| Benzene, 1,2-dimethoxy- | 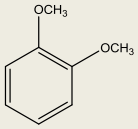 | Methoxy aromatic hydrocarbons | 0.39 |
| 3,4-Dimethoxytoluene | 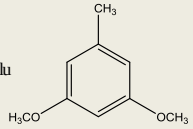 | Methoxy aromatic hydrocarbons | 1.00 |
| Benzene, 1-ethyl-4-methoxy- | 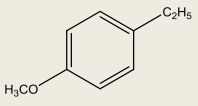 | Methoxy aromatic hydrocarbons | 2.40 |
| 2-Cyclopenten-1-one, 3-methyl- | 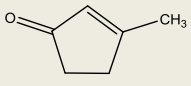 | Cyclic pentenones | 0.78 |
| 2-Cyclopenten-1-one, 2,3-dimethyl- | 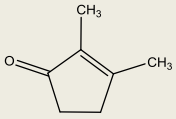 | Cyclic pentenones | 0.58 |

| Name | Structure | Group | Area% |
|---|---|---|---|
| 2-Cyclopenten-1-one, 3-ethyl- | 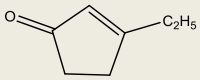 | Cyclic pentenones | 0.25 |
| Phenol | 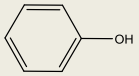 | Phenols | 4.16 |
| Phenol, 2-methyl- | 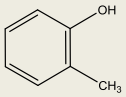 | Phenols | 5.71 |
| Phenol, 2,3-dimethyl- | 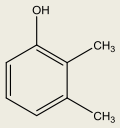 | Phenols | 1.22 |
| Phenol, 4-methyl- | 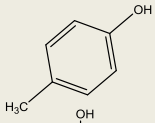 | Phenols | 8.14 |
| Phenol, 2-ethyl- | 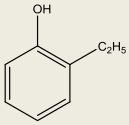 | Phenols | 1.60 |
| Phenol, 2,4-dimethyl- | 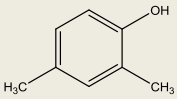 | Phenols | 6.64 |
| Phenol, 2,4,6-trimethyl- | 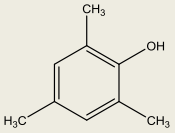 | Phenols | 0.92 |
| Phenol, 4-ethyl- | 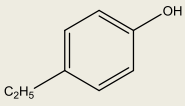 | Phenols | 1.92 |
| 1,4-Benzenediol, 2,3,5-trimethyl- | 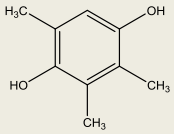 | Phenols | 1.27 |
| Phenol, 2,3,5-trimethyl- | 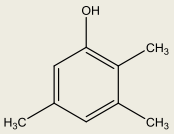 | Phenols | 0.31 |
| 3-Methyl-4-isopropylphenol | 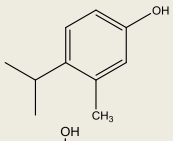 | Phenols | 0.78 |
| 2-Allylphenol | 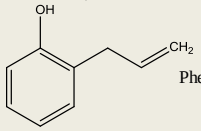 | Phenols | 0.28 |
| Phenol, 2-methoxy- | 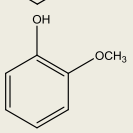 | Methoxy phenols | 15.25 |

**Table S6.3.** Identified components in the condensable phase with $Na_2CO_3/Al_2O_3$ material

| Name | Structure | Group | Area% |
|---|---|---|---|
| Phenol, 3,5-dimethyl- | 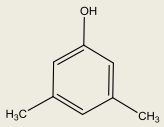 | Phenols | 20.70 |
| Phenol, 2-methyl- | 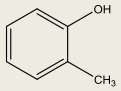 | Phenols | 16.43 |
| Phenol, 3-ethyl-5-methyl- | 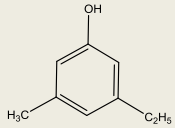 | Phenols | 6.41 |
| Phenol, 2-ethyl- | 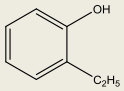 | Phenols | 5.58 |
| Phenol, 3,4,5-trimethyl- | 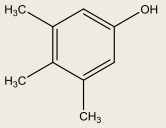 | Phenols | 5.33 |
| 3-Methyl-4-isopropylphenol | 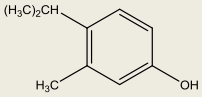 | Phenols | 4.38 |
| Phenol, 2,6-dimethyl- | 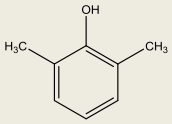 | Phenols | 4.34 |
| Phenol, 2,4,6-trimethyl- | 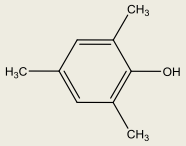 | Phenols | 3.89 |
| 2,3-Dimethylanisole | 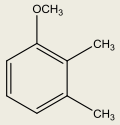 | Methoxy aromatic hydrocarbons | 4.55 |

| Name | Structure | Group | Area% |
|---|---|---|---|
| Benzene, 1-methoxy-4-methyl- | 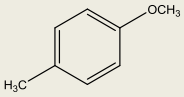 | Methoxy aromatic hydrocarbons | 4.35 |
| Benzene, 1-ethyl-4-methoxy- | 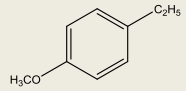 | Methoxy aromatic hydrocarbons | 2.48 |
| Benzofuran, 2-methyl- | 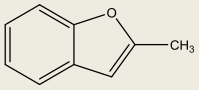 | Methoxy aromatic hydrocarbons | 2.13 |
| 2-Cyclopenten-1-one, 3-methyl- | 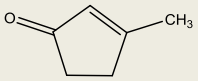 | Cyclic pentenones | 7.28 |
| 2-Cyclopenten-1-one, 2,3-dimethyl- | 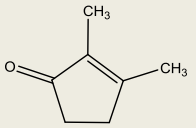 | Cyclic pentenones | 5.85 |
| 2-Cyclopenten-1-one, 3,4-dimethyl- | 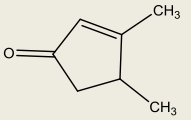 | Cyclic pentenones | 2.18 |
| 2-Cyclopenten-1-one, 2,3,4-trimethyl- | 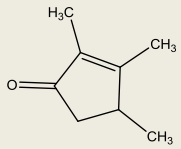 | Cyclic pentenones | 1.82 |
| Cyclohexene, 2-ethenyl-1,3,3-trimethyl- | 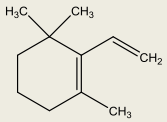 | Aromatic hydrocarbons | 2.30 |

**Table S6.4.** Identified components in the condensable phase with $Al_2O_3$ material

| Name | Structure | Group | Area % |
|---|---|---|---|
| Naphthalene, 2-methyl- | 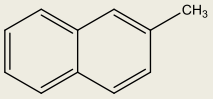 | Aromatic hydrocarbons | 10.9573 |
| o-Xylene | 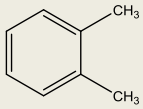 | Aromatic hydrocarbons | 8.21 |
| Naphthalene | 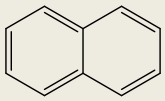 | Aromatic hydrocarbons | 7.1053 |
| 2-Methylindene | 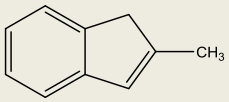 | Aromatic hydrocarbons | 5.3506 |
| Phenanthrene, 1-methyl- | 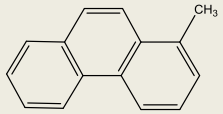 | Aromatic hydrocarbons | 5.2077 |
| Phenanthrene | 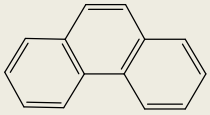 | Aromatic hydrocarbons | 4.4156 |
| Phenanthrene, 2-methyl- | 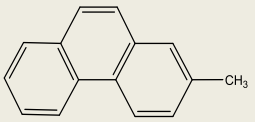 | Aromatic hydrocarbons | 3.806 |
| Indene | 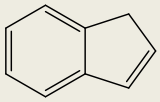 | Aromatic hydrocarbons | 3.0722 |
| p-Xylene | 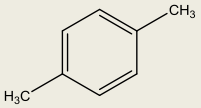 | Aromatic hydrocarbons | 2.8269 |
| Benzene, 1,2,3-trimethyl- | 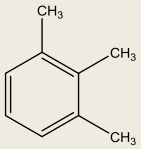 | Aromatic hydrocarbons | 2.6086 |
| Other aromatic hydrocarbons | – | Aromatic hydrocarbons | 58.76 |

# References


[1] Huber GW, Iborra S, Corma A. Synthesis of Transportation Fuels from Biomass: Chemistry, Catalysts, and Engineering. Chem Rev 2006;106:4044.

[2] Nguyen TS, Zabeti M, Lefferts L, Brem G, Seshan K. Catalytic upgrading of biomass pyrolysis vapours using faujasite zeolite catalysts. Biomass Bioenerg 2013;48:100.

[3] Nguyen TS, Zabeti M, Lefferts L, Brem G, Seshan K. Conversion of lignocellulosic biomass to green fuel oil over sodium based catalysts. Bioresource Technology 2013;142:353.

[4] Carlson TR, Vispute TP, Huber GW. Green Gasoline by Catalytic Fast Pyrolysis of Solid Biomass Derived Compounds. ChemSusChem 2008;1:397.

[5] Hassan E-b, Steele P, Ingram L. Characterization of Fast Pyrolysis Bio-oils Produced from Pretreated Pine Wood. Appl Biochem Biotechnol 2009;154:3.

[6] Bhattacharya P, Steele PH, Hassan EBM, Mitchell B, Ingram L, Pittman Jr CU. Wood/plastic copyrolysis in an auger reactor: Chemical and physical analysis of the products. Fuel 2009;88:1251.

[7] Papadikis K, Gu S, Bridgwater AV. CFD modelling of the fast pyrolysis of biomass in fluidised bed reactors: Modelling the impact of biomass shrinkage. Chemical Engineering Journal 2009;149:417.

[8] Vispute TP, Zhang H, Sanna A, Xiao R, Huber GW. Renewable Chemical Commodity Feedstocks from Integrated Catalytic Processing of Pyrolysis Oils. Science 2010;330:1222.

[9] Demirbaş A. Biomass resource facilities and biomass conversion processing for fuels and chemicals. Energy Conversion and Management 2001;42:1357.

[10] Ragauskas AJ, Williams CK, Davison BH, Britovsek G, Cairney J, Eckert CA, et al. The Path Forward for Biofuels and Biomaterials. Science 2006;311:484.
[11] Brower KR. Measuring the Efficiency of Biomass Energy. Science 2006;312:1744.
[12] Jae J, Tompsett GA, Lin Y-C, Carlson TR, Shen J, Zhang T, et al. Depolymerization of lignocellulosic biomass to fuel precursors: maximizing carbon efficiency by combining hydrolysis with pyrolysis. Energy & Environmental Science 2010;3:358.
[13] Ralph J, Lundquist K, Brunow G, Lu F, Kim H, Schatz P, et al. Lignins: Natural polymers from oxidative coupling of 4-hydroxyphenyl- propanoids. Phytochemistry Reviews 2004;3:29.
[14] Czernik S, Bridgwater AV. Overview of applications of biomass fast pyrolysis oil. Energ Fuel 2004;18:590.
[15] Mohan D, Pittman CU, Steele PH. Pyrolysis of Wood/Biomass for Bio-oil: A Critical Review. Energy & Fuels 2006;20:848.
[16] Chakar FS, Ragauskas AJ. Review of current and future softwood kraft lignin process chemistry. Industrial Crops and Products 2004;20:131.
[17] Dorrestijn E, Laarhoven LJJ, Arends IWCE, Mulder P. The occurrence and reactivity of phenoxyl linkages in lignin and low rank coal. Journal of Analytical and Applied Pyrolysis 2000;54:153.
[18] Iatridis B, Gavalas GR. Pyrolysis of a Precipitated Kraft Lignin. Industrial & Engineering Chemistry Product Research and Development 1979;18:127.
[19] Jiang G, Nowakowski DJ, Bridgwater AV. Effect of the Temperature on the Composition of Lignin Pyrolysis Products. Energy & Fuels 2010;24:4470.
[20] Nowakowski DJ, Bridgwater AV, Elliott DC, Meier D, de Wild P. Lignin fast pyrolysis: Results from an international collaboration. Journal of Analytical and Applied Pyrolysis 2010;88:53.
[21] Vuori AI, Bredenberg JBs. Thermal chemistry pathways of substituted anisoles. Industrial & Engineering Chemistry Research 1987;26:359.
[22] Klein MT. Department of Chemical Engineering: Massachusetts Institute of Technology; 1981.
[23] Schlosberg RH, Szajowski PF, Dupre GD, Danik JA, Kurs A, Ashe TR, et al. Pyrolysis studies of organic oxygenates: 3. High temperature rearrangement of aryl alkyl ethers. Fuel 1983;62:690.
[24] Masuku CP. Thermal reactions of the bonds in lignin. IV. Thermolysis of dimethoxyphenols. 1991.
[25] http://www.nist.gov/srd/nist1a.cfm.
[26] Shin E-J, Nimlos MR, Evans RJ. A study of the mechanisms of vanillin pyrolysis by mass spectrometry and multivariate analysis. Fuel 2001;80:1689.
[27] Kabalka GW, Pagni RM. Organic reactions on alumina. Tetrahedron 1997;53:7999.
[28] Dawson WH, Kaiser SW, Ellis PD, Inners RR. Carbon-13 cross-polarization magic-angle-spinning NMR study of butylamine adsorbed on .gamma.-alumina: characterization of surface acid sites. Journal of the American Chemical Society 1981;103:6780.
[29] Weingarten R, Tompsett GA, Conner Jr WC, Huber GW. Design of solid acid catalysts for aqueous-phase dehydration of carbohydrates: The role of Lewis and Brønsted acid sites. Journal of Catalysis 2011;279:174.
[30] Ma Z, Troussard E, van Bokhoven JA. Controlling the selectivity to chemicals from lignin via catalytic fast pyrolysis. Applied Catalysis A: General 2012;423–424:130.
[31] Mullen CA, Boateng AA. Catalytic pyrolysis-GC/MS of lignin from several sources. Fuel Process Technol 2010;91:1446.
[32] Blanksby SJ, Ellison GB. Bond Dissociation Energies of Organic Molecules. Accounts of Chemical Research 2003;36:255.

# Chapter 7

## *In situ* catalytic hydro-deoxygenation of lignocellulose during pyrolysis

*To be submitted to Applied Catalysis B: Environmental*

**Abstract.** Pyrolysis of biomass followed by catalytic hydro-deoxygenation of the pyrolysis vapour were studied at 500 $^{o}$C and atmospheric pressure, applying platinum and sodium based catalysts. CO chemisorption has shown that platinum particles are well dispersed in $Pt/Al_2O_3$ catalyst while they get agglomerated in $Pt\text{-}Na_2CO_3/Al_2O_3$. The Pt-Na co-impregnated or sequentially impregnated catalysts have not shown improvement compared to either $Na_2CO_3/Al_2O_3$ or $Pt/Al_2O_3$ catalysts when it comes to quality of bio-oil. A dual bed system in which $Na_2CO_3/Al_2O_3$ and $Pt/Al_2O_3$ are packed in two consecutive beds has combined the advantages of all catalytic systems, resulting in a bio-oil with better fuel quality than fuel oil. The only drawback of the system is the low yield of bio-oil, which can be overcome by fine-tuning the conditions of the hydro-deoxygenation process. N-butane shows comparable performance compared to $H_2$ gas in hydro-deoxygenation, opening new possibility for economical hydrogen sources for bio-oil treating.

## 7.1. Introduction

It has been shown in Chapter 4 and summerised in Table 7.2 that the presence of $Na_2CO_3/\gamma$-$Al_2O_3$ catalyst results in bio-oils with significantly better quality compared to non-catalytic oil, such as being almost neutral in terms of acidity/basicity, having significantly lower oxygen content compared to non-catalytic oil and having energy density close to that of fuel oil (37 MJ $kg^{-1}$). However, the drawback was the increase in carbonyl content (ketones, aldehydes), which are known to be the precursors for the instability of bio-oil (Table 6.2). Our investigation in Chapter 3 showed that the content of high molecular weight components (> 400 g $mol^{-1}$) in bio-oil increased during storage. This increase was later shown to be caused by condensation reactions between carbonyls compounds and alcohol /phenols in bio-oil (Chapter 3). An extra hydro-de-oxygenation step may of bio-oil may be useful to remove these harmful carbonyl groups as well as to further lower the oxygen content of bio-oil to make it compatible for fuel application.

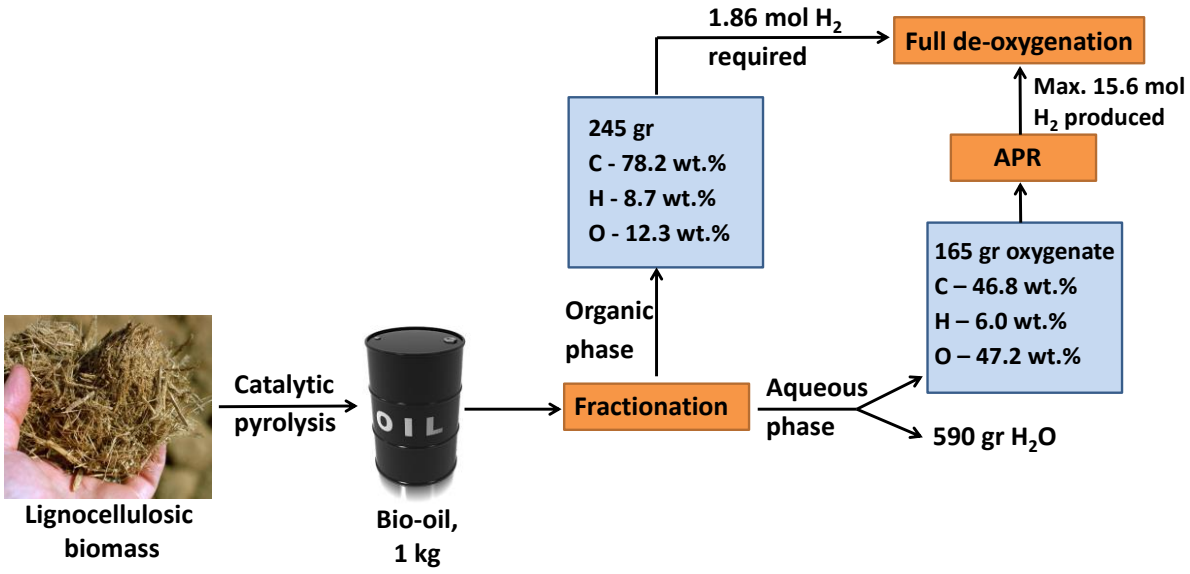


**Figure 7.1.** Estimation of hydrogen economic in bio-refinery of lignocellulosic biomass

The amount of hydrogen required for upgrading of the organic phase of bio-oil can be calculated and the details are shown in Figure 7.1. It is seen that per kg of catalytic bio-oil (obtained with $Na_2CO_3/\gamma$-$Al_2O_3$ catalyst) consists of 245 g of organic phase, 165 g of water-soluble oxygenates and 590 g of $H_2O$. Since the organic phase has an oxygen content (12.3 wt.%), the amount of hydrogen required for a complete hydro-deoxygenation was calculated to be 1.86 mol or 3.7 g $H_2$ per kg bio-oil (Figure 7.1).

As a reference, and in agreement, it was reported by Bridgwater [1] that around 16 g of $H_2$ was required to achieve full de-oxygenation of 1 kg of "non-catalytic" bio-oil (contains 250 g of organic phase, [O] content ~40 wt%, compared to catalytic oil in our case ~12 wt%). Competing side-reactions (e.g. hydrogenation of unsaturated bonds, hydrogenolysis and small alkane formation, *etc*.) during de-oxygenation accounts for the slight extra hydrogen required [11] to achieve full de-oxygenation. The $H_2$ required for the hydro-de-oxygenation of the organic phase can be obtained (i) from fossil sources, e.g methane steam reforming or (ii) "sustainably" *via* the aqueous phase reforming (APR) of the oxygenates in the aqueous phase (Figure 7.1). If hydrogen can be generated from the aqueous phase of the bio-oil, the pyrolysis process does not need to import hydrogen from fossil sources and becomes a completely green process. In one of our earlier studies, it was shown that a maximum theoretical value of 15.6 mol or 31.2 g of $H_2$ could be produce *via* APR of the oxygenates dissolved in the aqueous phase in 1 kg of bio-oil [2]. These calculations show that the amount of hydrogen obtained from the aqueous phase is enough for full de-oxygenation of the organic phase, when the hydrogen selectivity of the reforming of the aqueous fraction is at least 12%. Earlier studies with model components present in the aqueous fraction of the biomass has shown hydrogen selectivites in the range of 18-19% [2].

Up to now most of the studies on hydro-de-oxygenation of bio-oil involves the post hydrogenation of the formed bio-oil at moderate temperatures (300-600°C) and at high-pressure $H_2$ in the presence of heterogeneous catalysts. Reviews on such studies have been written by Furimsky [3] and Elliott *et al*. [4] Most hydro-deoxygenation work has focused on sulfided Co-Mo and Ni-Mo based materials, which are industrial hydro-treating catalysts used for the removal of sulfur, nitrogen, and oxygen from refinery feedstocks/products. Pt/ $SiO_2$-$Al_2O_3$ [5], vanadium nitride [6], and Ru have also been used for hydro-deoxygenation. Significantly it was shown in the reviews that the energy content of the fuel was significantly increased, and the stability of the fuel increased after hydro-deoxygenation. A hydro-treating step is useful to bring the bio-oil closer to application in the current fuel pool.

A variant to this option is to apply hydro-de-oxygenation of bio-oil vapours *in situ*, as in a hydrocracking process, and is discussed here. In this chapter attempts were made upgrade the pyrolysis vapours from lignocellulosic biomass in hydrogen/argon flow and in the presence of multiple catalytic systems which are able to catalyze both de-oxygenation/cracking and hydrogenation reactions. It was shown in Chapter 4 that with the

de-oxygenation/cracking over $Na_2CO_3/\gamma$-$Al_2O_3$ catalyst a low level oxygen content in bio-oil (12.3 wt.%) was already achieved. Moreover, some countries, for *e.g.* Brazil, legalize the use of fuel with relatively high oxygen content (oxygen content of a legal ethanol/gasoline blend in Brazil is ~ 9 wt.%). For these reasons, only a mild hydrogenation is required in the case of the pyrolysis oil obtained over $Na_2CO_3/\gamma$-$Al_2O_3$ catalyst. We have chosen the hydrogenation to be carried out at the same conditions as in de-oxygenation/cracking reaction in order to simplify the process, *i.e.* 550 $^oC$ and at atmospheric pressure. This relatively high temperature and low pressure is not optimal for hydrogenation (requires lower temperatures and higher pressures from thermodynamic considerations for favourable equilibrium) but since only a mild hydrogenation is required and also taking into account the high reactivity of the oxygenates in bio-oil, this approach can be a promising one.

*In situ* hydro-deoxygenation of bio-oil was studied over Pt (hydrogenation) and Na (de-oxygenation) based catalysts. The differences in catalytic activities for $Pt/\gamma$-$Al_2O_3$, Pt-$Na/\gamma$-$Al_2O_3$ and a dual bed catalytic system ($Na/\gamma$-$Al_2O_3$ + $Pt/\gamma$-$Al_2O_3$) were investigated. As a proof of concept, hydrogen was replaced by n-butane to investigate the possibility of a more economical hydrogen source. The goal of this chapter was to effect in situ hydrogenation and develop an efficient catalyst system for the combined processes of pyrolysis, de-oxygenation and hydro-de-oxygenation of biomass into a good quality fuel precursor.

## 7.2. Experimental

### *7.2.1. Catalyst preparation and characterisation*

$Na_2CO_3/\gamma$-$Al_2O_3$, $Pt/\gamma$-$Al_2O_3$, Pt-$Na/\gamma$-$Al_2O_3$ catalysts were prepared as described in section 2.2.2. Catalysts were characterized by XRF, BET, TGA, and CO chemisorption. These techniques are further described in section 2.3.1.

### *7.2.2. Catalytic testing*

The experimental set-up and applied definitions are described in detail in Chapter 2. In this chapter, catalytic experiments were carried out in one of the 2 modes, namely single-bed and dual-bed mode, which were explained in section 2.1. In single-bed operation, 2 g of biomass and 1 g of catalyst were used. For dual-bed operation, 2 g of biomass and 1 g of each catalyst were applied. In the model compound experiment, quartz wool, which was previously

soaked in methyl ethyl ketone (b.p. 80 $^{o}$C), was packed into the biomass bed. At the beginning of the experiment, the quartz wool with methyl ethyl ketone were quickly brought to the boiling point of the ketone using the infra-red furnace. The vapour was then pushed by a $H_2$/Ar flow into the dual catalyst bed where it was converted. Temperature of the pyrolysis and catalyst beds was set at 500$^{o}$C. Duration of all experiments was 10 min. The flow rate of Ar was 70 mL.min$^{-1}$. Products of the catalytic pyrolysis process were subjected to GC, elemental analysis and bomb calorimetry. Details of these analyses were given in section 2.3.2.

## 7.3. Results and discussion

*7.3.1. Catalyst characterisation*

The properties of all catalysts are summarised in Table 7.1. The BET surface area of γ-$Al_2O_3$ after calcination at 550 $^{o}$C is 257 m$^2$ g$^{-1}$. It exhibits type IV isotherm which is a characteristic of mesoporous materials. The average pore diameter is 10 nm with a pore volume of 0.8 mL g$^{-1}$. There were no changes in the properties on loading of 0.6 wt.% Pt on γ-$Al_2O_3$. However, the BET surface area and pore volume decreased to 196 m$^2$ g$^{-1}$ and 0.46 mL g$^{-1}$, respectively, on loading of 20 wt.% $Na_2CO_3$. This may be due to filling of pores of the support by sodium carbonate particles. The two Pt-$Na_2CO_3$/ γ-$Al_2O_3$ catalysts prepared by (i) co- or (ii) sequential impregnation showed further decrease in surface area and pore volume compared to γ-$Al_2O_3$. This can be attributed to the interaction between the two precursors, namely choloroplatinic acid and sodium carbonate. It is known that choloroplatinic acid is a strong acid [7] while sodium carbonate is a basic salt. Thus the exothermic nature of the acid – base reaction between these two precursors can result in the collapse some of the mesopores, leading to lower surface area. The BET surface area and pore volume of the catalyst prepared by co-impregnation is higher than that of sequential impregnation with the same loading of platinum and sodium carbonate. It can be explained by the fact that in the case of sequential impregnation, alumina surface is completely covered with sodium carbonate.

The dispersion of Pt on γ-$Al_2O_3$ is 67% but it decreases in the co-catalysts, both sequential and co-impregnation, indicating larger particles. This may be due to decrease in surface area of γ-$Al_2O_3$ during impregnation as discussed previously. In conclusion, CO

chemisorption indicates that platinum particles are well dispersed in Pt/γ-$Al_2O_3$ catalyst while they get agglomerated in Pt-Na/γ-$Al_2O_3$.

**Table 7.1.** Surface properties of the catalyst

| Catalyst | Loading[c] (wt.%) | Dispersion[d] (%) | Average Pt particle size[d] (nm) | Surface area ($m^2$ $g^{-1}$) | Pore volume (mL $g^{-1}$) |
|---|---|---|---|---|---|
| γ-$Al_2O_3$ | _ | _ | _ | 257 | 0.80 |
| $Na_2CO_3/Al_2O_3$ | 20.76 | _ | _ | 196 | 0.46 |
| $Pt/Al_2O_3$ | 0.67 | 67 | 1.7 | 262 | 0.80 |
| Pt- $Na_2CO_3/Al_2O_3$ seq.[a] | 0.65-20.44 | 20 | 6.0 | 100 | 0.32 |
| Pt- $Na_2CO_3/Al_2O_3$ co.[b] | 0.64-20.34 | 32 | 3.5 | 141 | 0.37 |

[a]prepared using sequential impregnation [b]prepared using co-impregnation
[c]derived from XRF measurement [d]derived from CO chemisorption

*7.3.2. Catalytic hydro-pyrolysis*

*7.3.2.1. Single-bed system*

The key aspects in non-catalytic and catalytic pyrolysis of lignocellulosic biomass were listed in Table 7.2. The first two experiments were carried out in Ar, one with $Na_2CO_3/Al_2O_3$ catalyst and the other is without catalyst (thermal).

It was already shown in Chapter 4 that bio-oil derived from experiment using $Na_2CO_3$/γ-$Al_2O_3$ catalyst contains remarkably less oxygen (~12 wt.%) and higher heating value (37 MJ $kg^{-1}$) compared to the bio-oil from the thermal pyrolysis experiment. This shows that $Na_2CO_3$/γ-$Al_2O_3$ is a very effective de-oxygenation catalyst. Moreover, study at the chemistry of the catalytic bio-oil by GC-MS reveals that carboxylic acids have been completely removed and the HC content has been increased significantly in the presence of $Na_2CO_3$/γ-$Al_2O_3$ catalyst. These above characteristics have make this catalytic oil a very

promising fuel precursor. However, low yield (9 wt.%) and high content of carbonyls (35.8%), known as precursors to instability, are the biggest drawbacks.

**Table 7.2**. Comparison of thermal and catalytic pyrolysis and hydro-pyrolysis of biomass

| Sample | Gas flow | Bio-oil properties | | | | | |
|---|---|---|---|---|---|---|---|
| | | Yield[a] | [O][b] | HHV[c] (MJ $kg^{-1}$) | Acids[d] | Carbonyls[d] | HCs[d] |
| Thermal | Ar | 41 | 42.1 | 19.0 | 12.0 | 14.1 | 0.5 |
| $Na_2CO_3/Al_2O_3$ | Ar | 9 | 12.3 | 37.0 | 0.0 | 35.8 | 17.8 |
| $Na_2CO_3/Al_2O_3$ | $H_2$&Ar | 10 | 12.5 | 37.0 | 0.0 | 37.3 | 18.6 |
| $Pt/Al_2O_3$ | $H_2$&Ar | 27 | 41.8 | 19.0 | 0.0 | 12.0 | 19.1 |

[a]yield in wt.% compared to biomass feed [b]oxygen content in wt.%
[c]higher heating value [d]the relative abundance based on the TIC area % in GC-MS analysis

In the next experiment, $Na_2CO_3/Al_2O_3$ material was again employed but now in presence of a mixture of 35 vol.% $H_2$ and 65 vol.% Ar. It can be seen that with this catalyst there is almost no change in the bio-oil's properties, whether or not $H_2$ was used (Table 7.2). This is expected since neither sodium nor alumina is known to catalyse hydrogenation reactions. In order promote hydrogenation, Pt/ γ-$Al_2O_3$, a typical hydrogenation catalyst, was used. The yield of bio-oil in presence of Pt/γ-$Al_2O_3$ catalyst was enhanced (from 10 to 27 %) but its quality (*i.e.* oxygen%, HHV) became worse compared to those obtained with Na/γ-$Al_2O_3$. However, GC-MS analyses do show that with platinum the lowest carbonyl (12.0 %) and highest HC (19.1%) contents among all the tested materials was achieved. Thus, carbonyls are susceptible to hydrogenation under the conditions of hydro-pyrolysis and thus shows promise. Up to this point, it can be concluded that Na/γ-$Al_2O_3$catalyst is responsible for the de-oxygenation of pyrolysis vapours while Pt/γ-$Al_2O_3$ accounts for the removal of carbonyls and enhancement of hydrocarbon, likely *via* hydrogenation. Thus both catalysts are required to achieve good quality oil.

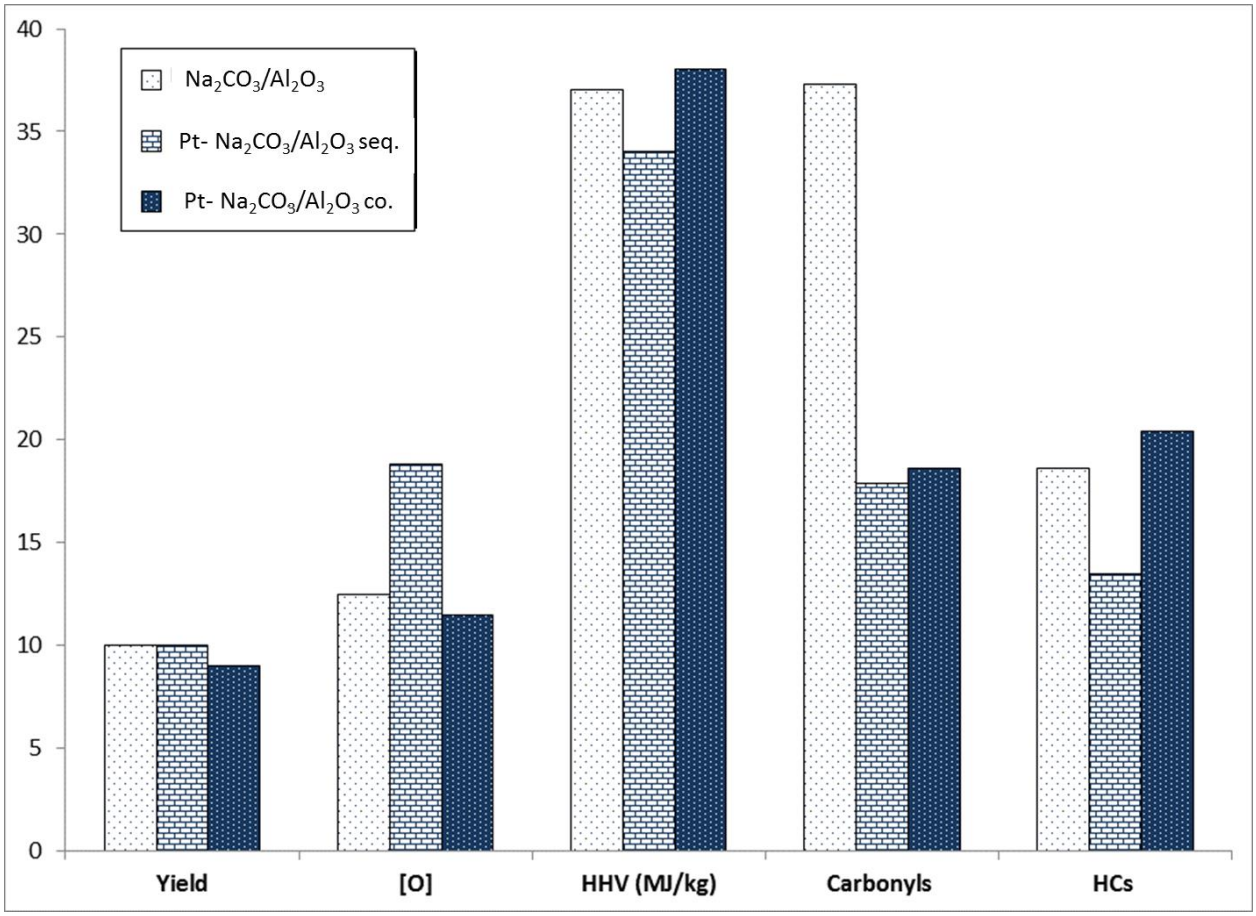


**Figure 7.2.** Comparison between two catalysts prepared by sequential impregnation and co-impregnation in biomass hydro- pyrolysis.

Platinum and sodium carbonate were loaded on γ-$Al_2O_3$ by sequential or co-impregnation methods to promote both hydrogenation and de-oxygenation, simultaneously. The results of the hydro-pyrolysis of pinewood using the two co-catalysts are compared to that of $Na_2CO_3$/γ-$Al_2O_3$ and illustrated in Figure 7.2. A decrease in carbonyl content was observed, coming down from 37.3 % ($Na_2CO_3$/γ-$Al_2O_3$) to 17.9 % and 18.6 % for seq., and co-impregnation catalysts, respectively. However, there is no noticeable improvement in terms of oxygen content and energy density. The catalyst prepared by sequential impregnation even shows slightly lower activity in this aspect, resulting in a bio-oil with higher oxygen content (18.8 %) and lower heating value (34 MJ $kg^{-1}$) compared to $Na_2CO_3$/γ-$Al_2O_3$. The activity towards hydro-pyrolysis of the 2 catalysts also correlates to the corresponding particle sizes of Pt as shown in Table 7.1. As expected, the co. impregnation catalyst with smaller particle size of Pt (3.5 nm) showed a superior catalytic performance in hydro-pyrolysis compared to that of the sequential impregnation material (with average Pt particle size of 6

nm). The fact that the two co-catalysts do not show improvement compared to the sodium catalyst can be due to the interaction of the platinum and sodium precursors, as discussed in section 7.3.1, leading to (i) the agglomeration of Pt particles (*i.e.* less contact between pyrolysis vapours and Pt catalyst) and (ii) lower surface area of the support.

*7.3.2.2. Dual-bed system*

In order to prevent the detrimental interaction between Pt and Na precursors as well as to increase the vapour-catalyst contact, the single-bed system with one single co-catalyst Pt-Na/γ-$Al_2O_3$ was changed to a dual-bed system as described in section 7.2.2. The first bed consisted of $Na_2CO_3$/γ-$Al_2O_3$ and the second bed was packed with Pt/γ-$Al_2O_3$. The results of such a system are shown in Figure 7.3. As can be seen, the hydrocarbon content increases tremendously from 18.6% (single-bed, $Na_2CO_3$/ γ-$Al_2O_3$) and 20.4% (single-bed, Pt-Na/$Al_2O_3$) to 55.3% in the dual-bed system. Some of the aliphatic carbonyls and their corresponding hydrogenation products (hydrocarbons) detected in bio-oils from single and dual-bed systems are shown in Table 7.3. The carbonyls shown on the left part of the table were completely removed in the dual-bed system while the hydrocarbons on the right part were not detected at all in the single-bed oil. This confirms that hydro-deoxygenation of carbonyls into HCs was facilitated in the dual-bed system.

To further confirm the activity of the catalysts of the dual-bed system in the conversion of carbonyls into hydrocarbons, an experiment with a carbonyl model compound (methyl ethyl ketone) was carried out as described in section 2.4. GC-MS analysis of the condensable products showed that unreacted methyl ethyl ketone makes up *ca.* 30% (based on TIC area %) of the detected products. 58% of the products are shown to be hydrocarbons (both aliphatic and aromatic) and the rest 12% are other products, for *e.g.* ketones, carboxylic acids, phenols *etc.* Among the detected hydrocarbons the two compounds with the highest area percentages are isobutylene (18%) and 2-pentene (10%). Butane and/or butene were expected to be present but none of them are detected among the products and instead the isomer of butene (*i.e.* isobutylene) was formed. However, this model compound experiment once again confirms the ability to convert carbonyls into hydrocarbons of the catalysts in the dual-bed system. Additionally, it can be seen in Table 7.3 that the transformation of carbonyls into the corresponding HCs likely occurred *via* two steps: (i) hydrogenation of carbonyls into

alcohols, which is catalysed on Pt and (ii) dehydration of these alcohols into HCs over acid sites on γ-$Al_2O_3$ surface.

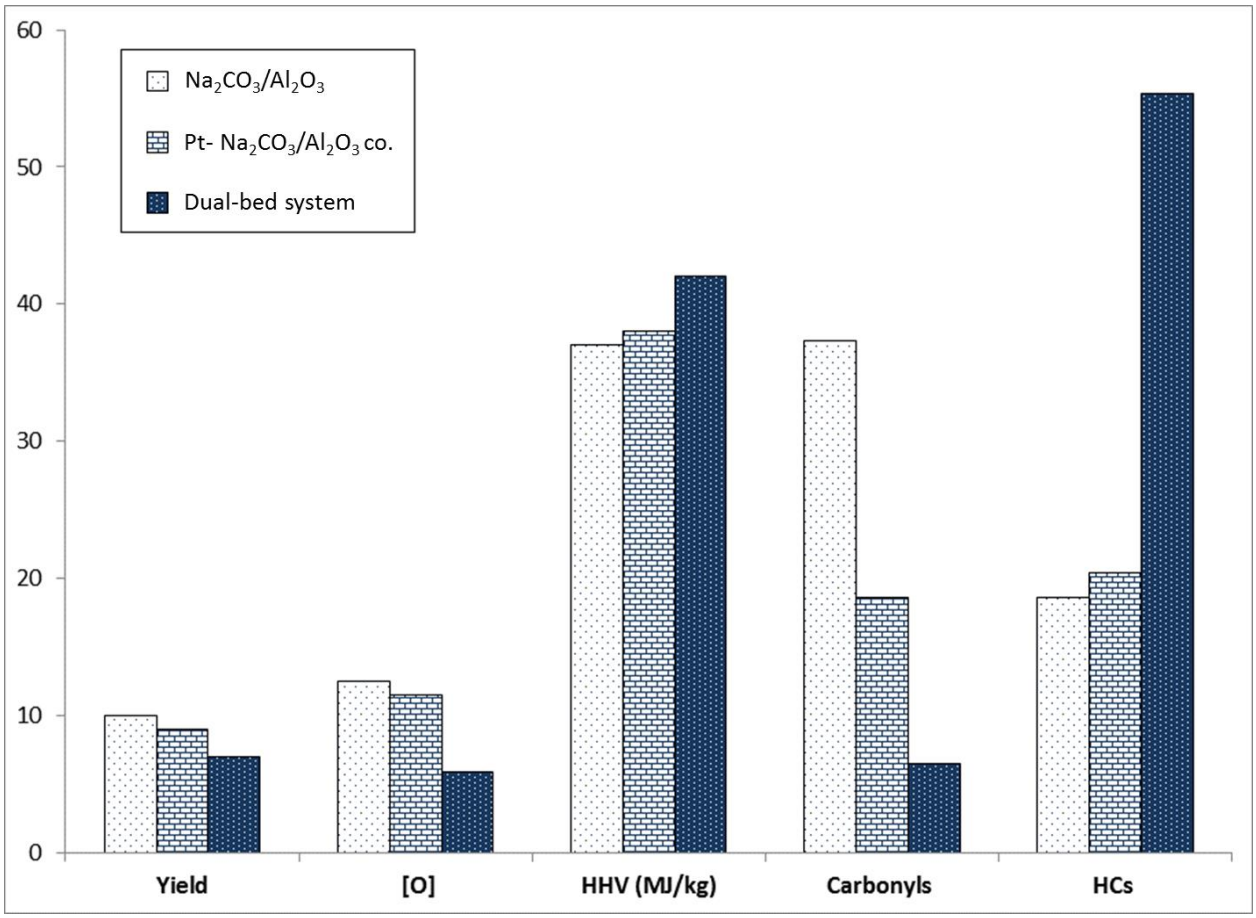


**Figure 7.3.** Comparison of single bed with dual bed towards bio mass hydro-pyrolysis

Oxygen and carbonyl content also decreases significantly in the double bed system, reaching extremely low values of 5.9% and 6.5%, respectively. The HHV value of bio oil from dual bed system is now 42 $MJ.kg^{-1}$ which approaches that of diesel (45 $MJ.kg^{-1}$). The biggest drawback of dual bed system is the lower yield of bio-oil (7 wt.%), which is caused by the higher yield of water and coke formed on the catalyst. This problem can be mitigated applying milder temperature and higher pressure, which facilitate hydrogenation and prevent unwanted coke formation. This approach will be investigated in future study.

**Table 7.3.** Detected compounds in single and dual-bed systems and their structures

| Single-bed system with $Na_2CO_3/\gamma\text{-}Al_2O_3$ catalyst | | Dual-bed system | |
|---|---|---|---|
| **Detected compound** | **Structure** | **Detected compound** | **Structure** |
| 3-Buten-2-one, 3-methyl- | 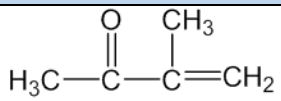 | Butane, 2-methyl- | 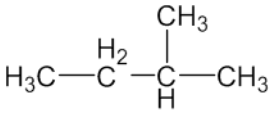 |
| 2-Butenal | 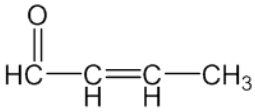 | n-Butane | 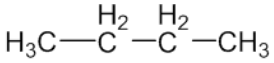 |
| Methyl Isobutyl Ketone | 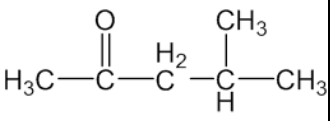 | 2-pentene, 4-methyl- | 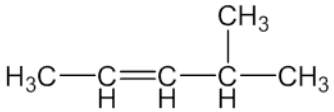 |
| 2-Heptanone | 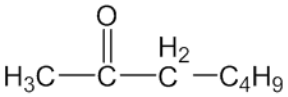 | 2-Heptene | 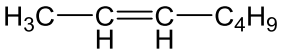 |

*7.3.2.3. Alternative source of hydrogen for the hydro-pyrolysis of biomass*

So far it has been shown that the dual-bed mode has resulted in oil with superior quality compared to the other systems. Each of the catalyst in this system has its own functionality and the combination of them is necessary for this achievement. APR of aqueous organic phase is still in the early stages of development and very promising results are still at the laboratory research scale. Upgrading of pyrolysis vapours using $H_2$ from fossil sources may not be optimal because of the cost and availability. In this aspect, low alkanes contained in natural gas, or LPG may be an option as a preferable source without going through the expensive reforming process. As a proof of concept $H_2$ was replaced by n-butane as the hydrogen donor. n-butane was chosen because of the fact that this gas is relatively easier compared to methane to decompose into hydrogen and thus it is a good point to start with. The results of hydro-pyrolysis of biomass in presence of n-butane or $H_2$ gas are compared in Table 7.4. It can be seen that using n-butane resulted in bio-oil with similar yield and quality compared to those of $H_2$. Hydro-pyrolysis in presence of butane also resulted in higher amount of coke (13%), which is a by-product from the decomposition of n-butane on Pt catalyst: $C_4H_{10} \rightarrow 4C + 5H_2$.

**Table 7.4.** Comparison between $H_2$ and n-butane as the hydrogen source for biomass hydro-pyrolysis

| Mode | Gas flow | Coke yield[a] | Bio-oil properties | | | | | |
|---|---|---|---|---|---|---|---|---|
| | | | Yield[a] | [O] | HHV (MJ $kg^{-1}$) | Acids | Carbonyls | HCs |
| Single-bed system Pt-$Na_2CO_3/Al_2O_3$ | $H_2$&Ar | 10 | 9 | 12.8 | 37 | 0 | 34.9 | 20 |
| Dual-bed system | $H_2$&Ar | 9 | 7 | 5.9 | 42 | 0 | 6.5 | 55.3 |
| Dual-bed system | n-$C_4H_{10}$ | 13 | 7 | 5.6 | 42 | 0 | 7.8 | 47.0 |

[a]in wt.% compared to weight of biomass

The fact that n-butane possesses similar performance compared to $H_2$ in hydro-pyrolysis of biomass has opened a new possibility of using natural gas as a hydrogen source in this domain. This approach is of great economical attractiveness and will be studied in the future.

**Table 7.5.** Summary of the progress achieved by hydro-pyrolysis in terms of quality of bio-oil

| Property | Non-catalytic | $Na_2CO_3/Al_2O_3$ | $Pt/Al_2O_3$ | Dual bed system | Fuel oil |
|---|---|---|---|---|---|
| **elemental composition, wt.%** | | | | | |
| **C** | 52 | 78.0 | 50.2 | 84.1 | 85 |
| **H** | 5.7 | 8.7 | 7.2 | 8.9 | 11 |
| **O** | 42 | 12.5 | 41.8 | 5.9 | 1 |
| **pH** | 2.6 | 6.5 | n.d[a] | n.d[b] | 5.7 |
| **higher heating value, MJ/kg** | 19 | 37 | 19 | 42 | 40 |
| **area % in GC-MS analysis** | | | | | |
| **acid** | 12.0 | 0 | 0 | 0 | 0 |
| **carbonyls** | 14.1 | 37.3 | 12 | 6.5 | 0 |
| **hydrocarbons** | 0.5 | 18.6 | 19.1 | 55.3 | 100 |

[a]not determined
[b]not determined, expected to be higher than 6.5

The progress we have made is summarized in Table 7.5. It can be seen that, from non-catalytic pyrolysis to catalytic pyrolysis using $Na_2CO_3$/ $\gamma$-$Al_2O_3$ catalyst and finally to hydro-pyrolysis using the dual bed configuration, Na/$\gamma$-$Al_2O_3$ + Pt/$\gamma$-$Al_2O_3$, most of the problems related to bio-oil have been solved. The obtained oil is now less corrosive and has

higher energy density than fuel oil. The drawback of Na/γ-$Al_2O_3$ catalytic system was successfully overcome, represented by the tremendous decrease in the carbonyl and increase in hydrocarbon contents.

The obtained oil is now less corrosive and has higher energy density than fuel oil. The drawback of $Na_2CO_3$/γ-$Al_2O_3$ catalytic system was successfully overcome, representing by the tremendous decrease in the carbonyl and increase in hydrocarbon contents.

## 7.4. Conclusion

Compared to non-catalytic pyrolysis, catalytic upgrading in the presence of $Na_2CO_3$/γ-$Al_2O_3$ results in higher level of selective de-oxygenation but leads to the formation of more harmful carbonyls. Hydro-pyrolysis using Pt-Na co-catalysts has reduced the amount of these harmful compounds in bio-oil. The dual-bed system in which the sodium and platinum components were separated has proven to be a very promising approach. Dual-bed operation has shown to achieve the highest de-oxygenation level of bio-oil among all the catalytic systems. This was achieved *via* the removal of harmful carbonyls and enhancement of the desirable hydrocarbons, leading to a heating value higher than that of traditional fuel oil (42 MJ $kg^{-1}$). n-butane can be used as a hydrogen source for biomass hydro-pyrolysis.

## References

[1] A.V. Bridgwater, Catalysis Today 29 (1996) 285-295.
[2] D.J.M.d. Vlieger, Design of efficient catalysts for gasification of biomass-derived waste streams in hot compressed water, University of Twente, 2012.
[3] E. Furimsky, Applied Catalysis a-General 199 (2000) 147-190.
[4] D.C. Elliott, D. Beckman, A.V. Bridgwater, J.P. Diebold, S.B. Gevert, Y. Solantausta, Energy & Fuels 5 (1991) 399-410.
[5] Y.H.E. Sheu, R.G. Anthony, E.J. Soltes, Fuel Processing Technology 19 (1988) 31-50.
[6] S. Ramanathan, S.T. Oyama, The Journal of Physical Chemistry 99 (1995) 16365-16372.
[7] W.A. Spieker, J. Liu, J.T. Miller, A.J. Kropf, J.R. Regalbuto, Applied Catalysis A: General 232 (2002) 219-235.

# Chapter 8

## Conclusions and recommendations

**Abstract.** The thesis is concluded with this chapter. Throughout the previous chapters, various aspects of the catalytic conversion of lignocellulosic biomass were discussed, with the goal to design an efficient catalyst for the generation of a high quality fuel/fuel precursor. This chapter summarizes main conclusions of the work carried out in this thesis followed by recommendations for the future.

## 8.1. Conclusions

Fast pyrolysis is a promising technique to convert lignocellulosic biomass into a liquid fuel/fuel precursor, also known as bio-oil. However, compared to conventional crude oil, bio-oil has much higher oxygen content which results in various detrimental properties and limits its application. Thus the first part of this thesis aims to develop an efficient catalyst to upgrade bio-oil into high quality fuel *via* de-oxygenation and hydro-deoxygenation *in situ* during pyrolysis. The second part is dedicated to study the nature of the active specie in the newly-developed catalyst and to gain more insights into the catalytic conversion of lignin *via* a model compound study.

The first part of the thesis begins with **Chapter 3**. In this chapter, Faujasite materials with different $H^+$ and $Na^+$ concentrations including H-FAU, $Na_{0.2}H_{0.8}$-FAU and Na-FAU were applied as catalysts in the pyrolysis of white pine, with the goal to lower the oxygen content of bio-oil. Two methods to establish the catalyst-biomass contact, *i.e.* both catalyst and biomass mixed in the pyrolysis zone and catalyst post to pyrolysis chamber, were compared and it was shown that the post-treatment was superior to *in-situ* when it comes to bio-oil oxygen removal efficiency. It was shown that the amount of $H^+$ and $Na^+$ of the catalyst plays an important role in the product yields and product distribution. The higher the concentration of $H^+$ of the catalyst is, the lower the liquid yield, and the higher the solid and gas yields are obtained. The two of major problems with bio-oil, namely the corrosiveness and instability, were shown to be mainly caused by carboxylic acids and carbonyl compounds, respectively. The best catalyst candidate is $Na_{0.2}H_{0.8}$-FAU, which reduced the most acid and carbonyl compounds while boosted the amount of the desirable phenolic and hydrocarbon compounds compared to non-catalytic experiment and to the other two catalysts. $Na_{0.2}H_{0.8}$-FAU also removed the most oxygen as $CO_2$, resulting in an oil with lowest oxygen content (38 wt.%) and highest energy content (24 MJ $kg^{-1}$) compared to other materials. It was shown possible to regenerate the spent catalyst without changing its crystalline structure and catalytic performance.

The catalytic system shown in **Chapter 3** was improved further in **Chapter 4** by employing $\gamma$-$Al_2O_3$ as the support for $Na^+$. $\gamma$-$Al_2O_3$ was selected because of its mesoporous nature, which allows access to bulkier biomass oxygenates and likely reduces the problem of coking/pore blockage compared to microporous FAU zeolites. Compared to non-catalytic

pyrolysis, catalytic upgrading in the presence of $Na_2CO_3/\gamma\text{-}Al_2O_3$ results in higher level of selective de-oxygenation with the oxygen ending up in heterogeneous char or removed as COx. Characterization of the catalyst using SEM and XRD has shown that sodium carbonate is well-dispersed on the support $\gamma\text{-}Al_2O_3$. TGA and $^{23}Na$ MAS NMR study suggested the formation of new hydrated sodium phase, which is likely responsible for the high activity of the catalyst. This hydrated phase is proposed to be formed by the coordination between sodium ion and the hydroxyl group of alumina. It has been shown that catalytic oil has much lower oxygen content (12.3 wt.%) compared to non-catalytic oil (42.1 wt.%). This comes together with a tremendous increase in the energy density (37 compared to 19 MJ $kg^{-1}$) approaching that of fuel oil (40 MJ $kg^{-1}$). Decarboxylation of carboxylic acids was favored on the catalyst, resulting in an oil almost neutral (TAN= 3.8 mg KOH/g oil and pH=6.5). However, the mentioned decarboxylation also resulted in the formation of carbonyls, which correlates to low stability of the oil.

**Chapter 5** continues with the study on the catalytically active site in $Na_2CO_3/\gamma\text{-}Al_2O_3$ catalyst mentioned in **Chapter 4.** It was shown possible to achieve very high de-oxygenation degree of bio-oil with $Na_2CO_3/\gamma\text{-}Al_2O_3$ catalyst compared to $Na_2CO_3$, $\gamma\text{-}Al_2O_3$ and non-catalytic experiment. XRD analyses have shown that a good dispersion of $Na_2CO_3$ on $\gamma\text{-}Al_2O_3$ was achieved using wet impregnation followed by calcination of the obtained materials. It was revealed in TGA analyses that, in the supported catalysts, the sodium active specie likely existed in a state different from that in pure $Na_2CO_3$. This was shown by the difference in decomposition temperature between the two. $^{23}Na$ and $^{1}H$ MAS NMR spectra also confirmed the presence of this phase. This state is later proposed to be hydrated sodium specie, formed by the coordination between sodium ions and hydroxyl groups on the surface of $\gamma\text{-}Al_2O_3$. The fact that the 20 wt.% $Na_2CO_3/\gamma\text{-}Al_2O_3$ sample the most active catalyst in the de-oxygenation of bio-oil suggests that this hydrated specie is the one responsible for this superior activity of the catalyst. $^{27}Al$ MAS NMR spectra of $\gamma\text{-}Al_2O_3$ and the supported catalysts with different $Na_2CO_3$ loadings have revealed two peaks corresponding to the tetrahedral and octahedral Al. It can be observed that there is a downshift in the resonance signal of the tetrahedral Al in the supported catalysts compared to that of $\gamma\text{-}Al_2O_3$. This can be a result of the interaction between absorbed $Na^+$ ions and oxygen atoms of γ-alumina which causes a deshielding effect on Al atoms. The chemical shifts of the octahedral Al also varied depending on the loading of sodium carbonate, but with a lesser extent. Regeneration of the catalyst was carried out in air

at 600 $^{o}$C and the regenerated material shows to have lower activity towards de-oxygenation compared to fresh catalyst. The alumina support was hardly affected during regeneration while there is change in the hydrated specie and this change is likely responsible for the deactivation of the catalyst.

In **Chapter 6**, the conversion of lignin-derived compounds in bio-oil over catalysts was studied using vanillyl alcohol as the model compound. It has been shown that this model compound undergoes consecutive reactions to form methoxy phenols, phenols, and eventually hydrocarbons with increasing degree of de-oxygenation. The degree of de-oxygenation of vanillyl alcohol was shown to increase with the increase in number of acid sites in catalysts. $\gamma$-$Al_2O_3$ material with the highest number of acid sites has resulted in the highest yield of aromatic hydrocarbons, accompanied by the highest yields of coke and gas compared to other materials used in this study. Two pathways have been shown to lead to the formation of hydrocarbons from vanillyl alcohol. These are: (i) decomposition of vanillyl alcohol into small olefinic hydrocarbon fragments and the subsequent aromatization into final products and (ii) direct de-oxygenation of this model compound over catalysts. Cyclic ketones, phenol derivatives and aromatic hydrocarbons were detected among the pyrolysis products of vanillyl alcohol and biomass. The concentrations of those components change in presence of different catalysts and the trends of changes are similar in both biomass and vanillyl alcohol pyrolysis. However, the rates of changes are different, which illustrates the difference in catalytic efficiency towards different biomass components.

The hydro-deoxygenation of bio-oil was investigated in **Chapter 7**. It was shown in **Chapter 5** that catalytic upgrading in the presence of $Na_2CO_3$/$\gamma$-$Al_2O_3$ results in higher level of selective de-oxygenation but leads to the formation of more harmful carbonyls. The study in **Chapter 7** was carried out trying to solve that problem using the combination of catalytic de-oxygenation and hydrogenation. It was shown that hydro-deoxygenation using Pt-$Na_2CO_3$/$\gamma$-$Al_2O_3$ co-catalysts reduced the amount of carbonyl compounds in bio-oil. However, the bulk quality of bio-oil (*i.e.* oxygen content, heating value) remained unchanged or became worse compared to the single catalyst, *i.e.* Pt/$\gamma$-$Al_2O_3$ and $Na_2CO_3$/$\gamma$-$Al_2O_3$. This low catalytic activity can be attributed to the interaction between the 2 precursors, namely choloroplatinic acid and sodium carbonate, which in turn resulted in the agglomeration of Pt particles and lower surface area of the support. The dual-bed system in which the sodium and platinum components were separated has proven to be a very promising approach. Dual-bed

operation has shown to achieve the highest de-oxygenation level of bio-oil among all the catalytic systems. This was achieved *via* the removal of harmful carbonyls and enhancement of the desirable hydrocarbons, leading to a heating value higher than that of traditional fuel oil (42 MJ $kg^{-1}$). n-butane possesses similar performance compared to $H_2$ as a hydrogen source for biomass hydro-pyrolysis, opening new possibility for economical hydrogen sources (for *e.g.* natural gas) for bio-oil hydro-treating

## 8.2. General recommendations

In this present work, a catalytic system has been developed with the goal to upgrade bio-oil into a high quality fuel precursor. Throughout the chapters in this thesis, attempts were made to answer a few critical questions related to this goal, such as: Which catalyst is the most active in the de-oxygenation of bio-oil? How can the catalyst be introduced in biomass pyrolysis? Is the newly-developed catalyst regenerable? Are we able to further improve the system by coupling catalytic de-oxygenation and hydrogenation? What is the active specie in the catalyst?, *etc.* Along the way new questions related to the catalytic material and ideas to further improve the system have also arisen.

An important aspect to take into account in any catalytic study is the regenerability of the catalytic material. In Chapter 5, the regenerablity of the $Na_2CO_3/\gamma$-$Al_2O_3$ catalyst was investigated. It was shown that the catalyst has lost some of its activity towards bio-oil de-oxygenation after being regenerated in air at 600 $^oC$. And this was attributed to the change in the catalytically active sodium specie, which was confirmed by comparing the $^{23}Na$ MAS NMR spectra of the fresh and regenerated catalyst samples. In order to improve the regenerabilty and thus applicability of the catalyst, it is necessary to identify the deactivation mechanism in this particular case. Does the change observed with the active specie result from (i) the interaction between catalyst-pyrolysis vapour during the upgrading process or by (ii) the regeneration step, *i.e* coke burning at 600 $^oC$ or both? If the factor which caused the change is the interaction between catalyst and the pyrolysis vapour, we can try to either reduce the severity of the upgrading process, *i.e.* temperature, retention time or to remove or neutralize the harmful compounds in bio-oil prior to upgrading, for *e.g.* carboxylic acids. If the change was caused by the regeneration step itself, certain promoters, for *e.g.* Pt, can be used to reduce the temperature needed for the coke burning. Moreover, promoters that are

able to limit the coke formation were extensively studied and well worth to try with the developed catalytic system.

In Chapter 7, it was shown that bio-oil obtained with the co-catalyst Pt-Na/γ-$Al_2O_3$ has higher oxygen content and lower heating value compared to that of the single catalyst Na/γ-$Al_2O_3$. This low catalytic activity was then attributed to the acid-base reaction between the 2 precursors, namely choloroplatinic acid and sodium carbonate, which resulted in the agglomeration of Pt particles and lower surface area of the support. One way to tackle this problem is to employ Pt precursor with neutral or basic properties, for *e.g.* $Pt(C_5H_7O_2)_2$ or $[Pt(NH_3)_4](OH)_2$. This will prevent the unwanted reaction between Pt and Na precursors and might result in a catalyst with higher activity.

Moreover, it was shown in Chapter 7 that a dual-bed system in which pyrolysis vapour was upgraded over two consecutive beds of de-oxygenation (Na/γ-$Al_2O_3$) and hydrogenation (Pt/γ-$Al_2O_3$) catalysts resulted in a liquid product (bio-oil) with higher energy content than fuel oil. However, the biggest drawback of such a system is the low yield of bio-oil (7 wt.%), which is caused by the high yield of water and coke formed on the catalysts. This problem can be mitigated applying milder temperature and higher pressure, which facilitate hydrogenation and prevent unwanted coke and water formation. Also in this chapter, n-butane was shown to be a feasible source of hydrogen for the hydrogenation reaction. It would be much more economically promising if we can prove that this approach also works with methane. Methane, which is the main component of natural gas, is widely available and cheaper than hydrogen gas. Thus replacing hydrogen gas with methane can offer great economical benefit.

An in depth study on the active specie in Na/γ-$Al_2O_3$ catalyst was carried out in Chapter 5, based on TGA and NMR analyses. It would be desirable to establish a theoretical model using Density Functional Theory (DFT) to look at the proposed active site and provide insights into sodium promoted catalyst. Such theoretical study complements the experimental data well and will help to establish a complete picture of the nature of the active catalytic sites in Na/γ-$Al_2O_3$ and provide an efficient catalyst design of this promising system.

The catalytic conversion of lignin-derived components in bio-oil was studied in Chapter 6 using vanillyl alcohol as a model compound. The results of such a model compound study were compared with the conversion of biomass (white pine) over the catalysts. Biomass consists of three main components, namely cellulose, hemicellulose and

lignin and the interaction between those components during catalytic pyrolysis can be complicated to follow and compared with the model compound. It is thus desirable to first carry out a study in which these three components were separated and converted independently. This will rule out the complication and allow to have a better understanding of the system.

# Scientific contributions

## Peer-reviewed journal articles

1. **T.S. Nguyen**, M. Zabeti, L. Lefferts, K. Seshan, "Conversion of lignocellulosic biomass to green fuel oil over sodium based catalysts" **Bioresource Technology** 142 (2013), p. 353-360.

2. **T.S. Nguyen**, M. Zabeti, L. Lefferts, G. Brem, K. Seshan, "Catalytic upgrading of biomass pyrolysis vapours using Faujasite zeolite catalysts" **Biomass and Bioenergy** 48 (2013), p. 100-110.

3. M. Zabeti, **T.S. Nguyen**, L. Lefferts, H.J. Heeres, K. Seshan, "*In situ* catalytic pyrolysis of lignocellulose using alkali-modified amorphous silica alumina" **Bioresource Technology** 118 (2012) p. 374-381.

## Manuscripts in preparation

1. **T.S. Nguyen**, L. Lefferts, K.B. Sai Sankar Gupta, K. Seshan, "Catalytic conversion of biomass pyrolysis vapours over sodium-based catalyst: A study on the state of sodium on the catalyst", **ChemCatChem**.

2. **T.S. Nguyen**, G. Raman, S. He, K. Seshan, "In situ catalytic hydro-deoxygenation of lignocellulose during pyrolysis", **Applied Catalysis B: Environmental.**

3. **T.S. Nguyen**, S. He, L. Lefferts, G. Brem, K. Seshan, "Study on the catalytic conversion of lignin-derived components in pyrolysis vapour using model component", **Catalysis Today**

## Oral presentations

1. **T.S. Nguyen**, A. Imran, L. Lefferts, G. Brem, K. Seshan, "Catalytic pyrolysis of biomass- Paving the way for a future of green energy", The Green Energy Initiative of University of Twente, Kick-off meeting, Enschede, The Netherlands, 2012.

2. **T.S. Nguyen**, Y. Guan, L. Lefferts, G. Brem, K. Seshan, "Influences of Faujasite catalysts on the fast pyrolysis of pinewood", 1st International Congress on Catalysis for Biorefineries, Malaga, Spain, 2011. Proceeding ISBN 978-849 3912 031, p.164-169.

3. **T.S. Nguyen**, L. Lefferts, G. Brem, K. Seshan, "Refinery feedstock via fast catalytic pyrolysis of biomass", Netherland Catalysis and Chemistry Conference NCCC XII, Noordwijkerhout, The Netherlands, 2011.

## Poster presentations

1. **T.S. Nguyen**, L. Lefferts, K. Seshan, "*In situ* catalytic pyrolysis of biomass using zeolite catalysts", Netherlands Process Technology Symposium NPS-10, Veldhoven, The Netherlands, 2010.

2. M. Verhoek, **T.S. Nguyen**, L. Lefferts, K. Seshan, "Flash pyrolysis of Vanillin as a model compound for lignin", Netherland Catalysis and Chemistry Conference NCCC XI, Noordwijkerhout, The Netherlands, 2010.

3. **T.S. Nguyen**, L. Lefferts, K. Seshan, "Introduction to the lab-scale catalytic pyrolysis of biomass", Energy and Resources Symposium, Enschede, The Netherlands, 2010.

4. **T.S. Nguyen**, L. Lefferts, K. Seshan, "Screening of catalysts for the pyrolysis of biomass using a lab-scale IR furnace set-up", Netherlands Process Technology Symposium NPS-09, Veldhoven, The Netherlands, 2009.

# Acknowledgement

Finally the time has come! My PhD journey in CPM has come to an end with plenty of beautiful and unforgettable moments that I treasure so much and keep with me for the rest of my life. This journey, like other adventures, has ups and downs but the most important part is all the lessons that I have learnt along the way, which shape me into the person that I am today. This part of my thesis is therefore dedicated to the people that taught me, inspired me, learnt alongside me, gave me unconditional love and supports, who all make this journey so memorable.

First, I would like to express my sincere gratitude to Seshan, my promoter and daily supervisor. You are a supervisor, a teacher, a parental figure and a friend that I can only dream of. Your door is always open for scientific discussion as well as informal talk. Your guidance and great support to my PhD, in both good and hard times, is much appreciated. I have learnt a lot from you, both as a scientist and as a person. I would like to show my gratefulness also to Jayanthi, your wife, for all the delightful gatherings with yummy food at your place. This makes my time in a country half a world away from home more enjoyable.

Leon, I would like to thank you for the opportunity to carry out my PhD research in CPM and for all scientific discussions we had, which helps me steering my project in the right direction. Your help in improving the way I wrote scientific papers is much appreciated. The annual CPM party at your place is always enjoyable!

Barbara and Arie, thank you for being there when we (PhD students) need you the most and for all your scientific advices. It is always a pleasure talking to you two. Barbara, your kind and cheerful personality makes our group a livelier place.

Bertolino, I would never be able to thank you enough for your support. Your immense technical knowledge and your unique view about life and people never fail to amaze me. It is my great pleasure to work with you.

My gratitude also goes to Tom, Ruben, Louise and Karin. Thank you for all your support along the years. Ruben, I had a lot of fun playing football in CPM team with you. Tom,

**Acknowledgement**

Louise, and Karin, I am grateful for the time that we had in our CPM borrels and during our annual group trips.

I would like to express my gratitude to Lianne, Sabine, Lidy and Maaike, our beloved secretaries. Thank you for your support at the various stages of my time in CPM. Your help is much appreciated.

Rao and Songbo, thank you for being my friends and paranimphs. Rao, thank you for being such a perfect officemate and for all your kind help in both work and in daily life. Your kind personality and your comprehensive knowledge in chemistry is much treasured.

My gratitude also goes to Frank De Groot who is carrying out his Master assignment in CPM. Thank you for the nice translation of the summary of my thesis into Dutch. Your help is much appreciated.

I supervised 2 students during my PhD, Julian and Maisha, and I would like to thank them for their contributions to my project. I wish you two the best with your career.

I would like to extend my sincerest thanks to Châu and Nhi, my fellow Shell Scholars. I wish you all the best with your career and your life.

Futhermore, I would like to thank my former colleagues and fellow CPMers, Shilpa, Sergio, Masoud, Arturo, Yingnang, Joline, Inga, Marijana, Cassia, Cristiano, Davide, Roger, Kamilla, Kaisa, Digijay, Kuma, Igor, Hrudya, Raman, Chris, Yejun, Berta, for such a pleasant time in CPM. You guys rock!

I also would to express my gratitude to Karthick from Leiden University for the fruitful collaborations and NMR analysis and to Mark Smither from Mesa+ for SEM and TEM analysis.

My special thank goes to my Vietnamese friends in Enschede, Hào, Loan, Minh, Giang, Lan Anh, Hành, Trung, Thanh, Hà, Hạnh, Hiển, Như, Tú, Tân, Đào, Trí, Tuấn (Hô), Hiếu, Trinh, Việt Anh, Đức, Hiếu (Eindhoven), Tuấn (Sói), Lâm, Tuấn (Jinn), Fima the Cat. You are my second family in Netherlands. Thank you all for your support and all unforgettable moments that we have shared together. Special thank goes to Việt Anh for letting me using your photos for the cover design of my thesis.

**Acknowledgement**

I cannot come to this point without the love and support of my family. Hằng, you are such a wonderful sister and I am always proud of you. During my time in the Netherlands I find myself so lucky that we are able to stick together. Without your and Tuấn's support I can never travel this far. Mom and Dad, thank you for your unconditional love and support. It is beyond words to appreciate your contribution to my life. I love you and this thesis is dedicated to you.

Last but not least, my deepest appreciation goes to my wife Bùi Hương Liên, my soul mate and the love of my life. You are always there for me, in happy and also hard times. In my most stressful time it is your love that gave me strength to keep moving forward. Your ceaseless faith in me and support made this happen. I love you!

Tang Son Nguyen was born in 1983 in Hanoi, Vietnam. In 2005, he graduated with a Bachelor degree in Chemistry from Hanoi University of Science, specializing in Catalysis. In 2006, he got a scholarship from the Royal Dutch Shell Centenary Fund to pursue a 2-year MSc program in Chemical Engineering at the University of Twente, the Netherlands. He conducted his final Master assignment in the Catalytic Processes and Materials group, investigating the influences of different catalytic materials to the thermal decomposition of biomass.

During the final Master assignment he gained a lot of interest in the field of renewable fuels and applied catalysis, which drove him to accept an offer for a 4-year PhD position in September, 2008. The goal of his PhD project is to develop an efficient catalytic system for conversion of lignocellulosic biomass into fuels via pyrolysis. The results of his PhD research are presented in this book.

ISBN 978-90-365-3796-4

UNIVERSITY OF TWENTE.